PL-TR-91-2214

SIO Ref. 91-33

ANALYSIS & INTERPRETATION OF SIMULATANEOUS MULTI-STATION WHOLE SKY IMAGERY

R. W. Johnson

J. E. Shields

T. L. Koehler

University of California, San Diego
Marine Physical Laboratory
San Diego, CA 92152-6400

30 September 1991

Final Report
30 December 1987 - 30 September 1991

APPROVED FOR PUBLIC RELEASE; DISTRIBUTION UNLIMITED

PHILLIPS LABORATORY
AIR FORCE SYSTEMS COMMAND
HANSCOM AIR FORCE BASE, MASSACHUSETTS 01731-5000

"This technical report has been reviewed and is approved for publication"

DONALD D. GRANTHAM
Contract Manager

DONALD D. GRANTHAM, Chief
Atmospheric Structure Branch

ROBERT A. McCLATCHEY, Director
Atmospheric Sciences Division

This report has been reviewed by the ESD Public Affairs Office (PA) and is releasable to the National Technical Information Service (NTIS).

Qualified requestors may obtain additional copies from the Defense Technical Information Center.

If your address has changed, or if you wish to be removed from the mailing list, or if the addressee is no longer employed by your organization, please notify PL/IMA, Hanscom AFB, MA 01731-5000. This will assist us in maintaining a current mailing list.

Do not return copies of this report unless contractual obligations or notices on a specific document requires that it be returned.

REPORT DOCUMENTATION PAGE

Form Approved
OMB No. 0704 0188

1 Agency Use Only *(Leave blank).*	2. Report Date. 1991 September 30	3. Report Type and Dates Covered. Final Report, 30 Dec 87 to 30 Sep 91

4. Title and Subtitle.

Analysis & Interpretation of Simultaneous Multi-Station Whole Sky Imagery

5. Funding Numbers.

F19628-88-K-0005
Program Element No. 63707F
Project No. 6670
Task No. 09
Accession No. AO

6. Author(s).

Richard W. Johnson, Janet E. Shields, and Thomas L. Koehler

7. Performing Organization Name(s) and Address(es).

University of California, San Diego
Marine Physical Laboratory of the
Scripps Institution of Oceanography
San Diego, CA 92093

8. Performing Organization Report Number.

SIO Ref. 91-33

MPL-U-98/91

9. Sponsoring/Monitoring Agency Name(s) and Address(es).

Phillips Laboratory
Hanscom AFB, MA 01731-5000

Contract Manager: Donald Grantham/GPAA

10. Sponsoring/Monitoring Agency Report Number.

PL-TR-91-2214

11. Supplementary Notes.

12a. Distribution/Availability Statement.

Approved for Public Release, Distribution Unlimited

12b. Distribution Code.

13. Abstract *(Maximum 200 words).*

This Final Report, under Contract No. F19628-88-K-0005, summarizes the development and use of a digital image data base containing approximately 900 Gigabytes of raw image data, and about 675 Gigabytes of processed data. These images represent 4614 data days geographically distributed among seven CONUS sites, and reside on approximately 900 eight millimeter tape cassettes.

The imagery was acquired by an automatic, computer controlled, electronic camera system previously developed and described in GL-TR-89-0061, Johnson, et al (1989).

In addition to the data base summary, this Final Report discusses selected aspects of the overall data processing procedures, the physical nature of the tape archive, the development of the automatic cloud decision algorithm, and several resultant applications of the data to comparative studies and model development.

The imagery yields statistical and specific case study representations which compare well with the classical observational formats reported by weather station personnel. The numerical data have served as preliminary inputs and conceptual baselines leading to the development of new stochastic modeling techniques (Hering 1989, 1990).

14. Subject Terms.

Automated Imaging, Cloud Cover, Cloud Distributions, Cloud Identification Algorithms, Cloud Free Arcs

15. Number of Pages. 84

16. Price Code.

17. Security Classification of Report.	18. Security Classification of This Page.	19. Security Classification of Abstract.	20. Limitation of Abstract.
Unclassified	Unclassified	Unclassified	SAR

Table of Contents

List of Illustrations

List of Tables

1.0 INTRODUCTION

Responding to a well recognized need by many in both the modeling and operational communities for an improved capability in the collection and assessment of whole sky cloud characteristics, a new generation of video based imaging systems was developed and fielded by the Marine Physical Laboratory (MPL) of Scripps Institution of Oceanography (Johnson, et al, 1989). This Final Report summarizes the development and use of a resultant data base, generated by these previously fielded systems, containing approximately 900 Gigabytes of digitized raw imagery. These images represent approximately 4600 data days geographically distributed among seven widely separated CONUS sites.

There were several inter-related tasks associated with the program pursued during the forty-six months covered in this Final Report. In their simplest form they were to, a) provide technical coordination and operational maintenance for the several on-site video systems, b) establish an image oriented, data management and archival facility at the Marine Physical Laboratory, c) conduct a cloud image analysis program directed toward the determination of Cloud-Free Line of Sight/Cloud Free Arc (CFLOS/CFARC) probability distributions and the refinement of analytical models for estimating these distributions, and d) initiate preliminary studies into the development of experimental procedures to enable temporally short term predictions of those cloud field dynamics associated with CFLOS/CFARC applications to the GBL mission. Each of these tasks has been addressed in accordance with the programs on-going adjustment of goals and priorities, and is discussed separately in the following sections of this Final Report.

2.0 AUTOMATED SYSTEMS FOR CLOUD ASSESSMENTS

The Whole Sky Imager (WSI), as an emerging operational system has been described previously in GL-TR-89-0061, Johnson, et al, 1989. In its final field ready configuration, reviewed briefly in this introductory section, the WSI system provided the data acquisition mechanism for generating the image oriented data base which is discussed in the body of this final report.

2.1 The Whole Sky Imager

The Whole Sky Imager (WSI) is a ground-based electronic imaging system, which monitors the upper hemisphere. It is a passive, i.e. non-emissive system, which acquires calibrated multi-spectral images of the sky dome. The system, shown in Fig. 2-1, views the sky through a series of spectral and neutral density filters,

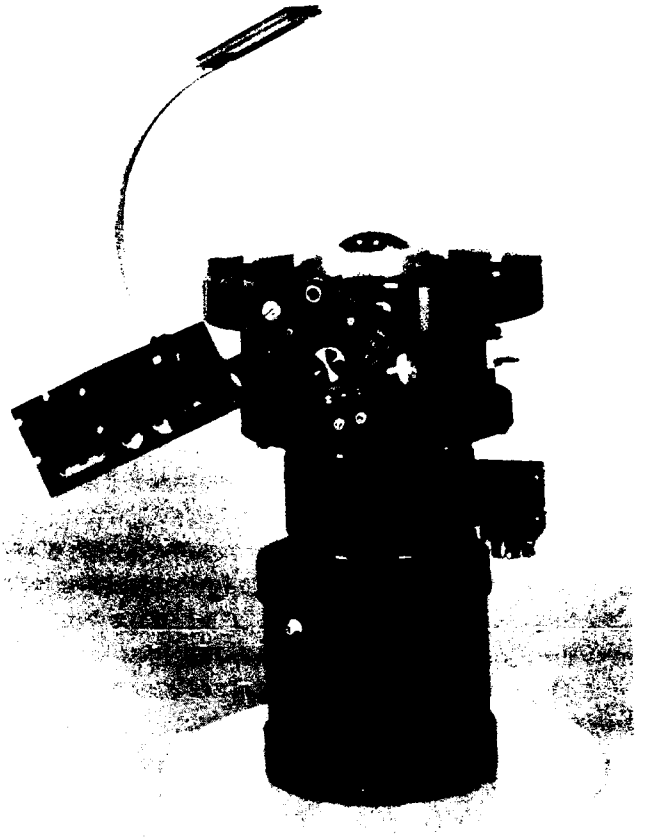

Fig. 2-1. Whole Sky Imager Camera Assembly

using a fisheye lens to acquire most of the sky dome. A fixed gain CID (charge injection device) solid state camera is utilized, and a full set of radiometric and geometric calibrations are acquired prior to fielding the system. Data are acquired in 512 x 480 format, which yields 1/3 degree spatial resolution. This corresponds to a 17 meter footprint, for a cloud layer at 3 km height.

In the field, cloud images are acquired under control of an IBM AT-class microcomputer. This is a stand-alone unit, requiring essentially no user intervention; control of all peripheral functions is fully automatic. Four digital images are acquired every minute, and archived on 8 mm tape, for post-processing. Approximately 1.2 gigabytes are acquired and archived per week at each site.

A sample radiance image is shown in Fig. 2-2. In this image, the center is at the zenith overhead, and the edges are near the horizon. The black square is the sun occultor, which shades the lens in order to minimize stray light. A tower may also be seen in the field of view near the occultor. In the processing, a determination is made at each point in the image, yielding a cloud decision image at full spatial resolution. The cloud decision image is illustrated in Fig. 2-3. In this illustration the areas

Fig. 2-2. Sample WSI Image, acquired at 650 nm

Fig. 2-3. Sample Cloud/No cloud Decision Image. This shows the full resolution results taken at 10 minute intervals.

identified as sky are dark grey, the occultor is black indicating a "no data" region, and the pixels identified as thin or opaque cloud are light grey through white respectively.

Full resolution images such as shown in Fig. 2-2 are saved every ten minutes. At one minute intervals, the subset shown in Fig. 2-4 is saved. (Fig 2-4 is the one minute cloud decision image.) This image consists of a subset of rows and columns, each saved at full resolution (i.e. we save 33 rows, and 33 columns, for 33 x 512 + 33 x 480 resolution). Thus for cloud free arc length statistics, we have full resolution, but for cloud areal statistics such as cloud cover, we have reduced resolution in the one minute data. Our early studies indicated an uncertainty of approximately a 1% in the cloud cover computed from the one minute data as compared with the ten minute full resolution data.

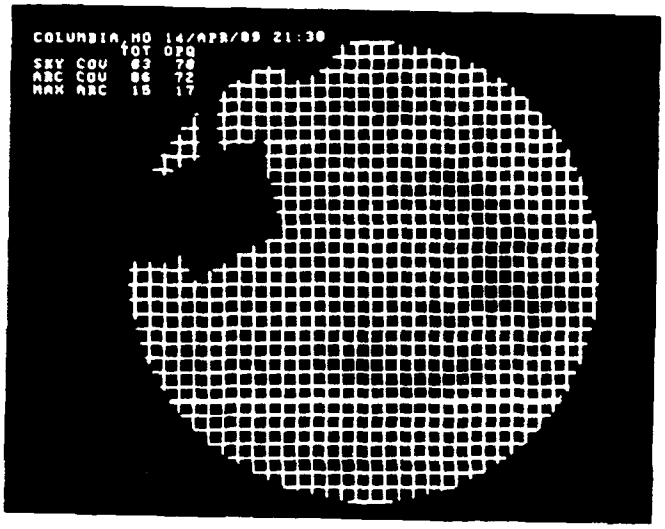

Fig. 2-4. Sample One-Minute Cloud/No cloud Decision Image. This shows the subset saved 1 minute intervals.

In summary, the Whole Sky Imager is a system for cloud assessment, specifically for the archival of cloud field spatial and temporal dynamics. The WSI acquires calibrated multi-spectral sky radiances every minute. From these, automatic cloud determinations are produced with 1/3 degree spatial resolution. The system was originally deployed at 7 sites throughout the country, illustrated in Fig. 2-5 and as of 1 Jan 91, had acquired an average of 26 months of data per site. The data will be further discussed in Section 3.

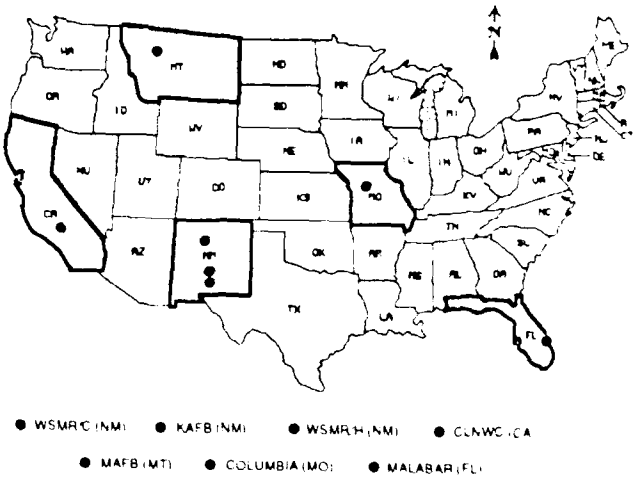

Fig. 2-5. Whole Sky Imager data sites

2.2 The Portable WSI

The portable WSI unit is shown in Fig. 2-6. This unit, designed for short term deployments and/or special applications, is similar to the WSI, but has a more transportable support and environmental control housing. The portable system was initially installed at the University

of Wisconsin, for a cooperative study with Eloranta and Grund, using their High Spectral Resolution Lidar (HSRL) lidar system. The intent was to acess techniques to relate the WSI cloud determinations to the cloud optical depth determined by the lidar system.

Fig. 2-6. Portable Whole Sky Imager

2.3 Supporting Instrumentation

The WSI cloud data base is stored in digital format on 8mm video tape cassettes (Sony P6-120MP, NTSC). These small cassettes, when used with the EXABYTE 8200 streaming tape sub-system, can hold up to 2.2 Gigabytes of digital information each. All WSI data manipulations conducted at MPL are built around this small compact tape system under the control of an IBM/AT class microcomputer. All software is MS-DOS compatible, and is generally written in either FORTRAN or C programming language.

The basic hardware configuration required for WSI image processing is essentially the same as that required for the initial acquisition. That is, a system able to read the 8mm data tapes, an image processing system able to handle the 512 X 480 pixel image format, and a host computer suitable for overall control. At MPL, the data acquisition system shown in Fig. 2-7 is also appropriate for all subsequent image processing tasks. For bulk processing, however, the basic computer unit is supplemented with an Eighteen Eight Labs PL1250 floating point array processor to accelerate the system throughput, and dual EXABYTE drives are attached to each control computer. The complete WSI system is illustrated in Fig. 2-6, which combines the photographic description with the basic system block diagram.

3.0 THE WSI IMAGE DATA BASE

The WSI cloud data base was acquired primarily to provide a reliably calibrated, computer friendly image library that could be used in a variety of model validation and model development activities. Of specific interest was its applicability to the generation of joint multi-site cloud free line of sight (CFLOS) and cloud free arc (CFARC) probabilities. This interest was in turn driven by concerns related to CFLOS/CFARC impacts upon ground based laser (GBL) applications. Within this context, it was important that the imagery within the data base provide computer access to a "micro-climatology" of cloud field characteristics, well defined in space and time, and at relatively high spatial and temporal resolutions. The fully automatic WSI system provided this acquisition capability.

3.1 Background

As can be deduced from the entries in Table 3.1, not all field systems produced equal shares of the resultant data base. On average, field system downtimes were at about a 20% rate, ranging from a low of about 14% at the Columbia NWS site to an unfortunate high of about 28% at the China Lake NWC site. For the most part, the no-data intervals at China Lake were due to power outages that exceeded the capacity of the WSI back-up battery pack. Early in the data collection interval, continuing problems related to the 8mm tape subsystem and the video frame grabber were experienced. Both problems were eventually resolved by retro-fitting additional cooling and air filtering capacity to the interior computer housing. Air conditioner failures in the external housing were a continuing irritation at the high humidity sites, leading to their eventual replacement with a chilled liquid coolant system. The efficacy of these basic system upgrades was reflected in the average months per maintenance visit which improved from an early two to three month average interval to a four to five month interval during the later portions of the program.

3.2 Current Extent of the Data Base

The Whole Sky Imager (WSI) data network, while fully implemented, consisted of seven independently operating, fully automatic electronic camera systems. Each system collected whole sky imagery for twelve hours a day, seven days a week. Each resultant weekly data tape currently in archive contains up to 1200 megabytes of image data, plus around 200 megabytes of housekeeping space. Thus, at the end of the data collection interval 31 Dec 90, the WSI cloud data base contained approximately 900 Gigabytes of raw image data. About 675 Gigabytes of these data have been processed through varying portions of the sequence discussed in Section 4. The data quantities are substantial, and have required carefully conceived and efficiently executed

Table 3.1

WSI DATA TAPE STATUS AS OF 31 JANUARY 1991								
		C-STA 30 MAR 88	HELSTF 29 MAR 88	KIRTLAND 17 MAY 88	CHINA LAKE 23 JUN 88	MALMSTROM 29 AUG 88	MALABAR 18 NOV 88	COLUMBIA 9 FEB 89
A	TOTAL DAYS IN FIELD	995	1008	953	897	478	735	691
B	TOTAL DAYS OF DATA	763	819	749	641	406	602	592
C	TOTAL FULL DATA DAYS (12 HR)	652	623	607	453	332	515	561
D	TOTAL PARTIAL DATA DAYS	111	196	142	188	74	87	31
E	TOTAL DAYS DOWN (NO DATA)	232	189	204	256	78	133	99
	DATE WITHDRAWN FROM SERVICE	19 Dec 90	31 Dec 90	25 Dec 90	6 Dec 90	20 Dec 89	19 Nov 90	31 Dec 90
	A = B + E B = C + D							

processing procedures to insure optimum downstream utilization. Elements of these procedures are summarized in Section 4.0.

The WSI cloud data base presently resides in the custody of the Marine Physical Laboratory (MPL), Scripps Institution of Oceanography, San Diego, CA, 92093. As of 1 Jan 91, imagery representing 4614 days, geographically distributed as shown in Table 3.1 and Fig. 3-1 have been collected and returned to MPL for processing and analysis. A reasonable estimate is that these raw data reside on approximately 900 data tapes.

The preparation of these 900 raw data tapes plus their appropriate output products with the procedural documentation deemed necessary for subsequent usages is essentially the task outlined in Section 4.0.

It should be noted that these data quantities do not include several relatively small case study sets collected by the portable system. The data listed in Table 3.1 and discussed in this report are only those associated with the multi-station network sponsored under Air Force contract F19628-88-C-0005. An inventory of the complete WSI Image Database, segregated by site, date and archival tape number is included as Appendix A. The data in Appendix A have been reviewed in accordance with our established QC procedures, and have been purged of all sets deemed inappropriate for further application. The material included in Appendix A has been previously released as Optical Systems Group, Technical Note No. 228, M. L. Ciandro, 1991.

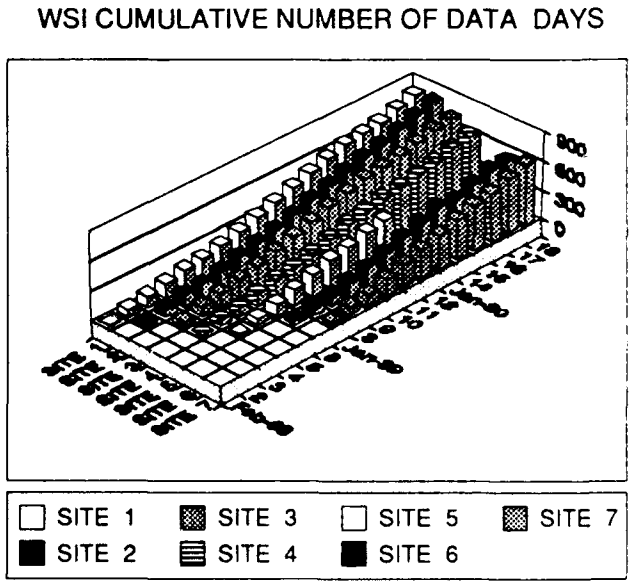

Fig. 3-1

4.0 DATA PROCESSING PROCEDURES

The general concept guiding the post-acquisition processing of the WSI data base is illustrated in Fig. 4-1, "WSI BASIC IMAGE PROCESSING FLOW CHART". This conceptual game plan is implemented through a series of proprietary software routines designed to impose strict quality and calibration controls upon the raw data, while simultaneously reducing the number of images required for insertion into the optimized cloud/no cloud decision processes. Carried to its nominal conclusion, this processing plan reduces the basic imagery (that

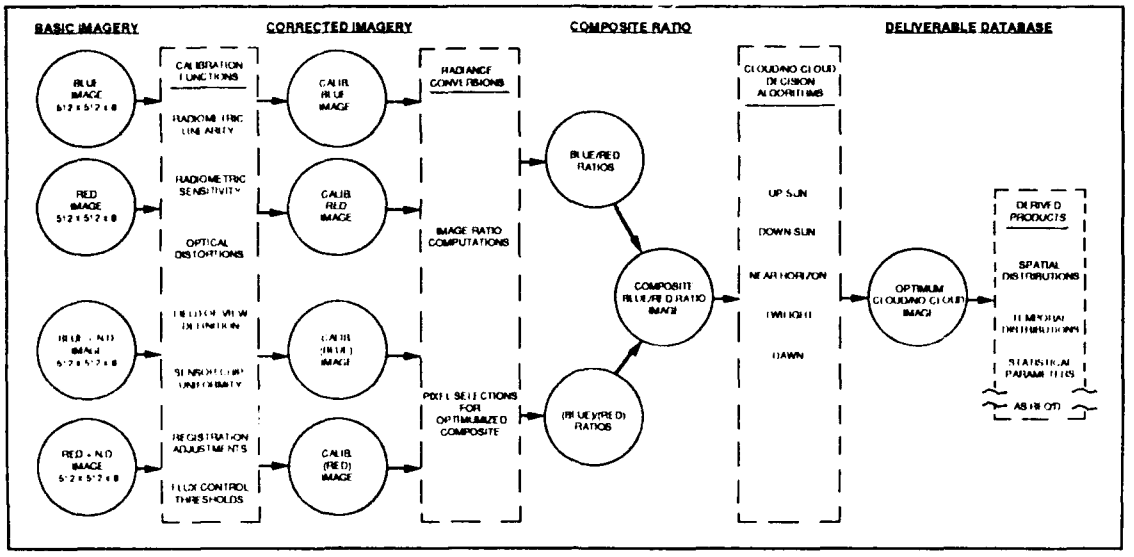

Fig. 4-1. WSI Basic Image Processing Flow Chart

created by each camera in the system) to about one fourth of its original volume at the composite ratio stage and then, if desired, by an additional increment depending upon the output format specified by the user of the derived products. The cloud/no cloud images are created at the same eight bit resolution as are the raw radiance and composite ratio images.

4.1 Data Processing Procedural Sequence

With the basic data tapes in hand, the processing hardware and software on-line, and the data base management system implemented, one can address the stepwise manipulation of all component elements from raw tape to delivered end product. In the following paragraphs this stepwise process will be described on the basis of a single data tapes sequential manipulation, and from this unit tape estimate, the overall program time estimates will be produced.

In assessing the following estimates of the processing times associated with each procedural sequence, one should be aware that throughput times are often heavily influenced by different machine/software interfaces even when determined on systems containing nominally "identical" hardware and code versions. With this caveat in mind, the estimates included herein and indicated on Fig. 4-2, were derived from actual full length processing episodes running in the hardware/software configuration listed in Table 4.1.

4.2 Data Processing Run Time Estimates

Processing the complete stepwise procedure required to convert a field tape containing seven days of raw unedited cloud imagery into a fully processed tape containing the same seven days of data in the form of cloud-no cloud imagery is illustrated in Fig. 4-2, and the run-time summary for both machine time and supporting analyst time is shown in Table 4.2.

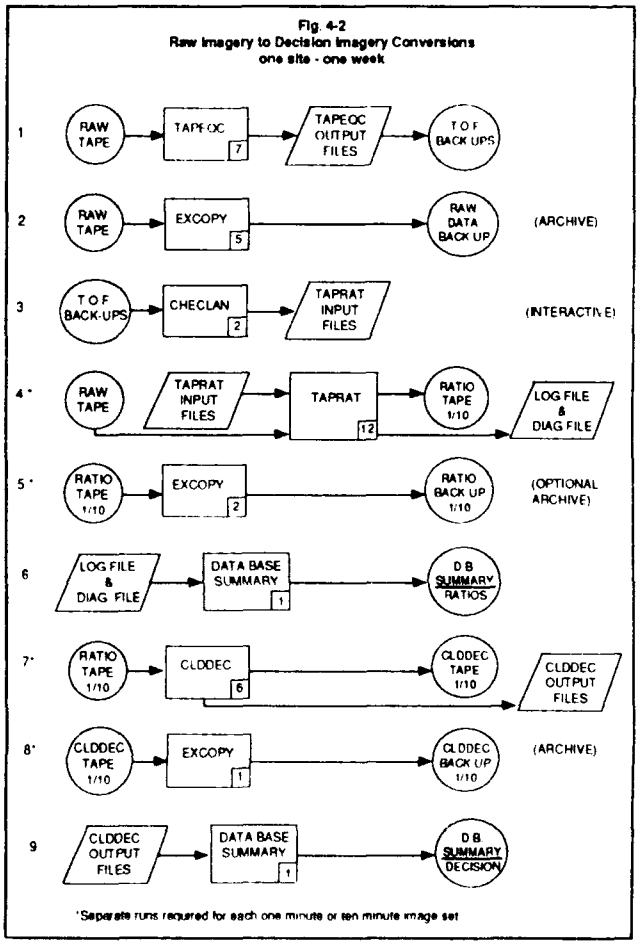

Table 4.1
WSI Standard Data Processing Configurations

HARDWARE		SOFTWARE	
TMI Model 2001A Computer		Proprietary Software Programs	
1. 80386	CPU	1. TAPEQC,	Version xxx
2. 80387	Co Processor	2. EXCOPY,	Version xxx
3. PL 1250	Array Processor	3. TAPRAT,	Version xxx
4. ASC-88	SCSI Interface	4. CLDDEC,	Version xxx
5. EXABYTE 8200, 2 ea w/ 4 S25 PROM			
6. Seagate 60 MB Hard Disc			

Table 4.2
Raw to Decision Conversions
Run Time Summary

Sequence No.	Machine Hours			Analyst Hours
(From Fig. 4-2)	Primary	File Copy	Total	Housekeeping &Oversight
1	7	2	9	2
2	5	.5	5.5	0.5
3	2	.5	2.5	2.5
4*	12+12	.5+.5	25	0.5+0.5
5*	2+2	.2+.2	4.4	0.5+0.5
6	1	.2	1.2	0.5
7*	6+6	.5+.5	13	0.5+0.5
8*	1+1	.2+.2	2.4	0.5+0.5
9	1	.2	1.2	0.5
Totals 1+10	58	6.2	64.2	10
1 or 10	37	4.8	41.8	8

* Separate runs required for each one minute or ten minute image set.
Times indicated are based upon "clean" runs without appreciable software or hardware glitches.

In estimating the overall processing task, as outlined in Fig. 4-2 & Table 4.2, it is important to note that the totals shown in Table 4.2 are really for best effort data "processing" only. They do not include the very substantial effort which is heavily related to "housekeeping and oversight", but which is more specifically oriented toward on-line data "interpretation and analysis" (I&A).. Nor do they include the more stylized but highly important implementation and maintenance of the appropriate Data Base Management functions.

The Table 4.2 comment related to "clean" runs is a comment ignored at extreme peril. One must keep in mind that all of WSI field systems were monitored by on-site host personnel with widely varying degrees of technical background and program related interests. Not all received the imposition of the WSI system into their daily routines with equal exuberance. The vagaries of local weather extremes, power fluctuations, hardware faults and conflicting on-site priorities all contributed to sometimes substantial variations in the normally full automatic mode that the WSI attempted to maintain. With this "real-world" context in mind, it is easy to visualize the nature of the on-line data interpretation and analysis that must accompany the more formalized data "processing" outlined in Fig. 4-2.

The primary tools employed by the analyst to diagnose and sanitize those raw data tapes which fail either their initial TAPEQC runs, or their subsequent TAPRAT runs, are the regularly produced TAPEQC output files, the Local Apparent Noon (LAN) image files, and the raw data tapes themselves, all in concert with the analysts highly honed understanding of the WSI hardware and software operating regimes. These diagnostic skills are not readily transferable and they are absolutely essential to the orderly and efficient data flow shown in Fig. 4-2.

Some estimate of the additional machine time required to support the "interpretation and analysis" (I/A) function plus the attendant requirement for data re-runs should be provided as part of the overall task definition. As a first approximation, one finds about 7% of the data designated as special handling. During the first quarter of calendar 1990, an estimated 10% of the accumulated data runs were repeated due to specific I/A decisions and another 10% were re-run due to miscellaneous hardware peculiarities, primarily EXABYTE incompatibilities. Thus one might assume a worst case requirement for up to 27% of miscellaneous re-runs, however as "production line" processing settles down, a 10 to 15% re-run estimate seems more reasonable.

Descriptive summaries of the software programs shown in Fig. 4-2, and their primary sub-routines are contained in Appendix B. Program listings and additional illustrative materials as are required by the Contract Data Requirements List are provided under separate cover

4.3 Data Processing Status

As noted in Section 3.1, there are approximately 900 raw data tapes currently in archive status, representing over 4600 separate data days. Some of these data tapes have been processed through all of the sequences illustrated in Fig. 4-2, however the majority have been through steps one and two only. An illustration of the data base

status as of 30 Sep 91 is shown in Fig. 4-3. A slightly more detailed representation broken down by major software program is shown in Table 4.3.

Table 4.3
Processed Data Tape Summary

Data Station	Raw Data Tapes	Major Software Programs					
		TAPEQC	CHECKLAN	TAPRAT 1	TAPRAT 10	CLD DEC 1	CMP DEC 10
C-Sta	190	190	70	70	70	70	70
Helstf	166	166		0			
Kirtland	142	142	69	69	69	69	69
China Lake	135	135		0			
Malmstrom	71	71	32	32	32	32	32
Malabar	104	104	27	27	27	27	27
Columbia	95	95	59	59	60	59	60
Totals	903	903	257	257	258	257	258

The processing sequence illustrated in Fig. 4-1 is descriptive of the preliminary run sequence used during the mid-1990 processing of the "one-minute" data subset. The output product for this preliminary sequence is a data base containing derived cloud/no cloud images based upon a fixed threshold decision algorithm (Apr. '90).

A major activity during late 1990 and early 1991 has been the development of an improved cloud decision algorithm. This effort has produced a new composite decision program called CMPDEC. The algorithm improves the thin cloud discrimination by correcting for aerosol scattering processes, as described in Section 5. The method is particularly effective at reducing the overdetermination of thin cloud found in regions near the sun and close to the horizon that was made by the earlier fixed threshold algorithm.

CMPDEC was used in place of CLDDEC in the processing of the "ten-minute" data sub-sets. Fig. 4-2 and Tables 4.1 and 4.3 are still valid if this substitution is recognized.

4.4 An Alternative Product: Calibrated Radiance

An alternative procedure involves the modification of the Fig. 4-2 sequence to generate calibrated radiance imagery, either in addition to or in lieu of the cloud/no cloud imagery. This sequence modification is not trivial since the calibrated radiance imagery is not normally held intact in image memory, but for maximum computational throughput is used piecemeal and not retained once the ratio computations are complete. An estimated time estimate for implementing this alternative can also be deduced from the estimates in Fig. 4-2.

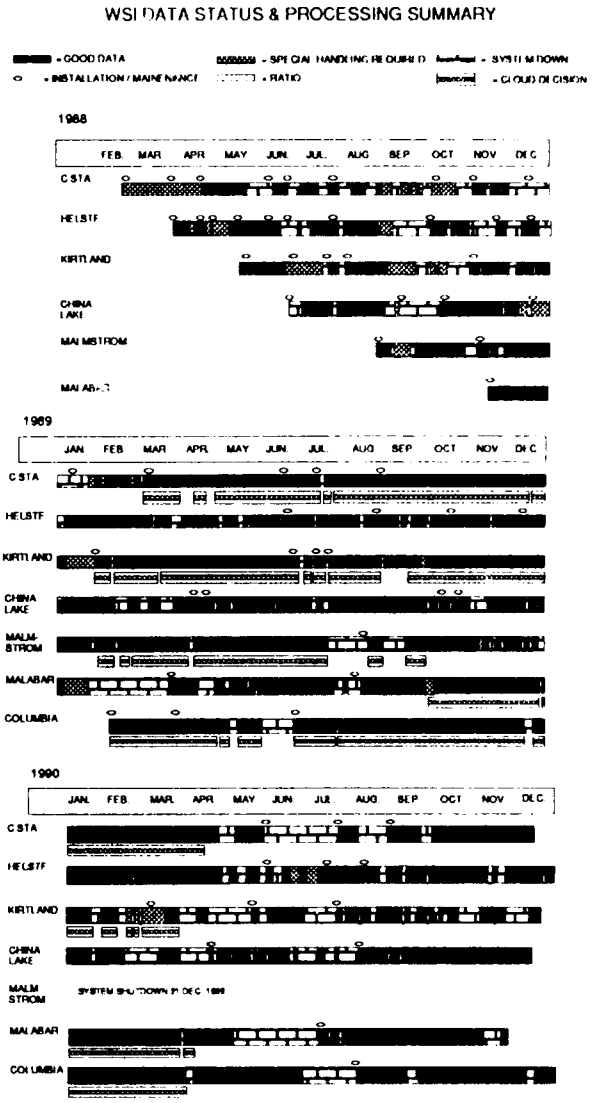

Fig. 4-3

Modifying the processing sequence shown in Fig.4-2 to produce output tapes of calibrated radiance imagery has not yet been implemented, but does not represent a major programming effort provided one makes a clean interrupt at the point of insertion within the software program TAPRAT. There will be however, changes to the logical flow within the program which may result in substantial increases in processing times. In any case, the creation of a calibrated radiance library would procedurally involve the re-running of modified steps 4, 5, & 6 shown in Fig. 4-2. These modifications would be of the form shown in Fig. 4-4, with programs ABSRAD and SELECT representing the necessary new code.

Since the absolute radiance values which are desired as output reside temporarily within the existing sequence, and their accumulation should be reasonably simple, the

machine time necessary to execute the ABSRAD task should represent a relatively short interval. A reasonable first approximation for the ABSRAD execution time is its being equivalent to or less than the CLDDEC runs. To the degree with which this approximation is true, then the incremental effort to execute the sequence shown in Fig. 4-4 can be estimated.

Fig. 4-4

Raw Imagery to Calibrated Radiance Data

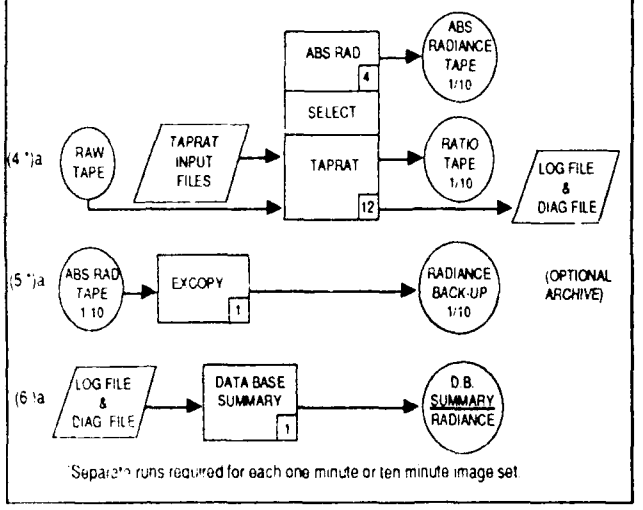

*Separate runs required for each one minute or ten minute image set

Assuming a clean insertion, it is reasonable to assume approximately 3 man-mo to code, test and debug the ABSRAD & SELECT software. Housekeeping and Oversight (H/O) analyst hours required for processing should not exceed the TAPRAT rate, nor should the I/A time. Thus an estimate of around 4 analyst-hours per radiance tape, about half the TAPRAT rate, seems reasonable.

Rerunning the nominal 100 raw data tapes through the SELECT/ABSRAD sequence represents an incremental increase of 600 machine hours and 400 analyst-hours (approximately 1.0 system-mo. and 2.3 analyst-mo.). An estimated incremental cost for implementing this alternative processing sequence is readily determinable.

5.0 THE AUTOMATED CLOUD DECISION ALGORITHMS

This section discusses the methods used to convert the WSI images to quantitative decisions regarding cloud cover. Whereas it is relatively straightforward to acquire WSI images which are pleasing and readily interpretable to the human user, the task of acquiring imagery which may be automatically assessed through image processing techniques is more demanding. Requiring that these image processing techniques be both fast and autonomous is also an important consideration. This section discusses first the acquisition and processing of the data to yield the ratio images, and then the cloud algorithms used to yield the cloud decision images.

5.1 Raw Data Characteristics

The CID (Charge Injection Device) sensor has a number of characteristics which are advantageous in acquiring full sky imagery. Most importantly is the fixed gain, allowing the measured signal to be directly related to the sky radiance for a given filter and aperture setting. The sensors also have very low blooming, so that even if a portion of the scene is significantly offscale bright, other portions of the scene are not corrupted radiometrically. The noise is also reasonably low, typically 2 counts on a scale of 0 to 255, in a reasonably new camera.

The sensors are somewhat limited in sensitivity range. We did not wish to use signals below 20 counts, where the least count change of 1 becomes a significant fraction of the signal. With this limitation, the overall sensitivity range is somewhat over 1 log (a factor of 10). Even with the sun filtered by a 4 log neutral density filter in the sun occultor, the radiance range of the upper hemisphere is larger than 1 log. For this reason, two pairs of filters were used: one set to acquire the darkest parts of the sky on scale, and the other buffered by a .5 log neutral density filter that puts the brighter portion on scale. (An offset of .5 log was chosen, rather than 1 log, to give a region of overlap to be used for accuracy assessment.) Thus the spectral filter wheel held a blue filter centered at 450 nm, a red at 650 nm, a blue with .5 log offset, and a red with .5 log offset.

The sensor package also included a neutral density filter wheel, to allow the sensor to adjust to the changing light levels during the day. Each minute, the system acquired images in the four neutral density positions, and made a decision regarding which filter to use for the next data acquisition. The flux control algorithm was designed to keep the minimum flux level above 40 counts. If there was insufficient radiant energy in the open hole (no attenuation) position, the aperture was automatically opened, in increments of 1/2 stop. The aperture was kept at f/16 when possible, however, to optimize the image quality by maximizing the depth of focus. (The depth of field with this system is essentially infinite, with both clouds and the bolts holding on the protective dome in focus. However, the analogous depth of focus at the image plane was quite low, resulting in defocusing near the edge of the image if the aperture was fully open.)

Following data acquisition, the data tapes were processed through a quality control program, which verified

that data were onscale, and that the signals in the corners of the imager's active area which are outside the optical image were dark, noise free, and balanced (i.e. no significant bias from left to right or top to bottom). The program also verified that all four spectral images were acquired, the flux control sequence was completed successfully, and no times were skipped. Any such problems were noted, so that systems could be repaired as necessary and special processing requirements could be addressed.

5.2 Processing to the Ratio Stage

Prior to the automated ratio processing, the data were checked in several additional respects. Images were evaluated to determine whether the clock time was correct, based on expected vs actual sun position, and to determine whether the occultor arm was properly aligned with respect to its readout. Special problems such as debris on the protective dome or use of an incorrect occultor arm are noted Any of these special considerations are noted digitally in an input file. Abnormalities such as time errors were corrected; others such as debris on the dome could not be corrected, but they were noted in the header of the ratio tape and thence the cloud tape, to make users aware of the anticipated data quality.

The first step in the ratio processing involves the linearity calibration. Whereas the camera signal is approximately linear with respect to the input flux, this calibration measures the response more precisely. The linearity correction is quite fast using a look up table (firmware on the image processing board), which replaces each measured signal with the corrected signal which is linearly related to the flux. The calibration is normally acquired prior to fielding the system, and the look up table is computed by a program designed to process the linearity calibration data.

Next, if the signals have a value less than 20 counts out of 255, the ratio is assigned a value of 0. This 0 value represents regions external to the optical image, and any other regions which may be offscale dark. For those picture elements (pixels) which are onscale, the ratio is computed from the equation

$$\text{Ratio} = 128 * \text{SPR} * \text{Radiance}(2)/\text{Radiance}(1) \quad (5.1)$$

The constants in this equation will be discussed below. For those pixels which are offscale bright in filter 1 or 2 (blue or red), the ratio must be computed using filters 3 and 4 (blue and red with offset), with the following equation.

$$\text{Ratio} = 128 * \text{SPR} * \text{NDR} * \text{Radiance}(4)/\text{Radiance}(3) \quad (5.2)$$

This creates a composite image, using the 2/1 pair at darker pixel locations, and the 4/3 pair at brighter pixel locations. Those pixels which are offscale bright in filter 3 or 4 are so indicated with a specific byte value in the ratio image and later in the cloud decision image.

In the above equations, the SPR is the spectral ratio, which corrects for the small differences in the passband of the red and blue filter (both nominally 70 nm), as well as the differences in the sensitivity of the CID at 450 and 650. The NDR is the neutral density ratio, which corrects for the small error induced by the fact that the .5 log offset filter is not quite neutral, and also corrects for differences between the 3,4 passbands in comparison with the 1,2 passbands. Both the SPR and the NDR ratios are normally determined from absolute calibrations, and verified or adjusted using the field data. The neutral density filters used for flux control are also slightly spectrally selective; the correction for this is included in the SPR and NDR terms. For this reason the SPR and NDR factors are dependent on the neutral density filter selected during flux control, and may therefore vary from image to image.

The above steps also include a correction for image size. Rather than ratioing the same pixels on the active array in image space, the program takes into account the size and placement of the optical image on the sensor array so that it ratios the pixels which are at the same look angle in object space. For example, if one imager is set up so that the optical image is offset 10 pixels to the right of the center of the active array, the radiance pixels 10 to the right of center will be placed at the center in the computed ratio image. Thus all imagers are corrected to a standard size and location. The exact placement of the radiance images vary somewhat from system to system, and also from filter to filter due to a 2% size difference between the red and blue images. Thus the image size correction is both system and filter dependent.

In the above equations, the choice of the 128 multiplier, and the choice to use red/blue rather than blue/red, were driven by several considerations. The equation should map the theoretically possible range of ratios into the 0 - 255 byte value range; a change of 1 in output byte value should correspond to roughly the same change in cloud density independently of cloud brightness; measurement noise should not be overly amplified in the ratio image; yet radiometric resolution in the radiance image should not be lost in converting to the ratio image.

The next step in the ratio computation is the overlay of the mask. Those pixels which should be obscured by the occultor, as well as any which are obscured by objects in

the field of view (primarily at the Columbia site) are set to a value of 0. Thus they are treated as "no data", just as the offscale dark values are. Following this step, the data are smoothed with a 3 x 3 kernal, to moderate the effects of system noise.

Finally, the data are written to tape, along with a header which contains identifying information regarding the data, its quality, and its processing. The filter 4 red image is also written to tape, to provide a means to evaluate the efficacy of the ratio and the cloud decision process.

In the resulting ratio image, the clear sky has a lower value than the clouds. Most of the variance in the clear sky radiance has been removed through ratioing, although the ratio is still higher in the aureole and near the horizon. Essentially, the brightness variation caused by changes in the scattering angle and changes in the optical depth of the path (such as near the horizon) have been removed. But color variation caused by differences between the Mie scattering properties at 450 and at 650 nm have not been removed. The opaque clouds have significantly higher ratios than the clear sky ratios in general. Grey storm clouds, even those darker than the adjoining sky, are also characterized by high ratios.

5.3 Geometric Calibration of the Images

Both the ratio images and the cloud decision images generated in the next stage of processing have been corrected to the standard image size and placement. The identification of the look angle associated with a given pixel location is then the same for all sites. To a first approximation, the fractional distance of a pixel to the edge of the image is linearly related to the zenith angle of the path of sight associated with the pixel. A more precise calibration has yielded a parabolic fit of the relation between this fractional distance on the image plane and the zenith angle. The result is the following equations, which give the zenith and azimuth angles as a function of pixel position.

$$\theta = 585\left(1-\sqrt{1-.001128\,R}\right) \tag{5.3}$$

$$\phi = \tan^{-1}\left[\frac{1.25(x-255)}{(y-240)}\right] \tag{5.4}$$

where

$$R = \sqrt{[1.25(x-255)]^2+(y-240)^2} \tag{5.5}$$

The inverse equations, for obtaining the pixel position for a given angular position, are

$$x = 255 + 0.8R\sin\phi \tag{5.6}$$

$$y = 240 + R\cos\phi \tag{5.7}$$

where r is now defined in terms of θ, by

$$R = \theta\,(3.032 - 0.00259\,\theta) \tag{5.8}$$

If the angular relation were truly linear, such that r were proportional to θ, where r is the fractional distance to the radius, then the solid angle seen by the pixel would be related to the area of the pixel by the following proportionality.

$$\frac{d\Omega}{dA} \alpha \frac{\sin\theta}{\theta} \tag{5.9}$$

With the parabolic relation, this proportionality becomes

$$\frac{d\Omega}{dA} \alpha \frac{\sin\theta}{\theta}\left[(3.032-0.00259\,\theta)(3.032-0.00518\,\theta)\right]^{-1} \tag{5.10}$$

An estimate of cloud cover may be obtained by counting the number of cloud vs no cloud pixels. It is more accurate to weight each pixel by $d\Omega/dA$, however it can be shown that the maximum error in the total sky cover which occurs from ignoring this weighting function is approximately 2.1%. For most purposes, this weighting correction is not necessary.

5.4 Fixed Threshold Algorithms

As previously noted, two automated cloud discrimination algorithms were developed. The fixed threshold algorithm (CLDDEC) was used in the 1-min cloud decision processing, while the more complicated composite fixed-variable threshold algorithm (CMPDEC) performed the 10-min decision. Descriptions of these two techniques were presented by Koehler, et al (1991) at the CIDOS-91 conference.

The simplest ratio cloud decision algorithm assigns a certain sky state to fixed ranges of ratio value. In our application, we want to discriminate between clear sky, thin cloud and opaque cloud. Two values, the thin and opaque thresholds, need to be defined. All pixels with a red/blue ratio exceeding the opaque threshold are then assumed opaque cloud. Those pixels with ratios between the thresholds are assumed thin cloud cover. Finally, those pixels with ratios below the thin threshold are assumed clear.

The fixed threshold algorithm does a reasonable job in defining opaque cloud, but in many circumstances fails to properly distinguish the true thin-clear boundary. This problem is illustrated in the example shown in Fig. 5-1. Two contrails are evident in this image: a denser one oriented roughly from top to bottom, and a narrower one angling from the upper left to the lower right. The region just below the solar occultor is brighter than other parts of the image due to its proximity to the sun's aureole, but should probably be classified as clear. Figure 5-2 shows two different thin threshold slices through the same ratio image. The cloud decision with a thin threshold of 120 fails to identify significant parts of the contrails. When the thin threshold is brought down to 70 to bring out the remainder of the contrails, the clear regions near the occultor and the horizon are misidentified as thin cloud. This occurs because the clear sky ratio background is not constant. The sky appears lighter blue near the horizon and near the sun than it appears in the downsun direction. Thus, a thin cloud in the downsun part of the sky may actually have a smaller ratio than clear sky near the sun or horizon. An improved algorithm would have to take this sky background variation into account.

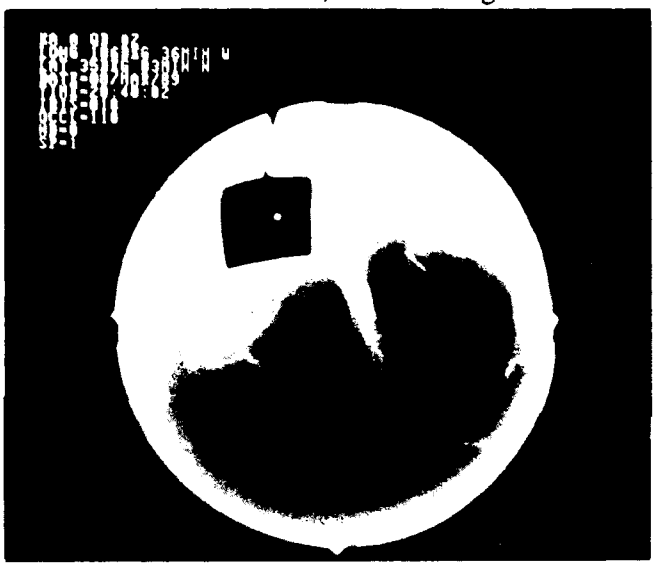

Fig. 5-1. WSI 650 nm radiance image from Kirtland AFB, 8 March 1989

5.5 Variable Threshold Algorithm

Several similar contrail cases were studied in an effort to determine the relationship between thin clouds and their background sky conditions. We found that the ratio of thin cloud red/blue radiance ratio to the clear sky background red/blue radiance ratio remains fairly constant along sections of contrails exhibiting uniform optical properties. If the clear sky background ratio were known, a thin cloud discrimination could then be based on whether the observed ratio exceeds the background ratio, and the degree of "thinness" could be estimated by the observed/background ratio. The thin cloud decision "problem" then becomes one of determining a reasonable estimate of the clear sky background ratio.

The red/blue clear sky ratio distribution is influenced by many factors the most important of which are the solar zenith angle, and the haze features of the atmospheric boundary layer. Figure 5-3 shows the variation of the ratio distribution as a function of solar zenith angle. Note how the clear sky background "whitens" (the ratio increases) as the sun approaches the horizon. Figure 5-4 illustrates the boundary layer haze influence, with the pristine February arctic air mass yielding "bluer" ratios than the haze laden air mass from July.

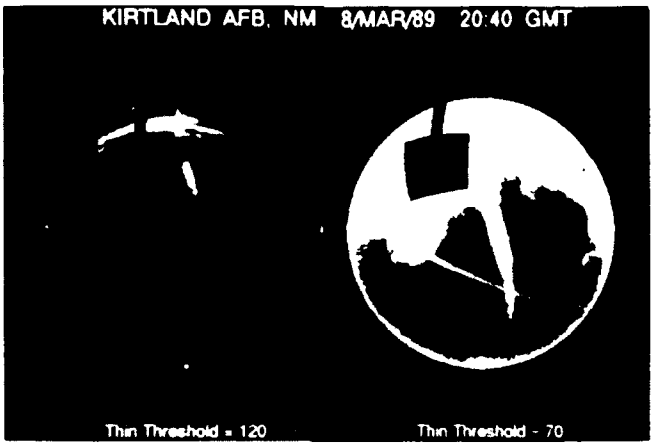

Fig. 5-2. Fixed threshold cloud decisions with two different thin cloud thresholds. Lighter shades indicate cloud, darker indicate clear sky.

Our new cloud decision algorithm uses clear sky background fields derived from clear day observations. The haze effect is normalized by dividing the image by the reference red/blue ratio from the intersections between the 45° look zenith circle, and the locus of points separated by a 45° scattering angle from the sun. The effect of the normalization is shown in Figure 5-5. In practice, a set of normalized clear sky ratio tables are extracted from many clear days at a specified site for each 5° solar zenith angle. The table consists of normalized ratios at 5° look zenith intervals from 0 to 75°, and azimuths relative to the solar azimuth at 15° intervals. Tables for each solar zenith angle set are then averaged together to provide the best normalized clear sky estimate.

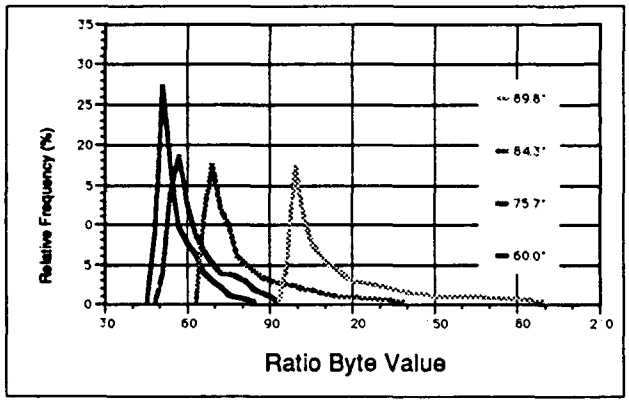

Fig. 5-3. Clear Sky Solar Zenith Angle Dependence: 11/Feb/89 - Columbia, MO

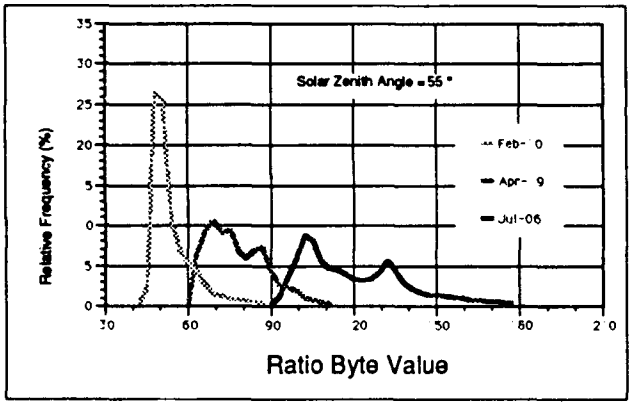

Fig. 5-4. Clear Sky Haze Layer Dependence: Columbia, MO, 1989

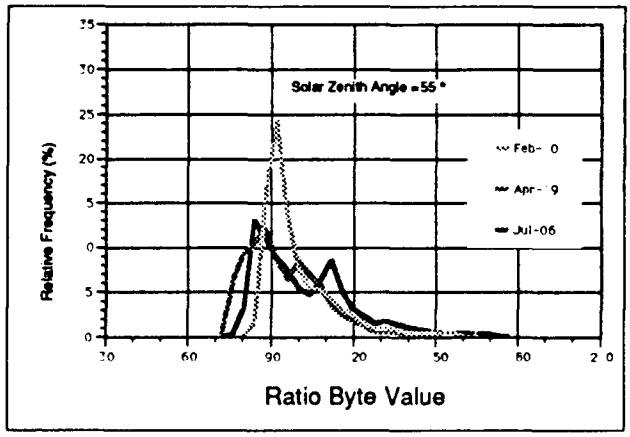

Fig. 5-5. Clear Sky Normalized to Minimize Haze Layer Dependence: Columbia, MO, 1989

In the cloud decision algorithm, the clear sky background for a particular image is determined as follows. First, the solar zenith angle is determined for the date, time and site location of the observation. A linear interpolation is then made between the two closest solar zenith angle tables to estimate the normalized background table for the image. Given the zenith and relative azimuth of a particular pixel in the image, its normalized clear sky ratio estimate is then computed by bilinear interpolation of the table values. This normalized value is then multiplied by a reference ratio value determined from an interactive procedure that examines the reference value variation for that day and time.

The cloud decision is then made by comparing the observed ratio to the fixed opaque threshold, and the clear sky ratio estimate. The pixel is then given a numerical value that defines whether it is categorized as clear, thin cloud, opaque cloud, obscured from view, or indeterminate. This last category occurs when the clear sky ratio estimate exceeds the opaque cloud threshold. The cloud decision image from the new algorithm for the contrail case is shown in Figure 5-6. Note how the contrails are identified without misidentifying the points near the sun and horizon.

Fig. 5-6. Variable threshold cloud decision image

In the resulting cloud decision image, those points identified in the ratio process as "no data", offscale

bright, or indeterminate, are identified by specific byte value. The indeterminate category represents cases where the clear ratio estimate exceeds the opaque threshold due to the presence of thick haze. This is analogous to the case when the observer cannot visually distinguish the white cloud in the haze.

The clear, thin, and opaque cloud identifications are each given a specific range of values in the cloud decision image, i.e. clear = 1 to 99, thin = 100 to 139, and opaque = 140 to 200. In the clear and opaque categories, the variance in the final representation is proportional to the ratio. But in the thin category, the variance is related to the perturbation of the ratio with respect to the sky background ratio, and thus related to the optical depth of the thin cloud.

This approach was used to satisfy two needs. If it is desired to simply count the number of pixels in the various categories such as clear or opaque, this may be done unambiguously. Yet the variance within each category is retained, so that the image can be false color displayed with its texture retained, and so that the cloud image may be reprocessed to investigate the effect of different threshold selections. The specific rules used in the cloud decision image format are given in Appendix B.

It should also be noted that the cloud decision images include headers, much like those used in the ratio images, which give information on the data, its quality, and its processing.

5.6 Data Base Processing with the New Algorithm

The new variable threshold, directionally-dependent algorithm has been used to process the 10-minute, cloud decision. The results are encouraging. The more reliable definition of thin cloud illustrated in the contrail example is the rule, not the exception. A measure of this improvement is shown in Figure 5-7. This figure illustrates the tenths of total sky cover category differences between the WSI and the human observer at Columbia from the 14-month sample. (For example, if the WSI detects 50% cloud cover and the observer 60%, this is a -1 category difference.)Values from both the old, fixed threshold, and new, variable threshold algorithms are shown. The new algorithm shows better agreement with the human observer. This comparison only indicates cases where the improvement was due to changing the WSI total sky cover amount. In many cases, the total sky cover did not change but the spatial distribution of that percentage improved.

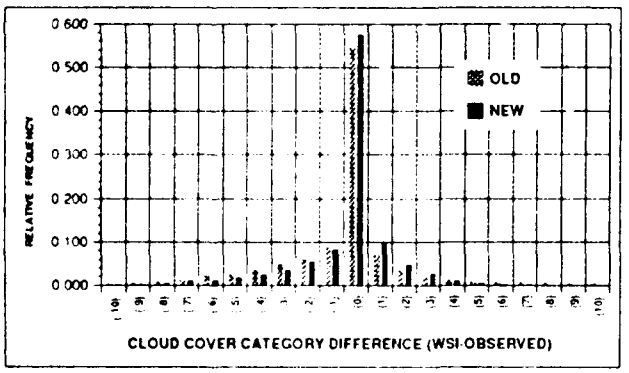

Fig. 5-7. Total Cloud Cover:
Columbia, MO 9 Feb 89 - 28 Mar 90

6.0 DATA BASE APPLICATIONS

It is a well accepted truism that as more and more vital elements of our national defense become increasingly sophisticated, they also become increasingly sensitive to the influences imposed upon them by their surrounding operational environment. This fact is nowhere more clearly illustrated than in the arena of electro-optical system performances in turbid, cloudy atmospheres where cloud attenuation of the sensor/target path of sight can result in the complete and near instantaneous negation of system performance. It is therefore only prudent that intense and innovative research into the development of techniques for the assessment and prediction of appropriate cloud population characteristics and cloud field dynamics, particularly at small spatial and temporal scales, be actively pursued.

The WSI image oriented data base, by virtue of its relatively high spatial and temporal resolution, is particularly appropriate for applications associated with the acquisition and tracking of earth orbiting devices. The statistical characterization of local cloud effects upon earth to space optical communication links is, of course, the reason the automatic multi-station data collection network was originally established. The generalized output product from this network, the temporally varying pixel by pixel definition of cloud thickness throughout the observable sky dome is directly applicable to all cloud free line of sight (CFLOS) and cloud free arc (CFARC) determinations either as real time operational support products, or as statistically predictive model inputs. Ground based laser operations which are particularly impacted by cloud field dynamics can employ the appropriate variations of CFLOS/CFARC persistence and recurrence statistics directly into mission planning scenarios with increasingly short response times.

Several examples illustrating the varied use of the WSI image data are presented in the following summaries. They are of course user specific applications con-

ducted under the general scope of this particular contractual effort, but readily typify the types of tasks for which the data base is deemed appropriate.

6.1 Concepts for Anti-Satellite (ASAT) Engagement Scenarios

With regard to determining the impact of cloud effects upon definition of a specific ASAT systems engagement space, it is clear that there are several contributing elements. The characteristics of the satellites orbit, the characteristics of the intervening atmosphere specifically including the nature of the prevailing cloud field, and the nature of the ground based laser itself must all be considered. Whereas it is appropriate to be fully cognizant of the methodology intended for the specification of these various characteristics, we feel that the optimum analytic scheme would employ as complete a decoupling between the major sub-elements as is practical. This is particularly true with regard to the atmospherics. To the degree that this decoupling of the cloud field statistics and related characterizations from the other performance characterizations within the general ASAT system performance model can be achieved, the more readily a truly definitive set of CFARC statistics can be generated. In the long term view, we feel that atmospheric decoupling is an extremely important issue and should be addressed early and creatively in defining the analytic approach.

For the application at hand, i.e., meteorological support products for application within a relatively generic ASAT Scenario, we will assume meteorological decoupling, and the production of statistical products from the WSI data base for White Sands Missile Range. The statistics have been extracted for a sample two week interval for procedural illustration only, i.e. for most realistic applications substantially longer sample intervals, seasonally weighted would be more appropriate. These concepts have been previously discussed in Optical Systems Group, Technical Note No. 219, T. L. Koehler and J. E. Shields (1990).

For this demonstration, an arbitrary arc trajectory, represented by pixel row 324 on the image, was chosen to provide a simulated satellite track, and a variety of sample statistics related to this arc were generated. The general question to be answered was: What is the probability of finding a cloud free arc length sufficient to allow a successful deposition of energy upon the satellite? In this example, "successful" was to be defined by the users system performance model in a manner decoupled from the meteorological determinations.

The first four figures illustrate the statistical data extracted from the two week sample of WSI imagery. The last three illustrate an assumed procedure for applying these statistical data to a generic ASAT engagement.

6.1.1 Graphics & Illustrations

Unconditional Probability Plots

Figure 6.1-1 shows the frequency distribution for start and end point of the longest cloud free arc occurring along the selected arc (row 324) within each image. Only those points which are neither completely clear nor completely cloudy are included on the plot. (The frequencies of clear and overcast cases are printed on the plot.) The shape of this curve appears reasonable; even for this small sample used in its derivation.

The second plot on this page, Fig. 6.1-2, gives the frequency distribution for arc length. (Again, clear and overcast are not included.) This is followed by Fig. 6.1-3, a plot of the cumulative frequency for arc length, both for the total sample, and for A.M. (the 3 hours before local apparent noon) and P.M.. (the three hours after), illustrating a simple temporal sorting option.

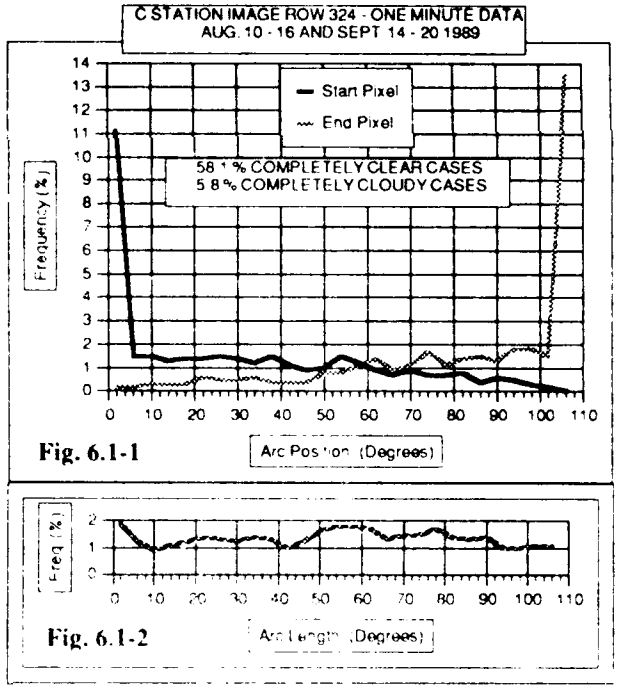

Fig. 6.1-1

Fig. 6.1-2

Unconditional Probability Interpretation

From the combined cumulative frequency plot, Fig. 6.1-3, one can see that the 20% value corresponds, for this sample, to an arc length of 45 degrees. Although these numbers should not be trusted at this point as definitive statistics, they can be used for illustrative purposes. In this sample, if one wishes an 80% success rate, one must be able to input sufficient energy in 45

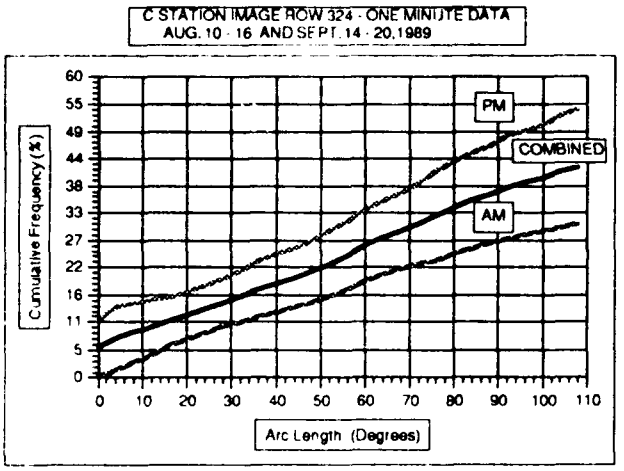

Fig. 6.1-3

degrees of transit time. Note that the afternoon was considerably more cloudy than the morning. In the morning one has over 60 degrees available, but in the afternoon only 30 degrees arc available, assuming a desired 80% success rate.

Conditional Probability Plot

The start point along a selected arc can also be quite critical in determinations of whether it is possible to input satisfactory energy levels onto the target vehicle. Therefore we also computed some conditional probabilities. One can first compute the probability that the start point is a given position. Then for a given start point, one can compute the conditional probability that the arc length is a given amount. The application of this approach is illustrated in the remaining plots and tables.

The first plot, Fig. 6.1-4 and Table 6.1.1, illustrate the arc length conditional probability, based on this limited data sample, given the start pixel position shown. For illustration only, the arc has been broken into 9 segments.

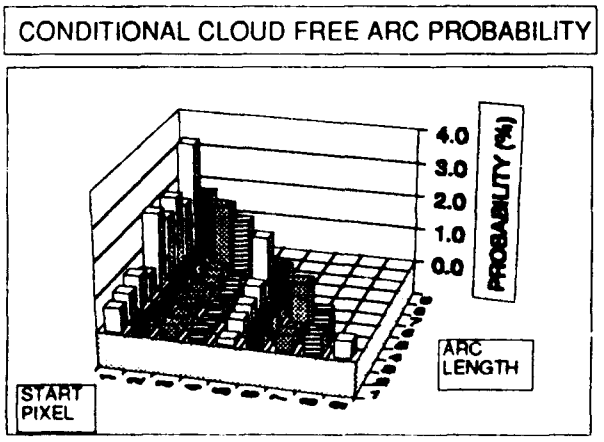

Fig. 6.1-4

Table 6.1.1

Conditional CFARC Probability (%)
Conditional Probability of ARC length, for each given start point
(Derived from Cloud Images)

		CFARC Length Category								
		1	2	3	4	5	6	7	8	9
	1	0.7	0.8	1.0	0.7	2.2	1.8	2.1	1.60	3.20
	2	0.5	0.2	0.1	0.2	0.3	0.4	0.4	2.00	
	3	0.4	0.3	0.3	0.4	0.3	0.4	2.0		
Start	4	0.3	0.2	0.3	0.3	0.5	1.9			
Pixel	5	0.2	0.4	0.5	0.7	1.8				
Cat.	6	0.4	0.5	0.4	1.3					
	7	0.5	0.3	1.3						
	8	0.6	0.9							
	9	0.5								

(These computations would normally be done at full pixel-by-pixel resolution.) Thus, for example, .7% of the cases had a start point within category 1 and arc length within category 1 (roughly 0-12 degrees).

Application of the Conditional Probability

Once similar conditional probabilities are computed for sufficiently long periods, these data could be used in the following way. The ASAT model could be used to generate the amount of energy which can be input for a given start point and arc length. This would be computed for all combinations of start point and arc length. This has been done for a simulated energy profile, in the figure labeled "Simulated Energy Matrix", Fig. 6.1-5 and Table 6.1-2.

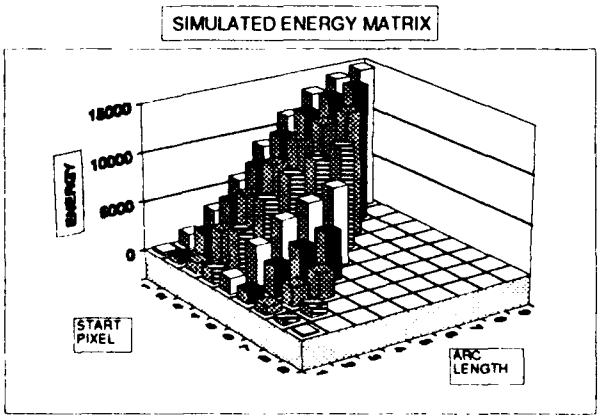

Fig. 6.1.5

If one knows the energy required for mission success, the energy matrix is thresholded at this known required energy. The resulting thresholded matrix is 0 if a given start point and arc length do not yield sufficient energy. A sample thresholded energy matrix has been plotted as Fig. 6.1-6 and listed in Table 6.1.3 for a successful engagement energy of 7000 relative units. This binary

matrix is then multiplied by the conditional cloud free arc length matrix shown earlier, to determine how often success is achieved. The sum of this final matrix yields percent success rate.

Table 6.1.2

Simulated Energy Matrix
Energy fluence for a given arc length and start point
(Normally derived from ASAT model)

		CFARC Length Category								
		1	2	3	4	5	6	7	8	9
	1	320	1420	3260	5820	8820	11380	13220	14320	14760
	2	700	2530	5090	8090	10650	12490	13600	14150	
	3	1070	3630	6630	9190	11030	12140	12810		
Start	4	1450	4450	7070	8840	9950	10740			
Pixel	5	1560	4120	5950	7060	7940				
Cat.	6	1210	3040	4150	4940					
	7	830	1940	2610						
	8	450	1010							
	9	140								

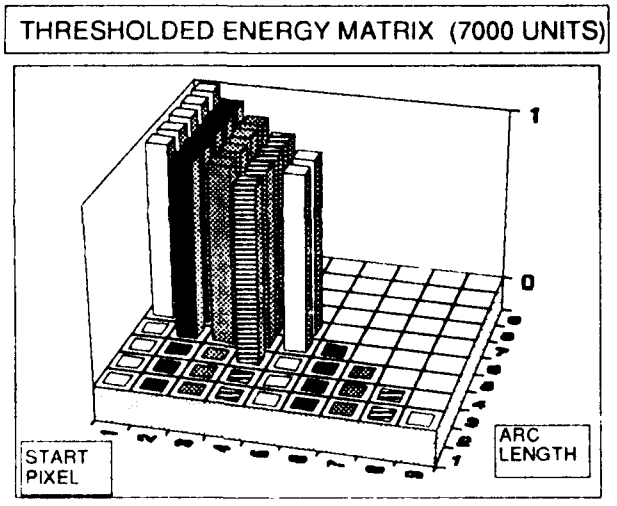

Fig. 6.1-6

Table 6.1.3

Decision Matrix (Energy > 7000)
from Energy Matrix thresholded at a sample required kill energy of 7000

		CFARC Length Category								
		1	2	3	4	5	6	7	8	9
	1	0	0	0	0	1	1	1	1	1
	2	0	0	0	1	1	1	1	1	
	3	0	0	0	1	1	1	1		
Start	4	0	0	1	1	1	1			
Pixel	5	0	0	0	1	1				
Cat	6	0	0	0	0					
	7	0	0	0						
	8	0	0							
	9	0								

Summation of the product of the CFARC table with this table yields 22.8% P_k
Addition of clear cases, 58.1%, yields net P_k = 80.9%

The final plot, Fig. 6.1-7, compares the resulting success rate for the unconditional and conditional probabilities. The unconditional probability gives a somewhat more conservative answer. That is, for a given required energy, the unconditional probability will yield a slightly lower estimate of the success rate. For a required energy of 7000, the conditional probability predicts a 2% higher success rate.

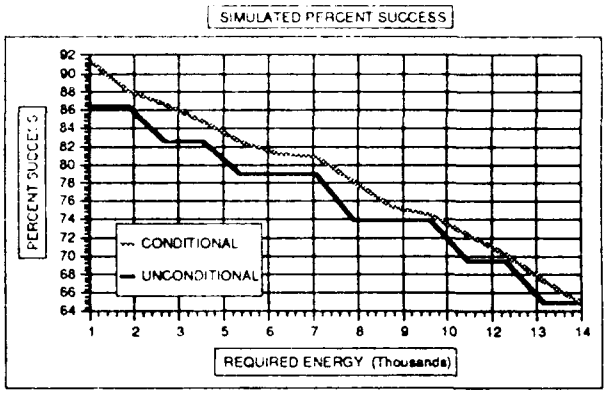

Fig. 6.1-7

For operational purposes, the important question is: how much will we overestimate the energy output requirements of the GBL if we use unconditional probabilities. Answering this directly requires multiple runs with different input energy profiles. However we can approach the problem indirectly by asking a slightly different question: what is the highest cumulative incident energy that could be achieved for a given fixed input energy. At the 80% point, the unconditional probability implies an energy of only 4700 units would be available on target; the conditional probability implies that 7200 units of energy would be available, for the same input profile. That is, the unconditional probability estimate implies at least 7200 energy units would be available 80% of the time. Thus in terms of energy, the conditional probability gives a much more favorable answer.

It should be noted that the stair-step nature of the unconditional percent success vs. required energy plot is an artifact of the coarse arc length resolution used for the illustration of concept in this sample. This artifact would disappear when the computations are made at full resolution.

Summary

The cumulative frequency of arc length based on the unconditional probability of arc length, yields a very convenient result. One can determine immediately the arc length in which sufficient energy must be input. This

is a very convenient format, as it uncouples the cloud statistics from the ASAT model; these distributions may be run for as many cases as desired, and input as distributions to the ASAT model.

The conditional probabilities also decoupled the cloud impact computations from the ASAT computations. That is, the cloud statistics may be determined independently from many cases, and input as a distribution to the ASAT model. They also, in our opinion, yield a somewhat more accurate result than the unconditional probabilities. They are not as convenient to interpret however, because determination of the final percent success rate requires use of an energy matrix from the ASAT model.

6.2 Preliminary Cloud Free Arc (CFARC) Statistics from WSI Imagery

Introduction

The study described in Section 6.1 was designed to illustrate the procedure for combining CFARC statistics with laser energy profiles to compute the probability of success in an ASAT scenario. The WSI data for that study was extracted from an arbitrary east-west row for two one-week samples that exhibited reasonable cloud cover variations. In contrast, the following section describes a brief study using CFARC information from WSI data collected at the C-Station site during the two extreme months of the year in terms of the climatological cloud cover at WSMR, along a north-south arc that better simulates a realistic satellite track. The preliminary one-minute cloud decision imagery generated with the fixed threshold algorithm available at the time of this study were employed.

6.2.1 White Sands Cloud Cover Climatology

Considering our desire to limit the resources allocated to this task, and the preliminary nature of the cloud/no cloud data available at the time of this study, we decided to focus on two monthly samples that illustrate the extremes in the cloud cover distributions at WSMR. Since the degree of cloud cover along an arc in the sky is strongly dependent on the total cloud cover, the selection of which monthly periods to examine was based on the climatological sky cover data from Stallion Site at WSMR illustrated in Fig. 6.2-1. The strong summer diurnal cycle with clearer mornings and cloudier afternoons is clearly evident. The extreme periods (black circles) occur in consecutive months, with June AM being the clearest on average, and June PM being cloudiest on average. The (+) symbols show the corresponding C-Station WSI average cloud covers from 1989. The WSI one year

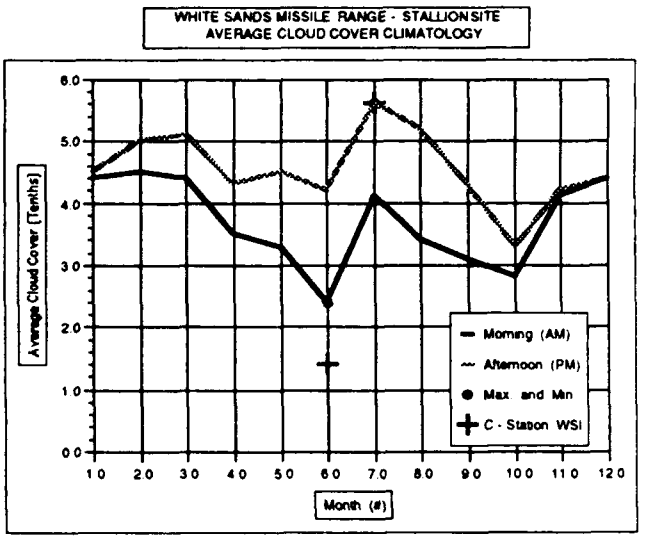

Fig. 6.2-1

average matches the Stallion 13-year site climatology in the July PM cloudy period. In contrast, the June AM averages differ significantly.

Fig.6.2-2 illustrates the cloud cover distributions from WSI and climatology for the periods of interest. The completely clear and completely cloudy categories are in close agreement for the June AM results. However, the sky cover amounts in the 3-9 tenths categories are smaller in the WSI results compared to climatology, appearing instead in the 1 tenth category, leading to the lower WSI average cloud cover. Similarly, the WSI results from July PM are smaller in the same 3-9 tenths categories than those from climatology, but both the 1 tenth and 10 tenths cases have increased, resulting in no difference in average total cloud cover. The differences noted can arise

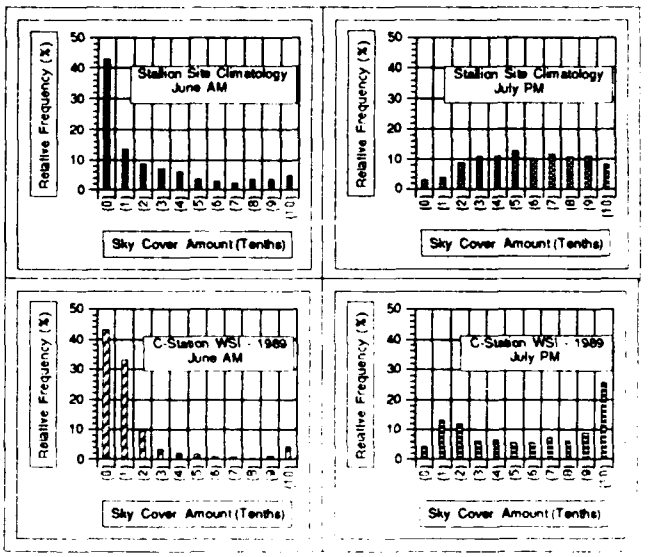

Fig. 6.2-2

from several sources, including natural year-to-year variability, different sites (C-Station is approximately 100 miles south of Stallion Site) and surrounding terrain, and known biases in the human observations vs. WSI (see, for example, McGuffie and Henderson-Sellers, 1989).

6.2.2 CFARC Data Reduction

The basic data employed in the study is a subset of the preliminary one-minute cloud/no cloud data release made earlier to The Analytic Sciences Corp. (TASC). Software was written to extract a 337 pixel cloud/no cloud sample from image column 255 starting at row 72 at 5 minute intervals. This column runs from south to north through zenith, and the sample is bounded by the 60° zenith circle (Fig. 6.2-3). For each subset extracted, the maximum arc free of either opaque (white) or thin (shaded) cloud pixels was determined, and the corresponding starting pixel and arc length values saved. The maximum CFARC in Fig. 6.2-3 is highlighted in dashed white. All available data from the C-Station site, 27 days for June 1989 and 28 days from July 1989, were processed in this manner.

Fig. 6.2-3

The results that follow are based only on the morning data from June and the afternoon data from July. Any period with an arc containing occulter mask pixels was ignored.

6.2.3 Resultant CFARC Distributions

General CFARC Distributions

The first step in the data analysis was to classify the maximum CFARC starting and ending pixel positions and the resulting arc lengths into 24 categories, each category representing an arc of 5° zenith angle. The June AM results are shown in Fig. 6.2-4. All three distributions do not include the completely cloudy arc (4.6%) or completely clear arc (75.4%) cases. As expected, the start pixel distribution has a maximum at the south edge, and the end pixel distribution has a maximum at the north edge. The start pixel distribution also has an unusual secondary maximum near the center of the arc, due primarily to spurious cloud identifications made near the sun, but outside the occulter mask in the 20 to 30 minute periods just before and after the mask intersects the arc of interest. A similar peak occurs in the center of the arc length distribution, implying that these are probably completely clear arc cases that have been misidentified as partial arc cases. Thus, the completely clear case frequency would be increased by almost 2%. Note also the the end pixel maximum exceeds the start pixel maximum by over 6%, indicating an azimuthal preference for clouds to the south compared to the north during the June mornings.

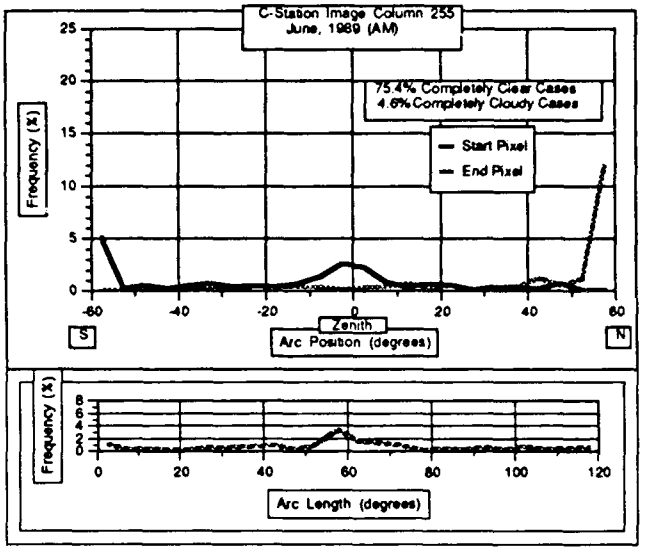

Fig. 6.2-4

As might be expected, the July PM results (Fig. 6.2-5) have greater frequency values than those from June AM, due to fewer completely clear cases. Maximum CFARCs starting at the southern edge now exceed those ending on the northern edge, suggesting a reversal in the cloud preference compared to June AM. The strong peak in the first arc length category (0° - 5°) is probably caused by anomalous clear pixels appearing in completely cloudy CFARC situations.

Cumulative CFARC Length Distributions

Users of CFARC information often ask for the probability of having an arc length of at least some specified value, or alternatively, the arc length that is met or exceeded some specified percentage of the time. Fig. 6.2-6 provides just such information, with the vertical

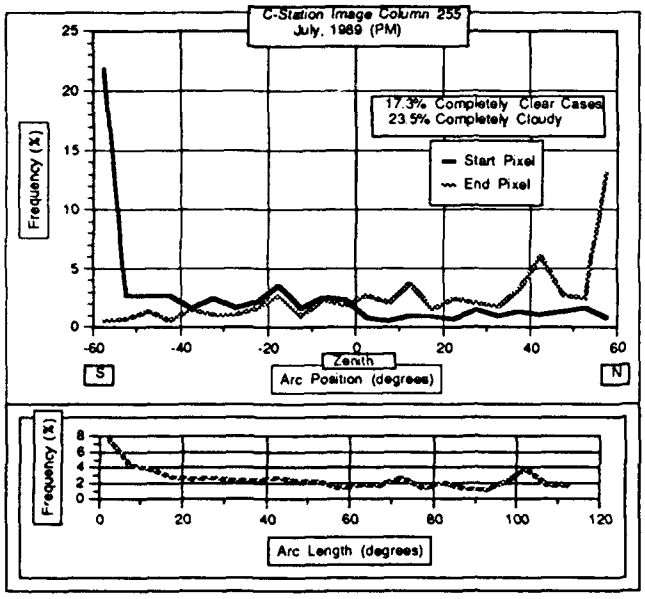

Fig. 6.2-5

axis depicting the probability of exceeding the maximum CFARC specified along the horizontal axis. For example, the maximum CFARC along the specified track is greater than 40° 90% of the time in the June AM sample, but only 48% in the July PM sample. Note also that the completely clear arc frequency appears at the right side of the diagram, and the completely cloudy frequency can be obtained by subtracting the value on the extreme left from 100%. Another interesting feature of these results is that fewer than 80% of the July PM cases have clear arcs of any length.

The following four figures provide additional insight needed for interpreting the results in Fig. 6.2-6. Fig. 6.2-7 combines the WSI cloud determination image from

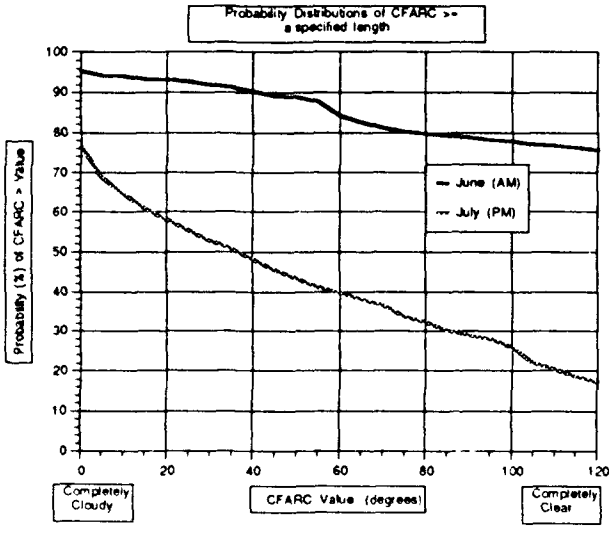

Fig. 6.2-6

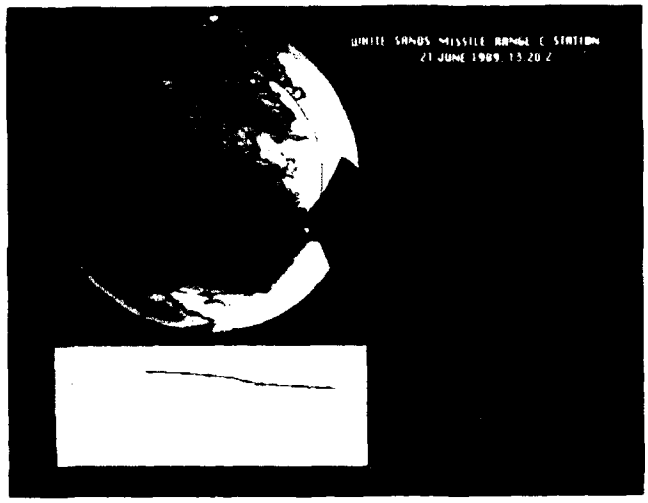

Fig. 6.2-7

Fig. 6.2-3 with the June AM curve from Fig. 6.2-6. The maximum CFARC for the image shown in Fig. 6.2-7 was 74°, as indicated by the dotted vertical line in the inset graph. This length was exceeded roughly 80% of the time in the June AM sample. In other words, 80% of the cases had maximum CFARCs clearer than this case.

In the worst case scenario (July PM), the 80% level must include completely cloudy arcs, as shown illustrated in Figs 6.2-8 and 6.2-9. While it is easy to see that a selected arc will be completely cloudy in an overcast situation (Fig. 6.2-8), one must also realize that completely cloudy arcs also arise in cases with partial cloud cover (Fig. 6.2-9). In further contrast with the best case example in Fig. 6.2-7, Fig. 6.2-10 illustrates a case with a 35° maximum CFARC. Only 50% of the July PM cases exceeded this value.

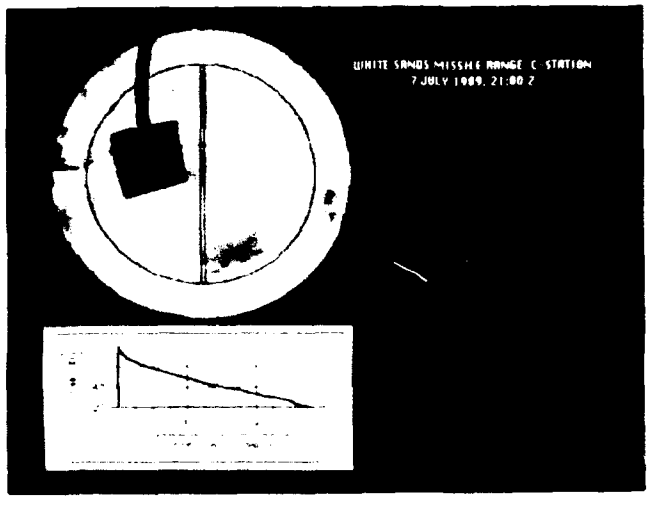

Fig. 6.2-8

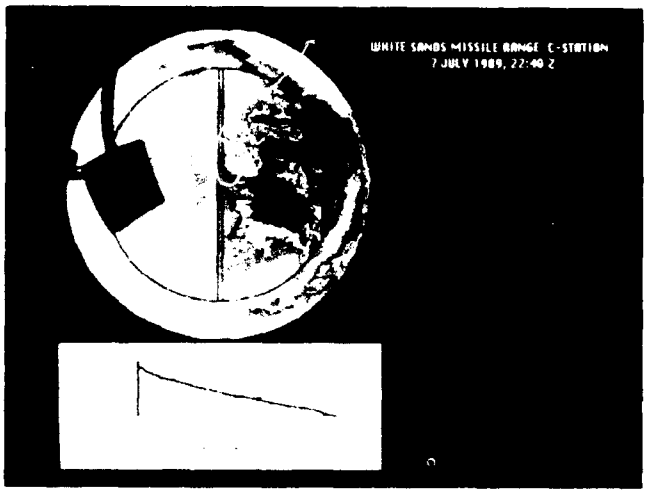

Fig. 6.2-9

Conditional Probability Distributions

In many laser scenarios, the position of the maximum CFARC can be almost as important as its length. Tables 6.2.1 and 6.2.2 give the percentage occurrences of maximum CFARC length, given that the CFARC begins at certain positions along the arc. The data have been organized in twelve 10° categories. For example, 0.4% of the 1572 July PM maximum CFARCs started in the southern 30° - 40° zenith angle interval and extended into the 30° - 40° arc length interval, as did the case shown in Fig. 6.2-10.

Table 6.2.1 - Conditional maximum CFARC probability (%) given arc start position for the June AM sample totaling 1365 cases.

		Arc Length Category											
	Zenith Angle Category	0° to 10°	10° to 20°	20° to 30°	30° to 40°	40° to 50°	50° to 60°	60° to 70°	70° to 80°	80° to 90°	90° to 100°	100° to 110°	110° to 120°
	60° to 50°	0.1	0.1	0.3	0.4	0.3	0.3	0.4	0.7	0.4	0.3	0.9	1.2
	50° to 40°	0.1	0.1	0.0	0.2	0.0	0.1	0.0	0.0	0.0	0.0	0.3	
S	40° to 30°	0.0	0.0	0.2	0.1	0.0	0.1	0.0	0.0	0.1	0.7		
	30° to 20°	0.1	0.0	0.0	0.0	0.2	0.0	0.0	0.1	0.5			
	20° to 10°	0.1	0.1	0.0	0.1	0.1	0.0	0.1	0.6				
Start	10° to 0°	0.0	0.0	0.0	0.1	0.0	1.4	2.5					
Pixel	0° to 10°	0.1	0.0	0.0	0.1	0.1	2.8						
	10° to 20°	0.0	0.0	0.1	0.1	0.8							
	20° to 30°	0.0	0.1	0.0	0.5								
N	30° to 40°	0.3	0.0	0.4									
	40° to 50°	0.4	0.5										
	50° to 60°	0.3											

Table 6.2.2 - Conditional maximum CFARC probability (%) given arc start position for the July PM sample totaling 1572 cases.

		Arc Length Category											
	Zenith Angle Category	0° to 10°	10° to 20°	20° to 30°	30° to 40°	40° to 50°	50° to 60°	60° to 70°	70° to 80°	80° to 90°	90° to 100°	100° to 110°	110° to 120°
	60° to 50°	1.8	1.4	1.8	1.4	1.3	1.3	1.8	2.6	1.8	2.2	4.3	2.9
	50° to 40°	0.5	0.8	0.4	0.3	0.3	0.6	0.3	0.1	0.6	0.1	1.4	
S	40° to 30°	0.6	0.3	0.3	0.4	0.4	0.1	0.3	0.5	0.2	0.9		
	30° to 20°	0.5	0.3	0.5	0.9	0.4	0.3	0.3	0.1	0.6			
	20° to 10°	0.8	0.4	0.4	0.3	0.8	0.4	0.3	0.8				
Start	10° to 0°	1.8	0.4	0.4	0.4	0.5	0.4	0.6					
Pixel	0° to 10°	0.5	0.1	0.1	0.3	0.1	0.4						
	10° to 20°	0.1	0.3	0.2	0.2	1.0							
	20° to 30°	0.6	0.8	0.3	0.4								
N	30° to 40°	1.0	0.6	0.7									
	40° to 50°	1.3	1.2										
	50° to 60°	2.3											

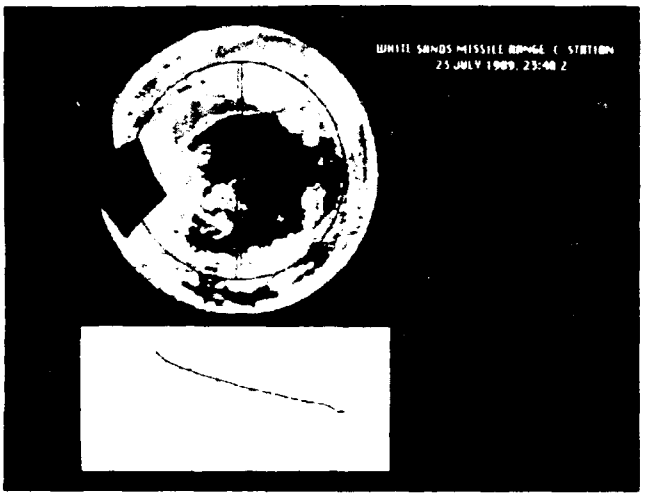

Fig. 6.2-10

Fig. 6.2-11 gives a graphical illustration of the conditional probability tables. The maxima in start pixel categories 6 and 7 (the region 10° on either side of zenith) in the June AM panel correspond to the secondary maximum noted previously in the start and end pixel distributions. The July PM maximum in arc length category 1 (0° - 5°) suggests that the peak in this category noted earlier in the bottom panel of Fig. 6.2-5 is localized in one part of the arc, and may be produced by nonuniformities in the imaging chip. Except for the problems just noted, the conditional probability values are quite reasonable, and are consistent in structure to those from other periods (not shown).

6.2.4 Concluding Remarks

Potential users of the WSI data base should find the results from this study encouraging. Previous comparisons reported in Shields, et al, (1990) showed reasonable agreement between overall sky cover estimates made by the WSI and the human observer. The CFARC results presented here imply that useful information regarding finer scale features, such as single arcs, can also be extracted from the WSI data.

These data and illustrations have been previously discussed in Optical Systems Group Technical Note No. 222, T. L. Koehler, 1990.

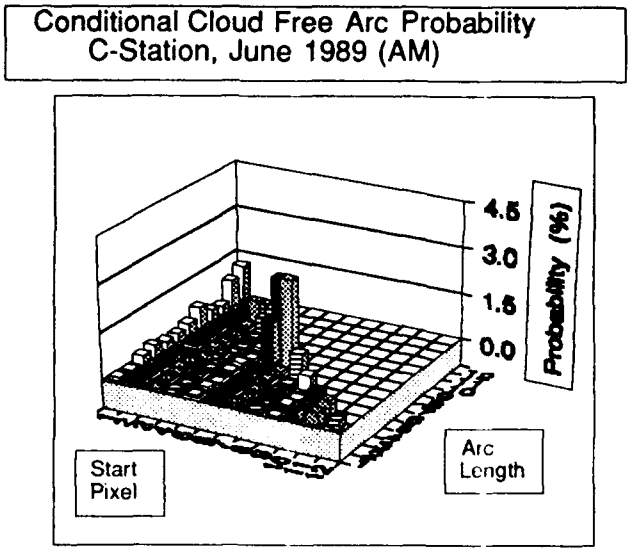

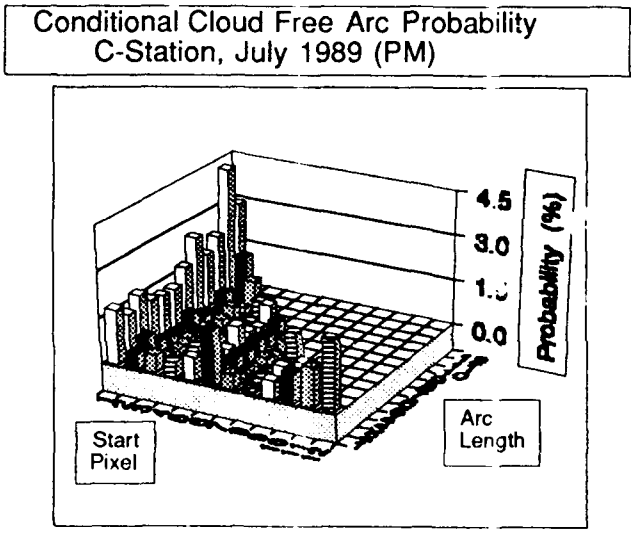

Fig. 6.2-11

6.3 Comparisons of WSI Cloud Determinations with Trained Observers

Whenever automatic machines are developed to mimic some specific element of human performance, there is an immediate and necessary demand to demonstrate credibility. The human's ability to perceive and interpret visible spectrum imagery in real time is, and will surely remain for some while, unchallenged. However, there are a myriad of human-like image acquisition and interpretation tasks that profit immensely from the ability to store and later retrieve images in a reliable manner. One of these tasks is obviously WSI cloud determination and documentation. A preliminary assessment of the WSI systems ability to mimic the human in this particular task is summarized below. This information has previously appeared in Shields, et al. 1990.

6.3.1 Total Cloud Cover Comparison

Much of the WSI data from the Columbia site was processed using the preliminary (fixed threshold) algorithm, in order to give a preliminary assessment of the accuracy of these techniques. Fig. 6.3-1 shows the cloud cover distribution from 7 months of WSI data, compared with the values of total sky cover reported on the National Weather Service Form 10's. The WSI values are from the one minute image at the reported time of the weather observation. This plot is for the six hours surrounding local apparent noon. The comparison between WSI and observer is in general quite good. The cloud algorithm identifies some clear cases as 1/10 cover, but in all other cloud categories the match in frequency of observance is excellent.

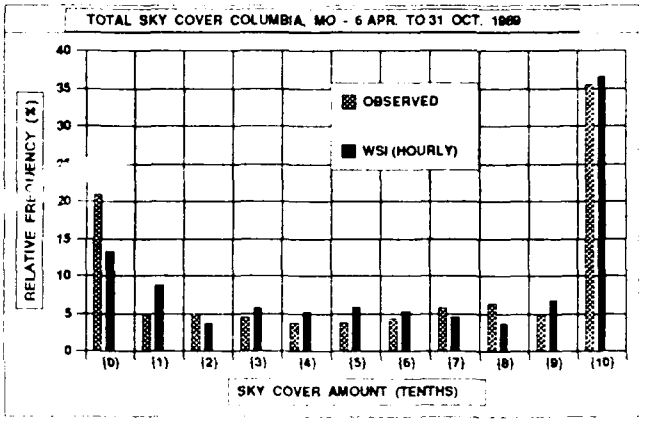

Fig. 6.3-1

Another indication of data quality is a direct case-by case comparison between WSI and observer. For Fig. 6.3-2, the difference between WSI and observer has been computed for each case. That is, a WSI value of 7/10 and observer value of 5/10 would be a difference of 2

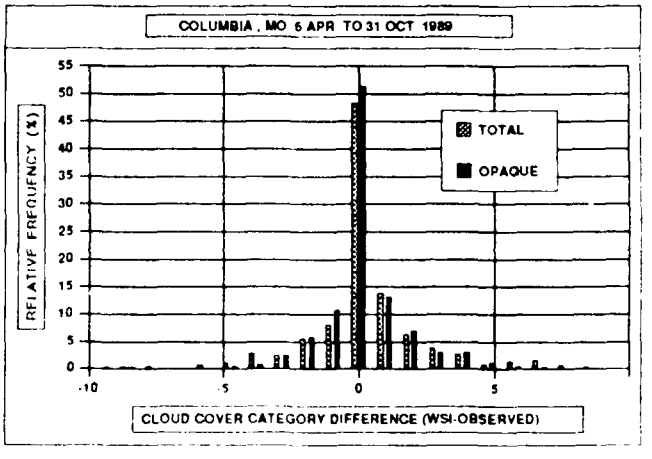

Fig. 6.3-2

categories. The distribution of category differences is shown in Fig. 6.3-2. The majority of the cases show a category difference of 0. The average difference is less than half a category, i.e. much less than 1/10 cloud cover.

6.3.2 Specific Temporal Dynamics Case Study

Although the observer to WSI comparison is generally good, the WSI data can show much more variance than the observer data, simply due to the limited temporal frequency of the observer values. One particularly dynamic day, 14 April at Columbia, Mo., is illustrated in Figs. 6.3-3 and 6.3-4. In Fig. 6.3-3, which shows the cloud cover determinations for both the WSI and the observer, the observer values are consistent with the WSI, but they certainly do not show the true variability, due to their limited temporal frequency. For example, at 1350 and 1450, both WSI and observer show approximately 20% cloud cover, but during the intervening hour the cloud cover increased to nearly 80%. The cloud images at the middle and end of this hour are shown in Figs. 6.3-5 and 6.3-6. The fastest rate of change during this hour occurred at between 1400 and 1413, when the cloud cover changed from 20 to 74%.

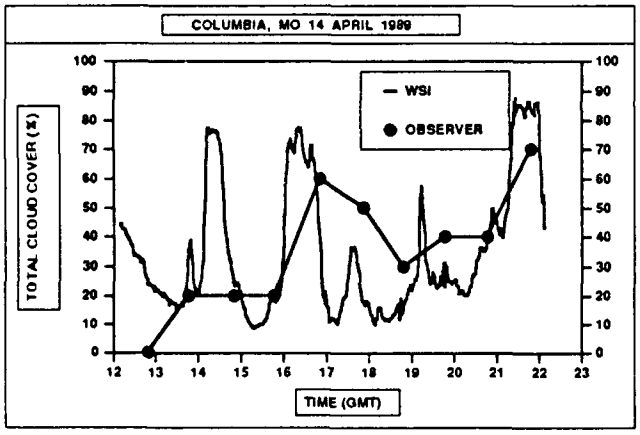

Fig. 6.3-3

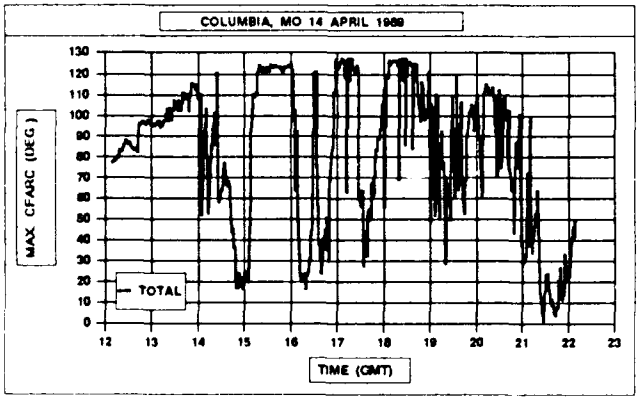

Fig. 6.3-4

Fig. 6.3-5

Fig. 6.3-6

One can also see, in Figs. 6.3-5 and 6.3-6, a horizontal line part way down the image in the Northern sky. This line represents an arc traveling from horizon to horizon, rising to a 45 degree zenith angle. The maximum cloud free arc length (CFARC) along this arc has been plotted in Fig. 6.3-4. Comparing Figs. 6.3-3 and 6.3-4, one can see that in general there is a tendency for short CFARCs to occur with high cloud cover. As expected however, the maximum CFARC is not always well related to the cloud cover at a given point in time. For example, at 1450, the cloud free arc length was quite short, in spite of the low cloud cover. Examination of the cloud image for this time (Fig. 6.3-6) shows that this occurred because the cloud band happened to lie over the selected arc.

6.4 Applications to Model Development and Evaluation

The emergence of the WSI cloud data base has prompted a variety of cloud model evaluations and reviews, many of which have been discussed within the

user community via the annual Proceedings of the Cloud Impacts on DoD Operations and Systems (CIDOS) conferences. Two short studies conducted at MPL related to the modeling of CFLOS/CFARC statistical properties have been presented previously as part of this currently reported research effort. Portions of these earlier reports have been abstracted, and are included in the following paragraphs.

6.4.1 Evaluation of Stochastic Models for Estimating the Persistence Probability of Cloud Free Lines-of-Sight

The report titled above, as is Section 6.4.1, was issued as GL-TR-89-0275, Scientific Report No. 1, 30 Sep 89, authored by Wayne S. Hering. Its abstract and introductory paragraphs are reproduced below.

Abstract

Stochastic models, based upon the Ornstein-Uhlenbeck (O-U) class of the simple Markov process have been used effectively to estimate the conditional probability of a variety of weather events (Gringorten, 1972). This study is directed toward extension of the analytical form of the O-U Markov model to yield estimates of the joint occurrence probability and duration of sky cover and cloud free lines of sight (CFLOS). As a first step, model estimates are made of the recurrence probability of CFLOS for specific categories of sky cover in tenths as a function of time. Then model calculations are made for the persistence probability of CFLOS and sky cover as a function of sky-cover category and time using an analytical representation of the mathematic solution of persistence probability for the O-U Markov process given by Kielson and Ross (1975). The model calculations of CLFOS recurrence and persistence are compared with the Columbia, MO, data base (Lund, 1973). Again using an analytical form of the O-U Markov model, calculations are made of the joint occurrence probability of sky-cover at two or more sites and compared with the observations from the central United States. Finally, analytic techniques are presented for calculating probability estimates of the duration of cloud-free or cloudy lines of sight from one or multiple ground sites to points in space. Trial calculations based upon climatic summaries of sky-cover are made for a selected group of sites in south western United States.

Introduction

Minute by minute determinations of sky-cover and cloud-free-line-of-sight (CFLOS) are being made in an experimental field program initiated in 1988 by the University of California, San Diego. Solid-state, whole-sky imagery (WSI) systems have been installed in a network configuration consisting of 6 field sites in the western United States. The primary goal is to obtain detailed observations of the joint occurrence frequency of CFLOS in time and space that are required to evaluate and extend sky-cover models. The stochastic sky-cover models are to be used for estimating the impact of clouds on ground-based systems that depend upon unobscured paths of sight to satellites in space.

A comprehensive statistical model has been developed by Boehm, et al, (1986) that specifically provides estimates of the duration of cloud free lines of sight from multiple ground sites to orbiting and geostationary satellites. The innovative method establishes the climatic probabilities through repetitive simulations of sky-cover distributions with the multidimensional Boehm Sawtooth Wave Model. The simulation model and its many component approximations are the prime candidates for test and evaluation with the new WSI data base.

Prominent among alternate approaches to the problem are models based on the Ornstein-Uhlenbeck (O-U) class of the simple Markov process. This approach has been applied successfully both in purely analytical form and by Monte Carlo simulation of probability distributions to estimate the joint occurrence and duration of a variety of weather events (Gringorten 1966, 1967, 1968, 1972). This study is directed toward extension of the analytical form of the O-U Markov model to yield estimates of the joint occurrence and persistence probability of cloud free lines of sight in time and space.

The ultimate objective of the modeling process is to determine the joint climatological probability of the duration of cloud free lines of sight to a point in space from one or more preselected ground sites, given the climatic summaries of sky-cover at each site. The solution to a number of intermediate modeling problems is required to achieve the desired objective. In Section 2, the application of existing models to estimate cloud free line of sight (CFLOS) probability as a function of sky-cover and the zenith angle of the path of sight is described. The basic O-U Markov modeling concepts are reviewed in Section 3. Estimates of the single station duration of CFLOS as a function of sky-cover using the Keilson-Ross procedure are discussed in Section 4. Estimates of the joint conditional probability of sky-cover at multiple sites is discussed in Section 5. Procedures for estimating the frequency of downtime intervals caused by cloud obscured lines of sight persisting concurrently at designated network sites are described in Section 6.

6.4.2 Probability Estimates of Cloud-Obscured Line-of-Sight

The report titled above, as is Section 6.4.2, was issued as Scientific Report No. 2, 30 May 90, authored by Wayne S. Hering. Its abstract and introductory paragraphs are reproduced below.

Abstract

The purpose of this study is to explore the basic relationships between the climatic frequency distribution of sky cover and the frequency and duration of Cloudy-Lines-of-Sight (CLOS) from one or more ground sites to points in space. Through a series of model calculations, estimates are made of the incremental changes in CLOS persistence and recurrence that correspond to changes in the climatic frequency of overcast, broken, scattered and clear sky conditions.

The determination of CLOS recurrence and persistence probability were made using the bivariate normal distribution (see Gringorten, 1972). The analytic stochastic model is based upon the Ornstein-Uhlenbeck class of the simple Markov process. A discussion of the procedures for modeling CLOS behavior is given in a previous report (Hering, 1989).

Model results are presented for CLOS as a function of sky cover and path of sight, CLOS recurrence and persistence probability relative to fixed categories of sky cover, and both single and multiple site CLOS recurrence and persistence probabilities.

Introduction

The purpose of this study is to explore the basic relationships between the climatic frequency distribution of sky cover and the frequency and duration of Cloudy-Lines-of-Sight (CLOS) from one or more ground sites to points in space. The determination of CLOS probability is of particular importance for the assessment of expected downtime of ground-based laser, optical data link and orbital surveillance systems. Through a series of model calculations, estimates are made of the incremental changes in CLOS persistence and recurrence that correspond to changes in the climatic frequency of overcast, broken, scattered and clear sky conditions.

The model calculations of CLOS behavior are of the following type:

a. Given the climatic frequency of sky cover at a selected ground site, what is the likelihood that a path of sight with zenith angle θ

1) will be obscured by clouds?

2) will be obscured by clouds at a particular time and then be obscured by clouds again after time interval t?

3) will be obscured by clouds continuously over time interval t?

b. Given the climatic frequency distribution of sky cover at a group of selected ground sites, what is the joint occurrence frequency and joint persistence probability of CLOS events such as those listed in (1), (2) and (3) above as a function of site separation distance d?

Modeling Procedures

The determination of CLOS recurrence and persistence probability in this study were made using the bivariate normal distribution (see Gringorten, 1972). The analytic stochastic model is based upon the Ornstein-Uhlenbeck class of the simple Markov process. A discussion of the procedures for modeling CLOS behavior is given in a previous report (Hering, 1989).

Markov model determinations of event probabilities are made through initial conversion of climatic frequency distributions of sky cover into corresponding values of Equivalent Normal Deviate (END). The transformation for any cumulative frequency distribution can be made using standard statistical tables or by computationally fast algorithms.

The fundamental modeling assumption is that the autocorrelation coefficients for sky cover decay exponentially with time or distance. Also, the correlation coefficient for CLOS under fixed sky cover conditions is assumed to decay exponentially with time. The expression for the temporal autocorrelation coefficient is simply

$$\rho_t = \exp(-t/\tau), \qquad (1)$$

where t is elapsed time and τ is the preselected relaxation time. The corresponding expression for the spatial autocorrelation coefficient is

$$\rho_d = \exp(-d/D), \qquad (2)$$

where d is the site separation distance and D is the input value for the relaxation distance. These correlation functions are used in determining recurrence probabilities.

In this study, nominal input values were used for sky cover relaxation time (16 hours), sky cover relaxation distance (500 mi) and CLOS relaxation time (30 min). The effects of uncertainties in these values will be assessed in association with some of the results as tabulated below.

The modeling procedures (Hering, 1989) are simple and easy to apply. The transformation to the equivalent normal deviate values are exact for any climatic cumulative frequency distribution. Once made, the model estimates of joint event (recurrence) probability are given by a simple regression equation for the bivariate normal distribution as follows:

$$y_t = \rho_t\, y_o + \sqrt{1-\rho_t^2}\ \eta_t \qquad (3)$$

where η_t is the END corresponding to the conditional probability $P_r\ (y \le y_t \mid y_o)$, and y_o and y_t are END equivalents of the cumulative frequency of the initial and final events, respectively. Thus, the expression yields the conditional probability of a weather event following a prescribed initial condition.

The value of y_o in Eq. 3 is defined uniquely for continuous variables by the cumulative frequency distribution at the initial time. For variables expressed only in categories, such as sky cover amount, it is important to subdivide the category probability range into subsets with smaller but equal ranges. The calculations of conditional probability should be carried out in turn using each of the subset midpoints as y_o and the results averaged to yield the composite result for the sky-cover category. Experience shows that division into 6 subsets is sufficient for good results.

A mathematical solution of persistence probability for the bivariate normal distribution is given by Keilson and Ross (1975). Since the computer routine for the formal solution is lengthy, an alternative analytical solution was developed for the CLOS determinations which provides reliable approximation of the formal solution over the desired range of output. The Keilson-Ross solution for the case where the climatic cumulative frequency of the weather event is 50 percent is simply

$$F_o = (1/\pi)\ \sin^{-1}\ (\exp -t/\tau) \qquad (4)$$

where F_o is the unconditional probability that $y \le y_o$ throughout the time interval t.

The solutions for $y_o \neq 0$ in this study were approximated by

$$f_r(y_o) = f(F_o) + y_o\left(1+0.13e^{-0.9\,t/\tau}\right)$$

$$\begin{bmatrix} -2 \le & y_o & \le 2 \\ 0 \le & e^{-0.9\,t/\tau} & \le 3 \end{bmatrix} \qquad (5)$$

where $f_r(y_o)$ is the END corresponding to the probability that $y \le y_o$ throughout the time interval, $f(F_o)$ is the END of F_o in Eq. 4, and y_o is the unconditional probability of the weather event. In contrast with Eq. 2 for recurrence probability, the persistence expression (Eq. 5) assumes that the climatic frequency of the event remains the same throughout the interval.

The sequence of four steps for the determination of CLOS recurrence and persistence for both single and multiple sites is as follows:

a. calculation of CLOS probability as a function of zenith angle q and particular category of sky cover amount,

b. calculation of CLOS recurrence and persistence probability as a function of time interval for specific individual categories of sky cover,

c. calculation of sky-cover amount recurrence and persistence probability as a function of time interval, site separation distance, and the climatic frequency distribution of sky cover.

d. given a, b and c, calculation of the recurrence and persistence probability of CLOS at a single site and for simultaneous recurrence and persistence of CLOS at multiple sites as a function of sky-cover frequency distribution, time interval and site separation.

7.0 RECOMMENDATIONS FOR FURTHER RESEARCH

The WSI cloud data base, summarized in Tables 3.1 and 4.3, provides an extensive selection of digitized cloud imagery suitable for a broad variety of modeling and case study applications. It has been compared with data derived from classical observations by meteorologically trained personnel, and found to produce equivalent statistical characterizations. Thus, it is well linked to other long term historical archives, for which it provides a useful high resolution supplement. Experience with the data to date clearly illustrates the technical viability of fully automatic digital systems as reliable vehicles for the acquisition and analysis of whole sky cloud cover characterizations.

Model validation studies, particularly those related to relatively short term phenomena, such as CFLOS or CLOS (Cloudy Line of Sight) recurrence and/or persistence statistics, are an appropriate arena for WSI class data. As abstracted from Hering (1990):

"The data base generated by the Whole Sky Imagery (WSI) network will enable validation of the many factors

involved in the CLOS modeling process. The trial calculations made in this study provide a first approximation of CLOS behavior relative to the climatic frequency distribution of sky cover. However, certain aspects of the modeling process remained to be analyzed and refined on the basis of more extensive CLOS data.

The relationships between CLOS frequency and the zenith angle of the path of sight will be examined in detail using the new WSI data base. Important refinements include the definition of CLOS dependence on zenith angle as a function of cloud type. In addition, it is important to take a close look at the relative importance of the azimuthal dependence of the climatic frequency of CLOS as revealed by the data from individual sites in the WSI network.

The temporal and spatial variations in sky cover have been analyzed rather extensively using the conventional climatic data base. Thus, the uncertainties in the model input values of sky cover relaxation time and distance and the resultant impact on CLOS probability estimates can be estimated. However, the more detailed WSI network data are necessary for comprehensive analysis of cloud-element relaxation time as defined in paragraph 4.0, and its variations with season and site location. Yet another factor requiring study is the potential variation in cloud-element relaxation time with the zenith angle of the path of sight. As shown by time lapse sequences of ground-based cloud imagery, apparent cloud motion overhead is more rapid than near the horizon."

Whereas the existing WSI imagery has proven its utility in a variety of daytime applications, its usefulness could be substantially broadened if it were to contain nighttime cloud data in addition to its current daytime inventory. A new day/night fisheye system has been developed at the Marine Physical Laboratory which will enable the addition of these low flux level images. The data obtained by these 24 hour/day imagers is directly applicable to extending the characterization of cloud field statistics throughout the 24 hour diurnal cycle. Studies of cloud field dynamics during the dawn and twilight transitions would be particularly informative, and readily achievable via an expanded 24 hr/day image archive. Two prototype systems, developed under cooperative tri-service support are currently operational at MPL under interactive computer control, with a technical assessment of full automatic operation under review. Applying systems of this class to the extension of the existing cloud data base provides exciting research opportunities that should promptly be pursued.

Continued research into the characterization of thin cirrus clouds, both daytime and nighttime, is an appropriate application for the WSI data base. With the implementation of the new cloud discrimination algorithm described in Section 5 of this report, the separation of clear sky background and thin cloud definition is substantially enhanced. Thus, the opportunity for thin cloud optical depth approximations is likewise improved, particularly when conducted as a joint exercise with active probing systems. Nighttime optical depth estimates using background starfields as the baseline reference level is an attractive and achievable experimental endeavor.

8.0 ACKNOWLEDGEMENTS

The work described in this Final Report was sponsored by the Geophysics Directorate, Phillips Laboratory, Hanscom AFB under contract number F19628-88-K-0005. Our thanks to Donald D. Grantham, J. William Snow, and Bruce A. Kunkle for their support and guidance.

The authors are indebted to their colleagues at the Marine Physical Laboratory for many, many hours of dedicated support, both in the Laboratory and in the field during the conduct of this progam. We particularly thank Eugene M. Zawadzki and Jack R. Varah for going the extra mile in support of many demanding installation and field maintenance requirements in addition to their normal laboratory software and calibration related activities. Harry G. Sprink and Monette E. Karr, members of our collaborating engineering staff, are thanked for their willing and prompt response to the inevitable quick fix emergencies that always appear. Melissa L. Ciandro deserves special gratitude for an outstanding performance in the organization and control of the major data processing task, as does Carole Robb for the excellence of this report's formatting and preparation.

Supporting organizations who provided host facilities for the WSI field installations provided much of the day to day care and feeding of the camera system for which we are greatly appreciative.

The organizations and our individual contacts were:

1. C-STATION, White Sands Forecast Station
   SLCAS-AT-WS
   WSMR, NM 88002
   Mr. Dave Novlan

2. HELSTF, HELSTF Test Facility
SLCAS-AT-H
WSMR, NM 88002-5501
Mr. Robert Endlich

3. KIRTLAND, Kirtland AFB

9.0 REFERENCES & BIBLIOGRAPHY

Allen, J. H. and J. D. Mahlick, (1983). *The frequency of cloud-free viewing intervals*, Preprint 21st Aerospace Science Meeting, 10-13 Jan. 1983, Reno, Nev.

Boehm, Albert, Irving A. Gringorten and Charles F. Burger, (1986). Private communication.

Ciandro, M. L. (1991). *WSI Data Base Catalog*, Marine Physical Laboratory, Optical Systems Group Technical Note No. 228, SIO, UCSD.

Duntley, S. Q., R. W. Johnson, J. I. Gordon, and A. I. Boileau, 1970: *Airborne Measurements of Optical Atmospheric Properties at Night*, University of California, San Diego, Scripps Institution of Oceanography, Visibility Laboratory, SIO Ref. 70-7, AFCRL-70-0137, NTIS No. AD 870 734.

Feller, W., (1966). *An introduction to probability theory and its applications*, Vol. II, John Wiley and Sons, Inc., New York, 626pp.

Gringorten, Irving I., (1966). *A stochastic model of the frequency and duration of weather events*, J. Appl. Meteorol. **5**:606-624.

Gringorten, Irving I., (1967). *Probabilities of moving time averages of a meteorological variate*, Tellus XX:461-472.

Gringorten, Irving I., (1968). *Estimating finite-time maxima and minima of a stationary Gaussian Ornstein-Uhlenbeck process by Monte Carlo Simulators*, J. Amer. Statistical Assoc., **63**:1517-1521.

Gringorten, Irving I., (1972). *Conditional probability for an exact noncategorized initial condition*, Monthly Weather Review, Vol. **100**, No. 1, 796-798.

Hering, W. S. and R. W. Johnson, 1985: *The FASCAT Model Performance Under Fractional Cloud Conditions and Related Studies*, University of California, San Diego, Scripps Institution of Oceanography, Visibility Laboratory, SIO Ref. 85-7, AFGL-TR-84-0168, NTIS No. AOA 085 451.

Hering, W. S., 1989: *Evaluation of Stochastic Models for Estimating the Persistence Probability of Cloud-Free Lines-of-Sight*, University of California, San Diego, Scripps Institution of Oceanography, Marine Physical Laboratory, GL-TR-89-0275, NTIS No. ADA 220283.

Johnson, R. W., W. S. Hering, and J. E. Shields, 1989: *Automated Visibility and Cloud Cover Measurements with a Solid-State Imaging System*, University of California, San Diego, Scripps Institution of Oceanography, Marine Physical Laboratory, SIO 89-7, GL-TR-89-0061, NTIS No. ADA 216 906.

Keilson, J., and H. F. Ross, (1975). *Passage time distributions for Gaussian Markov (Ornstein-Uhlenbeck) statistical process*, Selected Tables in Mathematical Statistics, Vol. **3**. Institute of Mathematical Statistics, American Mathematical Society, Providence, R. I.

Lund, I. A., 1973. *Persistence and recurrence probabilities of cloud-free and cloudy lines-of-sight through the atmosphere*, J. Appl. Meteor., 12, 1222-1228.

Lund, I. A., (1973b). *A model for estimating the joint probabilities of cloud-free lines-of-sight through the atmosphere*, J. Appl. Meteorol. 12:1040-1043.

Lund, I. A., and D. D. Grantham, (1980). *Estimating the joint probability of a weather event at more than two locations*, J. Appl. Meteor., 19, 1091-1100.

Lund, I. A., and M. D. Shanklin, (1973). *Universal methods for estimating probabilities of cloud-free-line-of-sight through the atmosphere*, J. of Appl. Meteor, **12**, 28-35.

McGuffie, K. and A. Henderson-Sellers (1989). *Almost a Century of "Imaging" Clouds Over the Whole Sky Dome*, Bulletin of the American Meteorological Society, Vol. **100**, No. 10, 1243-1253.

Ross, H. F., (1980). *An algorithm for $F_\theta(y)$ using cubic B-Splines*, AFGL-TR-81-0068 AD A103468, Air Force Geophysics Laboratory, Hanscom AFB, MA.

Shields, J. E., T. L. Koehler, M. E. Karr and R. W. Johnson (1990). *Automated Cloud Cover & Visibility Systems for Real Time Applications*. Tech. Note 217, Optical Systems Group, Marine Physical Laboratory, SIO, UCSD.

APPENDIX A

OPTICAL SYSTEMS GROUP
TECHNICAL NOTE NO. 228

Apr 1991

WSI DATA BASE CATALOG

(STATUS AS OF 31 DEC 1990)

M. L. Ciandro

UNIVERSITY OF CALIFORNIA SAN DIEGO

SCRIPPS INSTITUTION OF OCEANOGRAPHY

MARINE PHYSICAL LAB San Diego, CA 92152-6400

Contract Monitor, Mr. B. Kunkel
Atmospheric Sciences Division

Prepared for
The Geophysics Directorate of the Phillips Laboratory
Air Force Systems Command, United States Air Force
Hanscom AFB, Massachusetts 01731
under contract No. F19628-88-K-0005

Technical Note No. 228

WSI Data Base Catalog (Status as of 31 Dec 90)

Summary

Responding to a well recognized need by many in both the modeling and operational communities for an improved capability in the collection and assessment of whole sky cloud characteristics, a new generation of video based imaging systems has been developed and fielded by the Marine Physical Laboratory. One of these systems, the Whole Sky Imager, has been deployed at several widely separated portions of the United States, and has gathered several million images appropriate for determining cloud cover at very high spatial and temporal resolution. Cloud cover estimates derived from a 7-month sample of these cloud images shows very good agreement with observed sky cover amounts. The capabilities of the Whole Sky Imager and an overview of the current status and quality of the WSI data base are discussed in Technical Note No. 226.

An inventory of the complete WSI Image Data base, segregated by site, date and archival tape number, is included herein. The data in this catalog has been reviewed in accordance with our established QC procedures, and has been purged of all sets deemed inappropriate for further application.

WSI DATA BASE CATALOG
STATUS AS OF 31 DEC 90

Table of Contents

APPENDIX A

WSI DATA BASE CATALOG
STATUS AS OF 31 DEC 90

List of Illustrations

1.0 INTRODUCTION

This catalog is a complete listing of all available data deemed of adequate quality for follow-on processing and analysis from each of the seven WSI sites. Figure 1 shows the location of each data site. Processing quality extends from excellent (new camera) to degraded but useable (old camera). As a camera ages the imagery becomes grainy in appearance, but this does not normally interfere with Ratio or Cloud/No Cloud processing or determination. Figure 2 shows the status of each site and the level of processing completed for that site. A summary of data quality for any site and time are available upon request.

Throughout the catalog there are gaps between tape sequence numbers. The data contained on these unlisted tapes is not deemed suitable for general distribution. In some cases the data can be retrieved but would require additional special processing. Further evaluation of this data is available upon request.

Each site was given a 3 character identifier as noted on Figure 1. This identifier is written to the header of every image on the tape.

When a station tape was received from the field it was labelled and assigned the next available sequence number starting with 001 for each station. The tape label consists of a 3 character station identifier and a 3 digit sequence number, e.g. "WSC112" identifies a tape from the White Sands C-Station site (WSC), which was the 112th tape received.

Users should be aware that sequential data days need not necessarily occur on tapes of consecutive sequence numbers due to occasional disruptions at the host facilities.

WHOLE SKY IMAGER DATA SITES

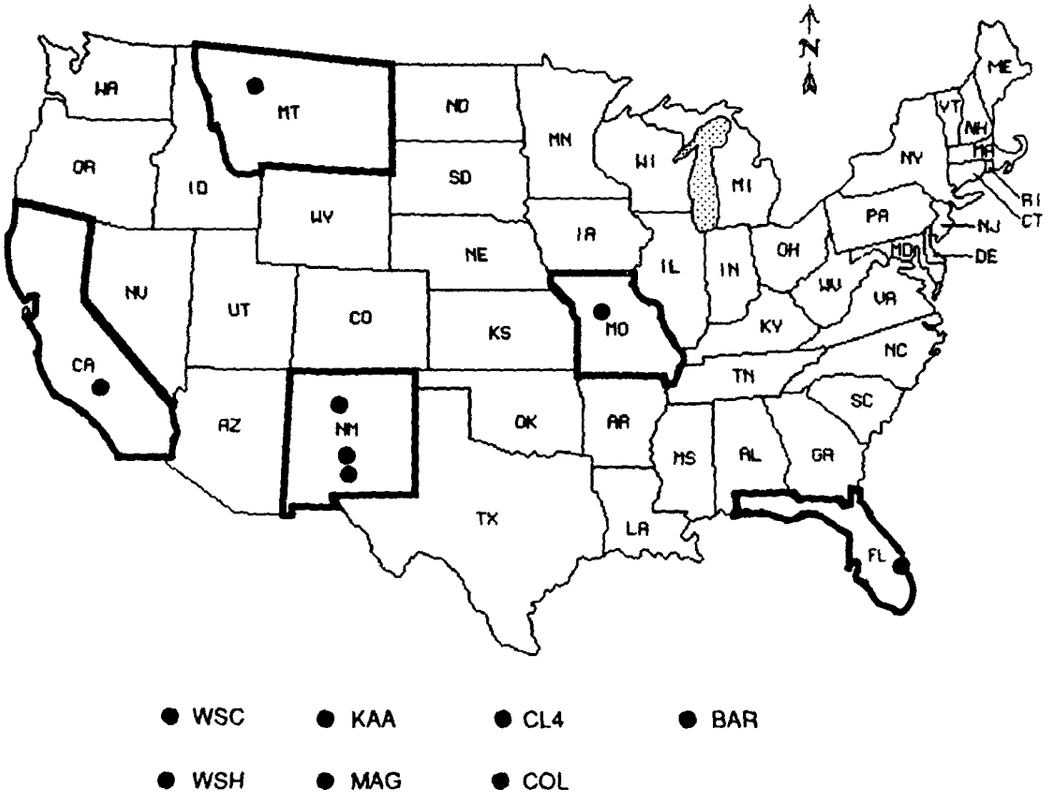

Figure 1

1988

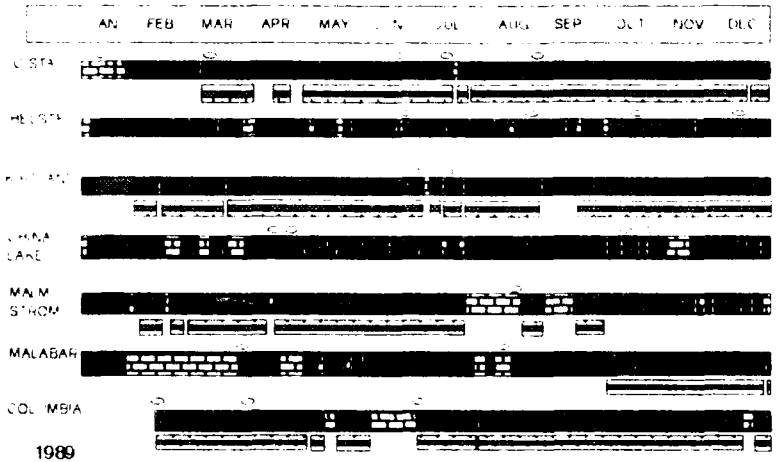

1989

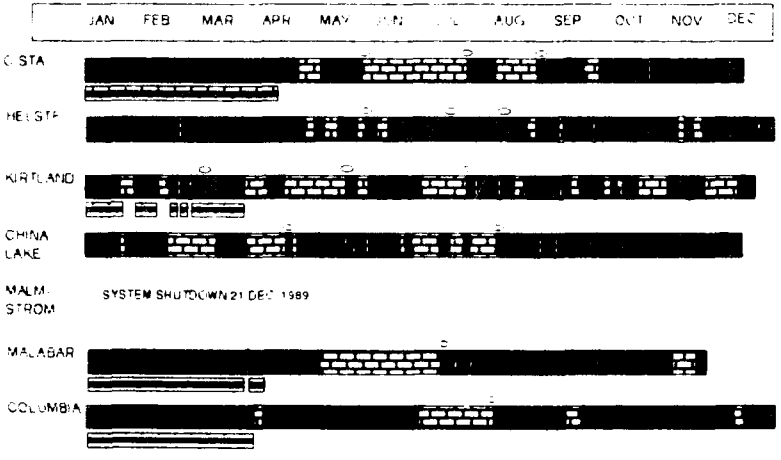

1990

WSI DATA STATUS & PROCESSING SUMMARY

= GOOD DATA

= INSTALLATION/MAINTENANCE

= SPECIAL HANDLING REQUIRED

= RATIO

= SYSTEM DOWN

= CLOUD DECISION

Figure 2

2.1 White Sands Missile Range/C-Station, New Mexico

TAPE #	DATE	START	STOP
YEAR = 1988			
WSC034	12-18/APR	05:50	17:48
WSC035	19-25/APR	05:50	17:48
WSC036	26-30/APR	05:50	17:48
	1-2/APR	05:50	17:48
WSC037	3-5/MAY	05:50	17:48
	6/MAY	05:50	07:48
WSC038	7-13/MAY	05:50	17:48
WSC039	14-17/MAY	05:50	17:48
WSC040	18-23/MAY	05:50	17:48
	24/MAY	05:50	09:00
* ALL DAYS FROM THIS POINT ON ARE ON ZULU-TIME			
WSC043	10/JUN	14:30	01:09
	11-15/JUN	13:10	01:08
	16/JUN	13:10	15:26
WSC044	16/JUN	18:10	01:08
	17-20/JUN	13:10	01:08
WSC045	29/JUN	16:50	01:11
	30/JUN	13:10	01:08
	1/JUL	23:09	00:58
WSC046	8/JUL	14:11	01:09
	9/JUL	13:10	17:46
WSC047	11/JUL	19:20	19:56
WSC048	14-18/JUL	13:20	01:18
	19/JUL	13:20	17:56
WSC049	20/JUL	20:10	01:19
	21-25/JUL	13:20	01:19
	26/JUL	13:20	15:20
WSC050	27/JUL	14:20	01:19
	28/JUL	13:20	15:19
WSC051	2/AUG	16:30	01:19
	3/AUG	13:20	01:19
	4/AUG	13:20	20:48
WSC052	5-11/AUG	13:20	01:19
WSC053	12/AUG	14:40	15:20
WSC054	21/AUG	13:10	09:11
	22/AUG	13:10	15:09
WSC055	23/AUG	14:50	01:19
	24-25/AUG	13:10	01:09
	26/AUG	13:10	07:11
WSC056	26/AUG	16:00	01:11
WSC057	27/AUG	17:40	01:09
	28/AUG	13:10	14:32
WSC071	3/NOV	17:40	00:49
	4-9/NOV	12:50	00:49
YEAR = 1989			
WSC084	27/JAN	14:40	01:19
	28-31/JAN	13:20	01:19
	1-2/FEB	13:20	01:19
WSC085	3/FEB	15:40	01:19
	4-6/FEB	13:20	01:19
	7/FEB	16:50	17:49
WSC086	8/FEB	23:30	01:19
	9-10/FEB	13:20	01:19
WSC087	11/FEB	14:20	01:19
	12-17/FEB	13:20	01:19
WSC088	18/FEB	13:20	01:19
WSC089	19/FEB	23:30	01:19
	20/FEB	13:20	01:19
	21/FEB	13:20	23:45
WSC090	22-25/FEB	13:20	01:19
	26/FEB	13:20	16:47
WSC091	26/FEB	23:20	01:19
	27/FEB	13:20	20:54
WSC092	2/MAR	22:20	01:19
	3-5/MAR	13:20	01:19

White Sands Missile Range/C-Station, New Mexico

TAPE #	DATE	START	STOP
WSC093	6-9/MAR	13:20	01:19
	10/MAR	13:20	23:11
WSC094	10/MAR	23:40	01:19
	11-16/MAR	13:20	01:19
WSC095	17/MAR	13:20	01:19
	18/MAR	13:20	23:17
WSC095	21/MAR	13:50	01:19
	22-27/MAR	13:00	01:19
WSC098	5-11/APR	13:10	01:09
WSC099	19/APR	14:10	01:09
	20-25/APR	13:10	01:09
WSC100	26-30/APR	13:10	01:09
	1-2/MAY	13:10	01:09
WSC101	3-9/MAY	13:10	01:09
WSC102	10-13/MAY	13:10	01:09
	14/MAY	14:00	01:09
	15-16/MAY	13:10	01:09
WSC103	17-23/MAY	13:10	01:09
WSC104	24/MAY	22:30	01:09
	25-30/MAY	13:10	01:09
WSC105	31/MAY	13:10	01:09
	1-3/JUN	13:10	01:09
	4/JUN	13:10	15:10
WSC106	4/JUN	17:40	01:09
	5-10/JUN	13:10	01:09
WSC107	11-12/JUN	13:10	01:09
	13/JUN	13:10	20:39
WSC108	14-19/JUN	13:10	01:09
WSC109	20/JUN	18:00	01:09
	21/JUN	13:10	15:36
WSC110	21/JUN	18:30	01:09
	22-23/JUN	13:10	01:09
WSC111	4-5/JUL	13:10	01:09
	6/JUL	13:10	21:47

TAPE #	DATE	START	STOP
WSC112	27/JUN	16:20	01:09
	28-30/JUN	13:10	01:09
	1-3/JUL	13:10	01:09
WSC113	6/JUL	22:20	01:09
	7-12/JUL	13:10	01:09
WSC114	13/JUL	14:40	23:08
WSC115	16-21/JUL	13:10	01:09
WSC117	23-29/JUL	13:10	01:09
WSC118	30-31/JUL	13:10	01:09
	1-3/AUG	13:10	01:09
	4/AUG	13:10	19:51
WSC119	5-9/AUG	13:10	01:09
	10/AUG	13:10	19:55
WSC120	10/AUG	21:40	01:09
	11-16/AUG	13:10	01:09
WSC121	17/AUG	14:20	01:09
	18/AUG	13:10	01:09
WSC122	19-22/AUG	13:10	01:09
	23/AUG	13:10	23:03
WSC124	24/AUG	23:02	01:09
	25-30/AUG	13:10	01:09
WSC125	31/AUG	13:10	01:09
	1-4/SEP	13:10	01:09
	5-6/SEP	13:00	00:59
WSC126	7-13/SEP	13:00	00:59
WSC127	14-20/SEP	13:00	00:59
WSC128	21-27/SEP	13:00	00:59
WSC129	28-30/SEP	13:00	00:59
	1/OCT	13:00	00:59
	2-4/OCT	12:50	00:49
WSC130	5-11/OCT	12:50	00:49
WSC131	12-15/OCT	12:50	00:49
WSC132	16-22/OCT	12:50	00:49

White Sands Missile Range/C-Station, New Mexico

TAPE #	DATE	START	STOP
WSC133	23-29/OCT	12:50	00:49
WSC134	30-31/OCT	12:50	00:49
	1-5/NOV	12:50	00:49
WSC135	6-12/NOV	12:50	00:49
WSC136	13-19/NOV	12:50	00:49
WSC137	20/NOV	12:50	00:49
	21/NOV	12:50	19:09
WSC138	21/NOV	19:40	00:49
	22-27/NOV	12:50	00:49
WSC139	28/NOV	14:40	00:49
	29/NOV	12:50	00:49
	30/NOV	13:00	00:59
	1-4/DEC	13:00	00:59
WSC140	5-10/DEC	13:00	00:59
WSC141	12-18/DEC	13:00	00:59
WSC142	19/DEC	13:00	18:20
WSC143	19/DEC	18:50	00:59
	20-22/DEC	13:00	00:59
	23-25/DEC	13:10	01:09
WSC144	26-31/DEC	13:10	01:09

YEAR = 1990

WSC144	1/JAN	13:10	01:09
WSC145	2-8/JAN	13:10	01:09
WSC146	9-15/JAN	13:10	01:09
WSC147	16-22/JAN	13:20	01:19
WSC148	23/JAN	13:20	17:41
WSC149	23/JAN	19:00	01:19
	24-29/JAN	13:20	01:19
WSC150	30/JAN	20:30	01:19
	31/JAN	13:20	01:19
	1-5/FEB	13:20	01:19
WSC151	6-12/FEB	13:20	01:19
WSC152	13/FEB	15:10	01:19
	14-19/FEB	13:20	01:19
WSC153	20/FEB	15:20	01:19
	21-26/FEB	13:20	01:19
WSC154	27/FEB	13:20	01:19
	28/FEB	13:20	20:06
WSC155	28/FEB	20:50	01:19
	1/MAR	13:20	01:19
WSC156	2-6/MAR	13:20	01:19
	7/MAR	13:20	18:18
WSC157	7/MAR	19:00	01:19
	8-13/MAR	13:20	01:19
WSC158	14/MAR	14:40	01:19
	15/MAR	13:10	01:09
	16/MAR	13:10	20:37
WSC159	16/MAR	22:00	01:09
	17-22/MAR	13:10	01:09
WSC160	23-29/MAR	13:10	01:09
WSC161	30/MAR	15:30	01:09
	31/MAR	13:10	01:09
	1-5/APR	13:10	01:09
WSC162	6-9/APR	13:10	01:09
	10/APR	13:10	17:58
WSC163	10/APR	18:20	01:09
	11-16/APR	13:10	01:09
WSC164	17/APR	13:10	01:09
	18-23/APR	13:00	00:59
WSC165	24-25/APR	13:00	00:59
	26/APR	13:00	00:00
WSC167	1/MAY	18:30	00:59
	2-7/MAY	13:00	00:59
WSC168	8-14/MAY	13:00	00:59
WSC169	15/MAY	13:20	00:59
	16-21/MAY	13:00	00:59

White Sands Missile Range/C-Station, New Mexico

TAPE #	DATE	START	STOP
WSC170	22-24/MAY	13:00	00:59
	25/MAY	13:00	23:45
WSC171	18-23/JUL	13:10	01:09
WSC172	24-30/JUL	13:10	01:09
WSC173	21/AUG	21:10	01:09
	22/AUG	13:10	01:09
	23/AUG	13:10	14:24
WSC174	23/AUG	16:20	01:09
	24-29/AUG	13:10	01:09
WSC175	30-31/AUG	13:10	01:09
	1-3/SEP	13:10	01:09
	4-5/SEP	13:00	00:59
WSC176	6-8/SEP	13:00	00:59
	9/SEP	13:00	13:09
WSC177	10/SEP	14:10	00:59
	11-16/SEP	13:00	00:59
WSC178	17/SEP	14:20	00:59
	18-23/SEP	13:00	00:59
WSC179	30/SEP	13:00	00:59
	1-6/OCT	12:50	00:49
WSC180	7-9/OCT	12:50	00:49
	10/OCT	12:50	18:06
WSC181	10/OCT	18:20	00:49
	11-16/OCT	12:50	00:49
WSC182	17-23/OCT	12:50	00:49
WSC183	24-30/OCT	12:50	00:49
WSC184	31/OCT	12:50	00:49
	1-6/NOV	12:50	00:49
WSC185	7-13/NOV	12:50	00:49
WSC186	14/NOV	15:30	00:49
	15-20/NOV	12:50	00:49
WSC187	22/NOV	15:50	00:49
	23-28/NOV	12:50	00:49
WSC188	29-30/NOV	13:00	00:59
	1-5/DEC	13:00	00:59
WSC189	6-12/DEC	13:00	00:59
WSC190	13-19/DEC	13:00	00:59

2.2 White Sands Missile Range/HELSTF, New Mexico

TAPE #	DATE	START	STOP
YEAR = 1988			
WSH001	29/MAR	16:00	18:00
WSH002	30-31/MAR	06:10	18:09
	1-4/APR	06:10	18:09
WSH004	11/APR	16:50	17:51
	12/APR	06:10	08:42
WSH005	12/APR	11:30	18:09
	13-18/APR	06:10	18:09
WSH008	2/MAY	09:10	18:09
	3-8/MAY	06:10	18:09
WSH009	9/MAY	08:20	18:09
	10-14/MAY	06:10	18:09
	15/MAY	06:20	12:12
WSH010	18/MAY	08:20	18:09
	19-24/MAY	06:10	18:09
WSH011	25/MAY	07:10	18:09
	26-31/MAY	06:10	18:09
WSH012	1/JUN	07:10	18:09
	2-7/JUN	06:10	18:09
WSH013	8/JUN	08:30	12:28
* ALL DAYS FROM THIS POINT ON ARE ON ZULU-TIME			
WSH014	9/JUN	21:30	01:09
	10-15/JUN	13:10	01:08
WSH015	16/JUN	14:10	01:09
	17/JUN	13:10	13:38
WSH017	29/JUN	15:20	01:09
	30/JUN	13:10	01:08
WSH018	5/JUL	16:30	20:46
WSH019	6/JUL	14:00	01:09
	7-8/JUL	13:10	01:08
WSH020	11/JUL	18:50	01:09
	12-17/JUL	13:20	01:18

TAPE #	DATE	START	STOP
WSH021	18/JUL	16:00	01:19
	19/JUL	13:20	01:18
	20/JUL	13:20	15:30
WSH022	20/JUL	17:10	01:19
	21-26/JUL	13:20	01:19
WSH023	27/JUL	14:20	23:20
WSH024	28/JUL	19:00	01:19
	29/JUL	13:20	21:00
WSH025	29/JUL	23:20	01:19
	30/JUL	13:20	17:36
WSH026	1/AUG	15:00	01:19
	2/AUG	13:20	00:12
WSH027	3/AUG	15:40	00:40
	4/AUG	13:20	20:23
WSH028	5/AUG	19:20	01:00
	6-7/AUG	13:20	01:19
	8-9/AUG	13:20	00:50
WSH029	12/AUG	20:10	01:09
	13/AUG	13:10	13:09
	14-15/AUG	13:10	01:09
WSH030	16/AUG	14:10	00:40
	17/AUG	13:10	01:09
	18/AUG	13:10	13:10
WSH031	18/AUG	15:00	01:09
	19/AUG	14:10	01:09
	20/AUG	13:10	01:09
	21/AUG	13:10	00:30
	22-24/AUG	13:10	01:09
WSH032	26/AUG	18:20	01:09
	27/AUG	13:10	23:32
WSH033	29/AUG	16:10	01:09
	30-31/AUG	13:10	01:09
	1/SEP	13:10	01:09
	2/SEP	13:10	15:10
WSH034	5/OCT	21:10	00:59
	6-11/OCT	13:00	00:59
WSH035	12/OCT	20:00	00:59
	13-18/OCT	13:00	00:59

White Sands Missile Range/HELSTF, New Mexico

TAPE #	DATE	START	STOP
WSH036	19/OCT	16:40	00:49
	20/OCT	12:50	00:49
WSH037	26/OCT	18:30	00:49
	27-31/OCT	12:50	00:49
	1/NOV	12:50	00:49
WSH038	3/NOV	16:10	00:49
WSH039	23/NOV	20:50	00:59
	24-29/NOV	13:00	00:59
WSH040	30/NOV	17:10	00:59
	1-6/DEC	13:00	00:59
WSH041	7/DEC	16:20	00:59
	8-13/DEC	13:00	00:59
WSH042	14/DEC	16:20	00:59
	15-16/DEC	13:00	00:59
	17-20/DEC	13:10	01:09
WSH043	21/DEC	15:30	01:09
	22/DEC	13:10	20:44

YEAR = 1989

WSH044	3/JAN	20:50	01:09
	4-5/JAN	13:10	01:09
	6/JAN	13:10	15:09
WSH045	6/JAN	17:10	01:09
	7-8/JAN	13:10	01:09
	9-10/JAN	13:20	01:19
	11/JAN	13:20	18:10
WSH046	12/JAN	19:30	01:19
	13-18/JAN	13:20	01:19
WSH047	19/JAN	17:00	01:19
	20-25/JAN	13:20	01:19
WSH048	26/JAN	18:10	01:19
	27-31/JAN	13:20	01:19
	1/FEB	13:20	01:19
WSH049	2/FEB	16:20	01:19
	3-8/FEB	13:20	01:19
WSH050	9-15/FEB	13:20	01:19

TAPE #	DATE	START	STOP
WSH051	16/FEB	16:50	01:19
	17-21/FEB	13:20	01:19
	22/FEB	13:20	18:19
WSH052	27/FEB	19:40	01:19
	28/FEB	13:20	01:19
	1/MAR	13:30	01:08
WSH053	2/MAR	17:00	01:19
	3-8/MAR	13:20	01:19
WSH054	10/MAR	15:50	01:19
	11-16/MAR	13:20	01:19
WSH055	17/MAR	16:20	01:19
	18-20/MAR	13:20	01:19
WSH056	21/MAR	17:30	01:19
	22/MAR	13:20	01:19
	23/MAR	13:20	23:10
WSH057	30/MAR	21:40	01:09
	31/MAR	13:10	01:09
	1-5/APR	13:10	01:09
WSH058	6/APR	16:30	01:09
	7-11/APR	13:10	01:09
	12/APR	13:10	19:09
WSH059	13/APR	15:40	01:09
	14-15/APR	13:10	01:11
	16/APR	14:30	01:09
	17/APR	13:10	01:09
	18/APR	13:50	01:09
	19/APR	13:10	01:09
WSH060	20/APR	15:30	01:09
	21/APR	13:10	01:20
	22-26/APR	13:10	01:09
WSH061	28/APR	15:40	16:00
WSH062	2/MAY	16:00	01:09
	3/MAY	13:10	21:19
WSH063	5/MAY	15:00	01:09
	6/MAY	13:10	01:09
	7/MAY	13:10	23:09
WSH064	8/MAY	15:20	01:09
	9/MAY	13:10	01:09

White Sands Missile Range/HELSTF, New Mexico

TAPE #	DATE	START	STOP
WSH065	10/MAY	15:20	00:42
WSH066	18/MAY	18:20	01:09
	19/MAY	13:10	01:09
	20/MAY	13:10	15:09
WSH067	22/MAY	15:40	01:09
	23/MAY	13:30	01:09
	24/MAY	15:30	01:09
WSH068	25/MAY	16:20	01:09
	26-29/MAY	13:10	01:09
	30/MAY	13:10	19:00
WSH069	1/JUN	15:10	01:09
	2-7/JUN	13:10	01:09
WSH070	12/JUN	15:10	01:09
	13/JUN	13:10	01:09
	14/JUN	13:10	19:54
WSH071	14/JUN	22:30	01:09
	15/JUN	13:10	01:09
	16/JUN	13:10	22:41
WSH072	19/JUN	15:20	01:09
	20-25/JUN	13:10	01:09
WSH073	26/JUN	15:20	01:09
	27/JUN	13:10	21:18
WSH074	28/JUN	16:40	01:09
	29-30/JUN	13:10	01:09
	1-3/JUL	13:10	19:09
	4/JUL	13:10	20:09
WSH075	5/JUL	15:30	01:09
	6-7/JUL	13:10	01:09
	8/JUL	13:10	21:09
	9/JUL	13:10	22:59
WSH076	11/JUL	15:40	01:09
	12/JUL	13:10	16:54
WSH077	12/JUL	18:30	01:09
	13-14/JUL	13:10	01:09
	15/JUL	13:10	00:09
	16-18/JUL	13:10	01:09
WSH078	19/JUL	15:10	01:09
	20-25/JUL	13:10	01:09
WSH079	26/JUL	15:10	01:09
	27-31/JUL	13:10	01:09
	1/AUG	13:10	01:09
WSH080	2/AUG	16:20	01:09
	3-8/AUG	13:10	01:09
WSH081	9/AUG	14:30	01:09
	10/AUG	13:10	01:09
	11/AUG	13:10	00:59
WSH082	15/AUG	16:20	01:09
	16/AUG	13:10	01:09
	17/AUG	13:48	01:09
	18-21/AUG	13:10	01:09
WSH083	22/AUG	19:30	01:09
	23/AUG	13:10	16:16
WSH084	24/AUG	17:40	19:11
WSH085	24/AUG	19:14	01:09
	25-30/AUG	13:10	01:09
WSH086	31/AUG	15:50	01:09
	1-2/SEP	13:10	01:09
	3/SEP	13:10	22:27
WSH087	5/SEP	15:50	00:59
	6-8/SEP	13:00	00:59
	9/SEP	13:00	00:19
WSH088	12/SEP	15:20	00:59
	13-18/SEP	13:00	00:59
WSH089	19/SEP	15:10	00:59
	20-25/SEP	13:00	00:59
WSH090	26/SEP	15:20	00:59
	27-28/SEP	13:00	00:59
	29/SEP	13:00	13:05
WSH091	3/OCT	13:50	18:31
WSH092	3/OCT	18:40	00:49
	4-5/OCT	12:50	00:49
	6/OCT	12:50	16:08
WSH093	6/OCT	16:20	00:49
	7-12/OCT	12:50	00:49

White Sands Missile Range/HELSTF, New Mexico

TAPE #	DATE	START	STOP
WSH094	13/OCT	15:30	00:49
	14-18/OCT	12:50	00:49
	19/OCT	12:50	16:27
WSH095	20/OCT	19:50	00:49
	21-26/OCT	12:50	00:49
WSH096	27/OCT	15:40	00:49
	28-31/OCT	12:50	00:49
	1-2/NOV	12:50	00:49
WSH097	3/NOV	16:00	00:49
	4-9/NOV	12:50	00:49
WSH098	10/NOV	17:40	00:49
	11-12/NOV	12:50	00:49
	13/NOV	12:50	21:29
WSH099	15-21/NOV	12:50	00:49
WSH100	22/NOV	16:50	00:49
	23-28/NOV	12:50	00:49
WSH101	29/NOV	15:10	00:49
	30/NOV	13:00	00:59
	1-3/DEC	13:00	00:59
	4/DEC	13:00	23:28
WSH102	5/DEC	13:00	17:40
WSH103	6/DEC	22:30	00:58
	7-12/DEC	13:00	00:58
WSH104	13/DEC	15:20	00:58
	14-19/DEC	13:00	00:58
WSH105	20/DEC	16:00	00:58
	21-22/DEC	13:00	00:58
	23-26/DEC	13:10	01:08
WSH106	27/DEC	15:39	18:15
WSH107	27/DEC	19:50	01:08
	28-31/DEC	13:10	01:08

YEAR = 1990

WSH107	1-2/JAN	13:10	01:08
WSH108	3/JAN	16:30	01:08
	4-9/JAN	13:10	01:08
WSH109	17/JAN	17:10	01:18
	18-23/JAN	13:20	01:18
WSH110	10/JAN	15:40	01:08
	11-15/JAN	13:10	01:08
	16/JAN	13:20	01:18
WSH111	24/JAN	16:10	01:18
	25-30/JAN	13:20	01:18
WSH112	31/JAN	15:20	01:18
	1-6/FEB	13:20	01:18
WSH113	7/FEB	16:10	01:18
	8-9/FEB	13:20	01:18
	10/FEB	13:20	21:22
WSH114	12/FEB	16:10	01:18
	13-18/FEB	13:20	01:18
WSH115	20/FEB	16:20	01:18
	21-26/FEB	13:20	01:18
WSH116	28/FEB	15:50	01:18
	1-6/MAR	13:20	01:18
WSH117	7/MAR	16:10	01:18
	8-13/MAR	13:20	01:18
WSH118	14/MAR	17:20	01:18
	15-20/MAR	13:10	01:08
WSH119	21/MAR	16:10	01:08
	22-26/MAR	13:10	01:08
	27/MAR	13:10	17:01
WSH120	27/MAR	20:20	01:08
	28-31/MAR	13:10	01:08
	1-2/APR	13:10	01:08
WSH121	3/APR	16:30	01:08
	4-9/APR	13:10	01:08
WSH122	10/APR	14:50	01:08
	11-16/APR	13:10	01:08
WSH123	17/APR	14:30	01:08
	18-23/APR	13:00	00:58

White Sands Missile Range/HELSTF, New Mexico

TAPE #	DATE	START	STOP
WSH124	24/APR	15:50	00:58
	25-26/APR	13:00	00:58
	27/APR	13:00	22:06
WSH125	30/APR	14:40	22:17
WSH126	1/MAY	16:30	00:58
	2/MAY	13:00	00:58
	3/MAY	13:00	17:39
WSH127	10/MAY	16:10	00:58
	11-15/MAY	13:00	00:58
	16/MAY	13:00	16:59
WSH128	17/MAY	16:20	00:58
	18-20/MAY	13:00	00:58
WSH129	24/MAY	19:40	00:58
	25/MAY	13:00	15:24
WSH130	25/MAY	20:00	00:59
	26-31/MAY	13:00	00:59
WSH131	5/JUN	16:50	00:59
	6-8/JUN	13:00	00:59
	9/JUN	13:10	01:09
	10/JUN	13:10	14:09
WSH132	11/JUN	16:00	01:09
	12-17/JUN	13:10	01:09
WSH133	18/JUN	14:50	01:09
	19-24/JUN	13:10	01:09
WSH135	9/JUL	17:20	01:09
	10/JUL	13:10	01:09
	11/JUL	13:10	15:36
WSH136	2/JUL	16:10	01:09
	3-6/JUL	13:10	01:09
	7/JUL	14:07	01:09
	8/JUL	13:10	01:09
WSH137	11/JUL	20:10	01:09
	12-17/JUL	13:10	01:09
WSH138	23/JUL	14:50	01:09
	24-26/JUL	13:10	01:09
WSH139	18/JUL	15:30	01:09
	19-22/JUL	13:10	01:09
	23/JUL	13:10	14:39
WSH140	27/JUL	16:10	01:09
	28-31/JUL	13:10	01:09
	1-2/AUG	13:10	01:09
WSH141	3/AUG	14:40	17:23
WSH142	3/AUG	19:10	01:09
	4-7/AUG	13:10	01:09
	8/AUG	13:10	14:10
WSH143	8/AUG	14:20	01:09
	9-14/AUG	13:10	01:09
WSH144	15/AUG	15:40	01:09
	16/AUG	13:10	01:09
	17/AUG	13:10	15:53
WSH145	20/AUG	14:30	01:09
	21-26/AUG	13:10	01:09
WSH146	27/AUG	16:10	01:09
	28-31/AUG	13:10	01:09
	1-2/SEP	13:10	01:09
WSH147	5/SEP	15:50	00:59
	6-8/SEP	13:00	00:59
WSH148	10/SEP	17:50	00:59
	11-16/SEP	13:00	00:59
WSH149	18/SEP	22:10	00:59
	19-24/SEP	13:00	00:59
WSH150	25/SEP	16:30	00:59
	26-27/SEP	13:00	00:59
	28/SEP	13:00	18:46
WSH151	28/SEP	19:10	00:59
	29-30/SEP	13:00	00:59
	1-4/OCT	12:50	00:49
WSH152	5/OCT	16:40	00:49
	6-8/OCT	12:50	00:49
	9/OCT	12:50	15:21
WSH153	9/OCT	15:50	00:49
	10-15/OCT	12:50	00:49
WSH154	16/OCT	16:30	00:49
	17-22/OCT	12:50	00:49

White Sands Missile Range/HELSTF, New Mexico

TAPE #	DATE	START	STOP
WSH155	23/OCT	14:50	00:49
	24-29/OCT	12:50	00:49
WSH156	30/OCT	18:40	00:49
	31/OCT	12:50	00:49
	1/NOV	12:50	00:49
	2/NOV	12:50	00:29
WSH157	5/NOV	16:30	00:49
	6-8/NOV	12:50	00:49
WSH158	13/NOV	17:40	00:49
	14/NOV	12:50	19:29
WSH159	14/NOV	21:20	00:49
	15/NOV	12:50	00:49
	16/NOV	12:50	17:08
WSH160	16/NOV	17:40	00:49
	17-19/NOV	12:50	00:49
	20/NOV	12:50	21:42
WSH161	20/NOV	22:00	00:49
	21-26/NOV	12:50	00:49
WSH162	27/NOV	16:40	00:49
	28/NOV	12:50	00:49
	29-30/NOV	13:00	00:59
	1-3/DEC	13:00	00:59
WSH163	4/DEC	16:40	00:59
	5-10/DEC	13:00	00:59
WSH164	11/DEC	16:00	00:59
	12-17/DEC	13:00	00:59
WSH165	18/DEC	16:10	00:59
	19-21/DEC	13:00	00:59
	22-24/DEC	13:10	01:09
WSH166	26/DEC	16:00	01:09
	27-31/DEC	13:10	01:09

2.3 Kirtland Air Force Base, Albuquerque, New Mexico

TAPE #	DATE	START	STOP
YEAR = 1988			
KAA001	17/MAY	19:30	01:08
	18-23/MAY	13:10	01:08
KAA002	24-30/MAY	13:10	01:08
KAA003	31/MAY	13:10	01:08
	1-2/JUN	13:10	01:08
	3/JUN	13:10	
KAA004	3/JUN	16:40	01:08
	4-9/JUN	13:10	01:08
KAA005	10-13/JUN	13:10	01:08
	14/JUN	13:10	
KAA006	14-20/JUN	13:10	01:08
KAA007	21-27/JUN	13:10	01:08
KAA008	28/JUN	13:10	18:02
KAA009	28/JUN	20:40	22:40
	29-30/JUN	13:10	00:10
	1-4/JUL	13:10	00:10
KAA010	5/JUL	13:10	01:09
	6-8/JUL	13:20	01:18
	9/JUL	13:20	00:58
KAA011	19/JUL	20:30	01:19
	20/JUL	13:10	01:19
	21/JUL	13:10	19:42
KAA012	21/JUL	20:30	01:19
	22-23/JUL	13:20	01:19
	24/JUL	13:20	00:00
KAA013	25/JUL	16:40	01:19
	26/JUL	13:20	17:14
KAA014	1/AUG	20:30	23:30
KAA015	2/AUG	17:30	01:19
	3-7/AUG	13:20	01:19
	8/AUG	14:20	21:04
KAA016	9/AUG	16:20	01:19
	10-15/AUG	13:20	01:19
KAA017	16/AUG	13:20	23:00
KAA018	17/AUG	13:50	01:09
	18-23/AUG	13:10	01:09
KAA019	24/AUG	13:10	20:30
KAA020	25/AUG	14:10	01:09
	26-31/AUG	13:10	01:09
KAA021	1/SEP	13:10	20:50
KAA022	1/SEP	21:20	01:09
	2-7/SEP	13:10	01:09
KAA023	8/SEP	13:50	01:09
	9/SEP	13:10	16:30
KAA024	12/SEP	14:00	01:09
	13/SEP	13:10	16:30
KAA025	14/SEP	16:10	01:09
	15/SEP	13:10	13:34
KAA026	15/SEP	13:50	01:09
	16/SEP	13:10	13:34
	17-21/SEP	13:00	00:59
KAA027	22/SEP	13:00	20:40
KAA028	23/SEP	16:30	19:00
KAA030	1/OCT	20:30	00:59
	2-3/OCT	13:00	00:59
	4/OCT	13:00	16:20
KAA031	6/OCT	16:40	00:59
	7/OCT	13:00	00:59
	8/OCT	13:00	18:50
KAA032	13/OCT	13:20	00:59
	14-19/OCT	13:00	00:59
KAA033	20/OCT	13:00	15:34
KAA034	2/NOV	23:40	00:49
	3-7/NOV	12:50	00:49
KAA035	9-13/NOV	12:50	00:49
	14-15/NOV	13:00	00:59
KAA036	16-20/NOV	13:00	00:59
	21/NOV	13:00	17:35

Kirtland Air Force Base, Albuquerque, New Mexico

TAPE #	DATE	START	STOP
KAA037	21/NOV	22:50	00:59
	22-27/NOV	13:00	00:59
KAA038	28/NOV	21:20	00:59
	29/NOV	13:00	00:59
	30/NOV	13:00	23:59
KAA039	5-10/DEC	13:00	00:59
	11/DEC	13:00	00:06
KAA040	12-14/DEC	13:00	00:59
	15-17/DEC	13:10	01:09
KAA041	19/DEC	16:00	01:09
	20-25/DEC	13:10	01:09
KAA042	26/DEC	14:20	01:09
	27-31/DEC	13:10	01:09

YEAR = 1989

KAA042	1/JAN	13:10	01:09
KAA047	30/JAN	20:10	01:19
	31/JAN	13:20	01:19
	1-5/FEB	13:20	01:19
KAA048	6/FEB	13:30	01:19
	7/FEB	13:20	17:22
KAA049	9/FEB	18:00	01:19
	10-15/FEB	13:20	01:19
KAA050	16-20/FEB	13:20	01:19
	21/FEB	13:20	16:20
KAA051	22/FEB	16:40	01:19
	23-28/FEB	13:20	01:19
KAA052	1-7/MAR	13:20	01:19
KAA053	8-14/MAR	13:20	01:19
KAA054	15-19/MAR	13:20	01:19
	20/MAR	13:20	22:48
KAA055	22-28/MAR	13:20	01:19
KAA056	29-30/MAR	13:20	01:19
	31/MAR	13:10	01:09
	1-4/APR	13:10	01:09
KAA057	5/APR	13:30	18:50
KAA058	5/APR	18:40	01:09
	6-11/APR	13:10	01:09
KAA059	12/APR	13:40	01:09
	13-15/APR	13:10	01:09
	16/APR	13:20	01:09
	17-18/APR	13:10	01:09
KAA061	20/APR	14:40	01:09
	21-26/APR	13:10	01:09
KAA062	27-30/APR	13:10	01:09
	1-3/MAY	13:10	01:09
KAA063	5-10/MAY	13:10	01:09
KAA064	11-17/MAY	13:10	01:09
KAA065	18-24/MAY	13:10	01:09
KAA066	25/MAY	13:20	01:09
	26/MAY	13:10	01:09
	27/MAY	13:10	13:30
KAA067	27/MAY	23:20	01:09
	28-31/MAY	13:10	01:09
	1-2/JUN	13:10	01:09
KAA068	3-9/JUN	13:10	01:09
KAA069	10-14/JUN	13:10	01:09
	15/JUN	13:10	20:17
KAA070	15/JUN	22:40	01:09
	16-20/JUN	13:10	01:09
	21/JUN	13:10	20:39
KAA072	29/JUN	15:20	01:09
	30/JUN	13:10	01:09
	1-5/JUL	13:10	01:09
KAA073	6/JUL	13:10	20:30
KAA075	14/JUL	22:20	01:09
	15-18/JUL	13:10	01:09
	19/JUL	13:10	18:46

Kirtland Air Force Base, Albuquerque, New Mexico

TAPE #	DATE	START	STOP
KAA076	7/JUL	23:00	01:09
	8-13/JUL	13:10	01:09
KAA077	19/JUL	22:00	01:09
	20-25/JUL	13:10	01:09
KAA078	26-31/JUL	13:10	01:09
	1/AUG	13:10	01:09
KAA079	2-8/AUG	13:10	01:09
KAA080	9-15/AUG	13:10	01:09
KAA081	16-22/AUG	13:10	01:09
KAA082	23/AUG	13:20	01:09
	24-27/AUG	13:10	01:09
	28/AUG	13:10	16:40
KAA083	29/AUG	17:00	01:09
	30-31/AUG	13:10	01:09
	1-4/SEP	13:10	01:09
KAA084	5-6/SEP	13:10	01:09
	7-11/SEP	13:00	00:59
KAA085	12/SEP	13:00	19:28
KAA086	13/SEP	21:30	00:59
	14-19/SEP	13:00	00:59
KAA087	20-26/SEP	13:00	00:59
KAA088	27-30/SEP	13:00	00:59
	1-3/OCT	13:00	00:59
KAA089	4/OCT	13:20	00:59
	5/OCT	12:50	13:49
KAA090	5/OCT	19:50	00:49
	6-11/OCT	12:50	00:49
KAA091	12/OCT	21:20	00:49
	13-18/OCT	12:50	00:49
KAA092	19/OCT	13:20	00:49
	20-25/OCT	12:50	00:49
KAA093	26/OCT	13:10	00:49
	27-30/OCT	12:50	00:49
	31/OCT	12:50	17:49
KAA094	2/NOV	12:50	16:41
KAA095	2/NOV	18:10	00:49
	3-8/NOV	12:50	00:49
KAA096	10-16/NOV	12:50	00:49
KAA097	17-23/NOV	12:50	00:49
KAA098	24-26/NOV	12:50	00:49
	27-29/NOV	13:00	00:59
	30/NOV	13:00	00:05
KAA099	1-6/DEC	13:00	00:59
KAA100	7/DEC	23:20	00:59
	8-13/DEC	13:00	00:59
KAA101	14/DEC	23:50	00:59
	15-20/DEC	13:00	00:59
KAA102	21-26/DEC	13:10	01:09
	27/DEC	13:10	22:21
KAA103	27/DEC	22:50	01:09
	28-31/DEC	13:10	01:09

YEAR = 1990

KAA103	1/JAN	13:10	01:09
	2/JAN	13:10	00:06
KAA104	3-8/JAN	13:10	01:09
KAA105	9/JAN	14:20	01:09
	10-12/JAN	13:10	01:09
	13-15/JAN	13:20	01:19
KAA106	16/JAN	14:10	01:19
	17-22/JAN	13:20	01:19
KAA107	6/FEB	14:00	01:19
	7-8/FEB	13:20	01:19
	9/FEB	13:20	00:19
KAA108	30/JAN	14:00	01:19
	31/JAN	13:20	01:19
	1-5/FEB	13:20	01:19

Kirtland Air Force Base, Albuquerque, New Mexico

TAPE #	DATE	START	STOP
KAA109	12/FEB	23:20	01:19
	13-15/FEB	13:20	01:19
	16/FEB	13:20	22:59
KAA110	16/FEB	23:10	01:19
	17/FEB	13:20	01:19
	18/FEB	13:20	19:13
KAA111	20/FEB	17:50	01:19
	21-23/FEB	13:20	01:19
	24/FEB	13:20	23:36
KAA112	26/FEB	15:00	01:19
	27-28/FEB	13:20	01:19
	1-4/MAR	13:20	01:19
KAA113	5/MAR	14:20	01:19
	6-7/MAR	13:20	01:19
	8/MAR	13:20	14:20
KAA114	9/MAR	21:20	01:19
	10-15/MAR	13:20	01:19
KAA115	16/MAR	14:10	01:19
	17-18/MAR	13:20	01:19
	19/MAR	13:10	01:09
	20/MAR	13:10	22:33
	21/MAR	13:10	17:28
KAA116	6/APR	21:20	01:09
	7-9/APR	13:10	01:09
	10/APR	13:10	19:06
	11/APR	13:10	20:12
	12/APR	13:10	00:34
KAA117	17/MAY	22:20	00:59
	18/MAY	13:00	16:07
KAA118	18/MAY	17:20	00:59
	19-24/MAY	13:00	00:59
KAA119	29/MAY	16:00	00:59
	30-31/MAY	13:00	00:59
	1-2/JUN	13:00	00:59
	3-4/JUN	13:10	01:09
KAA120	6/JUN	15:20	01:09
	7-12/JUN	13:10	01:09
KAA121	13/JUN	21:20	01:09
	14-19/JUN	13:10	01:09
KAA122	20/JUN	20:10	01:09
	21/JUN	13:10	21:42
KAA123	22/JUN	17:16	17:31
KAA124	18/JUL	22:40	01:09
	19-24/JUL	13:10	01:09
KAA125	3/AUG	15:40	01:09
	4-8/AUG	13:10	01:09
	9/AUG	13:10	17:00
KAA126	26/AUG	20:40	01:09
	27-31/JUL	13:10	01:09
	1/AUG	13:10	01:09
KAA127	9/AUG	17:20	01:09
	10-15/AUG	13:10	01:09
KAA128	20/AUG	14:20	01:09
	21-26/AUG	13:10	01:09
KAA129	27/AUG	14:50	01:09
	28-31/AUG	13:10	01:09
	1-2/SEP	13:10	01:09
KAA130	4/SEP	18:50	01:09
	5/SEP	13:10	01:09
	6-7/SEP	13:00	00:59
	8/SEP	13:00	15:00
KAA131	12/SEP	17:30	00:59
	13-18/SEP	13:00	00:59
KAA132	20/SEP	14:30	00:59
	21-26/SEP	13:00	00:59
KAA133	1/OCT	15:40	00:59
	2-3/OCT	13:00	00:59
	4/OCT	12:50	00:49
	5/OCT	12:50	17:07
KAA134	11/OCT	14:50	00:49
	12-16/OCT	12:50	00:49
	17/OCT	12:50	14:16
KAA135	17/OCT	14:30	00:49
	18/OCT	12:50	16:32
KAA136	24/OCT	13:50	00:49
	25/OCT	12:50	00:49
	26/OCT	12:50	20:59

APPENDIX A

Kirtland Air Force Base, Albuquerque, New Mexico

TAPE #	DATE	START	STOP
KAA141	11/DEC	21:30	00:59
	12-17/DEC	13:00	00:59
KAA142	19/DEC	15:10	00:59
	20-25/DEC	13:10	01:09

2.4 Naval Weapons Center, China Lake, California

TAPE #	DATE	START	STOP
YEAR = 1988			
CL4001	23/JUN	19:30	01:08
CL4002	23/JUN	23:00	01:52
CL4004	1-4/JUL	14:00	01:58
	5/JUL	14:00	19:26
CL4005	5/JUL	19:50	01:59
	6-11/JUL	14:00	01:12
CL4006	12-18/JUL	14:00	01:12
CL4007	19/JUL	19:10	01:59
	20/JUL	14:00	00:10
CL4008	21-22/JUL	14:00	01:12
CL4009	22/JUL	23:30	01:30
	23-28/JUL	14:00	01:12
CL4010	29-31/JUL	14:00	01:58
	1/AUG	23:59	01:58
	2-3/AUG	14:00	01:58
	4/AUG	14:00	19:59
CL4011	5-11/AUG	14:00	01:58
CL4012	12-13/AUG	14:00	01:59
CL4013	14-15/AUG	14:00	01:58
	16/AUG	14:00	00:58
	17/AUG	14:00	01:58
	18/AUG	14:00	00:58
CL4014	19-20/AUG	14:00	01:58
	21/AUG	14:00	23:58
	22/AUG	14:00	00:58
	23/AUG	14:00	01:58
CL4015	24/AUG	14:00	01:59
CL4016	25/AUG	17:20	01:59
	26/AUG	14:00	20:50
CL4017	26/AUG	21:10	01:58
	27/AUG	14:00	01:58
	28/AUG	14:00	01:04
CL4018	29/AUG	16:50	01:59
	30-31/AUG	14:00	01:58
CL4019	5-8/SEP	13:50	01:48
	9/SEP	13:50	18:30
CL4023	4/NOV	20:40	01:39
	6-7/NOV	13:40	01:39
	8/NOV	13:40	17:14
CL4024	8/NOV	21:00	01:39
	9-14/NOV	13:40	01:39
CL4025	15-19/NOV	13:40	01:39
	20/NOV	14:50	01:39
	22/NOV	13:40	01:39
CL4026	23-24/NOV	13:40	01:39
	25/NOV	13:40	14:59
	26/NOV	15:00	01:39
CL4027	28/NOV	20:10	01:39
CL4028	29/NOV	17:50	01:39
CL4029	30/NOV	19:00	01:39
CL4030	1/DEC	16:00	01:39
CL4031	2/DEC	17:30	01:39
CL4032	3/DEC	15:20	01:49
	4/DEC	13:50	01:49
CL4033	5/DEC	15:40	01:49
CL4034	6/DEC	18:20	01:49
CL4035	7/DEC	16:00	01:49
	8-9/DEC	13:50	01:49
	10/DEC	21:51	21:00
CL4036	11/DEC	23:10	15:58
CL4037	13/DEC	16:20	17:19
CL4038	13/DEC	17:30	01:49
	14/DEC	23:56	00:36
	16/DEC	13:50	01:49
	17/DEC	15:40	23:27
CL4039	21/DEC	15:10	01:49
	22-24/DEC	13:50	01:49

Naval Weapons Center, China Lake, California

TAPE #	DATE	START	STOP
CL4040	27/DEC	18:50	01:59
	28/DEC	15:00	00:51
	29/DEC	14:00	15:20
YEAR = 1989			
CL4041	4/JAN	14:58	01:59
	5/JAN	14:19	01:59
	6/JAN	13:58	01:59
	7/JAN	15:43	00:48
	8/JAN	16:24	00:48
	9/JAN	15:11	10:50
	10/JAN	14:00	01:59
CL4042	11/JAN	15:20	01:59
	12/JAN	15:46	06:14
	13/JAN	23:00	07:18
	14/JAN	15:07	01:08
	15/JAN	15:07	08:01
CL4043	17/JAN	13:58	01:59
	18-19/JAN	15:18	01:59
CL4044	20/JAN	16:04	01:59
	21/JAN	15:20	02:09
	22/JAN	15:50	02:09
	23/JAN	15:34	02:09
	24/JAN	15:20	02:09
	25/JAN	11:40	11:40
	26/JAN	14:10	02:09
CL4045	27/JAN	14:08	06:01
	28/JAN	15:40	02:09
	29/JAN	15:56	02:09
	30/JAN	15:46	02:09
	31/JAN	02:09	02:09
	1/FEB	15:10	02:09
	2/FEB	14:20	02:09
CL4046	3/FEB	14:08	02:09
	4/FEB	15:36	01:05
	6/FEB	14:56	02:09
	7/FEB	15:57	00:28
	8/FEB	15:14	04:17
	9/FEB	14:10	02:09
	11/FEB	15:04	01:28

TAPE #	DATE	START	STOP
CL4047	20/FEB	18:40	02:09
	21/FEB	15:10	02:09
	22/FEB	14:50	02:09
	23/FEB	14:15	02:09
	24-25/FEB	14:08	02:09
	26/FEB	02:09	02:09
CL4049	6/MAR	14:45	02:09
	7/MAR	22:50	02:09
	8/MAR	14:08	02:09
	9-10/MAR	14:40	02:09
	11/MAR	16:50	02:09
CL4050	12/MAR	14:08	14:10
	13/MAR	13:00	01:59
CL4051	16/MAR	17:00	00:15
CL4053	5/APR	23:20	01:59
	6-9/APR	13:58	01:59
	10/APR	21:29	21:29
CL4054	11/APR	18:40	01:59
	12-14/APR	14:00	01:59
	15-17/APR	13:50	01:49
CL4055	17-23/APR	13:50	01:49
CL4056	24/APR	13:50	01:49
CL4057	25/APR	13:50	01:49
	26/APR	13:50	21:02
CL4058	29/APR	20:10	01:49
	30/APR	13:50	01:49
	1-5/MAY	13:50	01:49
CL4059	6/MAY	13:50	01:49
	7/MAY	13:50	21:23
CL4061	15-20/MAY	13:50	01:49
CL4062	21-27/MAY	13:50	01:49
CL4063	31/MAY	17:00	01:49
	1-5/JUN	13:50	01:49
CL4064	7/JUN	17:00	01:49
	8-13/JUN	13:50	01:49

Naval Weapons Center, China Lake, California

TAPE #	DATE	START	STOP
CL4065	14-16/JUN	13:50	23:59
	17/JUN	13:50	01:49
	18-20/JUN	13:50	23:59
CL4066	23-29/JUN	13:50	01:49
CL4067	30/JUN	20:00	01:49
	1-4/JUL	14:00	01:59
	5/JUL	14:00	21:45
CL4068	9/JUL	17:10	01:59
	10-15/JUL	14:10	01:58
CL4069	18-24/JUL	14:00	01:58
CL4070	25-31/JUL	14:00	01:58
CL4071	1/AUG	15:10	01:58
	2-7/AUG	14:00	01:58
CL4072	8/AUG	17:30	01:58
	9-14/AUG	14:00	01:58
CL4073	15/AUG	15:00	01:59
	16-19/AUG	14:00	01:59
	20-21/AUG	13:50	01:49
CL4074	22-28/AUG	13:50	01:48
CL4075	29/AUG	15:10	01:49
	30-31/AUG	13:50	01:49
	1-4/SEP	13:50	01:48
CL4076	5/SEP	14:10	01:49
	6-8/SEP	13:50	01:48
	9/SEP	14:30	01:48
	10-11/SEP	13:50	01:48
CL4077	12-18/SEP	13:50	01:49
CL4078	19/SEP	14:20	01:39
	20-22/SEP	13:40	01:39
	23/SEP	13:53	01:39
	24/SEP	14:00	01:39
	25/SEP	13:40	01:39
CL4079	26/SEP	17:30	01:39
	27-28/SEP	13:40	01:39
	29/SEP	13:40	20:14
CL4080	1-4/OCT	13:40	01:39
CL4081	6/OCT	22:30	01:39
	7-8/OCT	13:40	01:39
	9/OCT	13:40	23:39
	10-11/OCT	13:40	01:38
	12/OCT	13:40	21:05
CL4082	12/OCT	23:10	01:39
	13/OCT	13:40	14:50
CL4083	13/OCT	16:10	01:39
	14/OCT	13:40	01:39
	15/OCT	15:11	22:56
CL4084	17/OCT	20:19	21:19
CL4085	18/OCT	21:30	01:39
	19/OCT	13:40	15:49
CL4086	20/OCT	16:50	01:39
	21/OCT	13:40	01:39
	22/OCT	13:40	15:02
CL4087	24/OCT	23:50	01:39
	25/OCT	13:40	19:46
CL4088	25/OCT	23:00	01:39
	26/OCT	13:40	01:39
	27-31/OCT	13:30	01:29
CL4089	1/NOV	13:30	15:07
CL4090	11/NOV	23:40	01:39
	12-15/NOV	13:40	01:39
	16/NOV	13:40	17:21
CL4091	20/NOV	18:00	01:39
	21-26/NOV	13:40	01:39
CL4092	27/NOV	17:10	01:39
	28-30/NOV	13:40	01:39
	1-3/DEC	13:40	01:39
CL4093	4/DEC	18:30	01:39
	5-7/DEC	13:40	01:39
	8/DEC	13:40	21:35
CL4094	10/DEC	20:50	01:39
	11/DEC	13:40	18:00
CL4095	12/DEC	23:50	01:49
	13/DEC	13:50	01:49
	14/DEC	13:50	16:38

Naval Weapons Center, China Lake, California

TAPE #	DATE	START	STOP
CL4096	15-18/DEC	13:50	01:49
	19/DEC	13:50	17:01
CL4097	21/DEC	20:20	01:49
	22-27/DEC	13:50	01:49
CL4098	28-31/DEC	13:50	01:49

YEAR = 1990

CL4098	1/JAN	13:50	01:49
	2-3/JAN	14:00	01:59
CL4099	4/JAN	21:30	01:59
	5-10/JAN	14:00	01:59
CL4100	11/JAN	21:20	01:59
	12-17/JAN	14:00	01:59
CL4101	21/JAN	21:30	01:59
	22-27/JAN	14:00	01:59
CL4102	29/JAN	21:50	01:59
	30-31/JAN	14:00	01:59
	1-4/FEB	14:00	01:59
CL4103	5-11/FEB	14:10	02:09
CL4104	7/MAR	19:40	01:59
	8-13/MAR	14:00	01:59
CL4105	14-17/MAR	14:00	01:59
	18/MAR	14:00	21:38
CL4106	18/APR	17:40	01:49
CL4107	23-29/APR	13:50	01:49
CL4108	1-7/MAY	13:50	01:49
CL4109	8/MAY	22:30	01:49
	9-14/MAY	13:50	01:49
CL4110	16/MAY	16:00	01:49
	17-18/MAY	13:50	01:49
	19/MAY	13:50	16:51
CL4111	21-27/MAY	13:50	01:49

TAPE #	DATE	START	STOP
CL4112	29/MAY	19:10	01:49
	30-31/MAY	13:50	01:49
	1-3/JUN	13:50	01:49
	4/JUN	13:50	18:02
CL4113	5-8/JUN	13:50	01:49
	9/JUN	13:50	19:57
CL4114	12/JUN	16:00	01:49
	13/JUN	13:50	01:49
	14/JUN	13:50	18:03
CL4115	3/JUL	20:30	01:59
	4-9/JUL	14:00	01:59
CL4116	19/JUL	21:20	01:59
	20/JUL	14:00	21:59
CL4117	2/AUG	20:00	01:59
	3/AUG	14:00	16:15
CL4118	3/AUG	18:00	01:59
	4-9/AUG	14:00	01:59
CL4119	10/AUG	16:40	01:59
	11-16/AUG	14:00	01:59
CL4120	17/AUG	16:30	01:59
	18/AUG	14:00	01:59
	19-23/AUG	13:50	01:49
CL4121	26/AUG	21:20	01:49
	27-31/AUG	13:50	01:49
	1/SEP	13:50	01:49
CL4122	4-10/SEP	13:50	01:48
CL4123	11-17/SEP	13:50	01:48
CL4124	18-24/SEP	13:40	01:39
CL4125	25-30/SEP	13:40	01:39
	1/OCT	13:40	01:39
CL4126	2-7/OCT	13:40	01:39
	8/OCT	23:00	01:39
CL4127	9-15/OCT	13:40	01:39
CL4128	16-22/OCT	13:40	01:39

Naval Weapons Center, China Lake, California

TAPE #	DATE	START	STOP
CL4129	23-25/OCT	13:40	01:39
	26-29/OCT	13:30	01:29
CL4130	30-31/OCT	13:30	01:29
	1-4/NOV	13:30	01:29
	5/NOV	13:40	01:39
CL4131	6-12/NOV	13:40	01:39
CL4132	13/NOV	15:40	01:39
	14-19/NOV	13:40	01:39
CL4133	20-24/NOV	13:40	01:39
CL4134	28-30/NOV	13:40	01:39
	1-3/DEC	13:40	01:39
CL4135	5/DEC	22:00	01:39
	6/DEC	13:40	21:28

2.5 Malmstrom Air Force Base, Montana

TAPE #	DATE	START	STOP
YEAR = 1988			
MAG001	30/AUG	20:40	01:29
	31/AUG	13:30	14:58
MAG002	31/AUG	16:20	21:10
MAG003	31/AUG	22:00	01:29
	1-6/AUG	13:30	01:29
MAG004	8/SEP	16:50	01:29
	9-12/SEP	13:30	01:29
	13-14/SEP	13:20	01:19
MAG005	16/SEP	15:40	01:19
	17-22/SEP	13:20	01:19
MAG006	23/SEP	13:50	01:19
	24-29/SEP	13:20	01:19
MAG007	30/SEP	14:50	01:19
	1-6/OCT	13:20	01:19
MAG008	7/OCT	14:20	01:19
	8-12/OCT	13:20	01:19
	13/OCT	13:10	01:09
MAG009	14/OCT	14:50	01:19
	15-20/OCT	13:10	01:09
MAG010	21/OCT	14:20	01:09
	22-27/OCT	13:10	01:09
MAG011	28/OCT	15:30	01:09
	29-31/OCT	13:10	01:09
MAG012	1/NOV	17:50	01:09
MAG013	9/NOV	23:30	01:09
	10-15/NOV	13:10	01:09
MAG014	16/NOV	18:10	01:09
	17/NOV	13:10	01:09
	18/NOV	13:10	13:46
MAG016	21/NOV	15:30	01:19
	22-23/NOV	13:20	01:19
	24/NOV	13:20	16:51
MAG017	29/NOV	22:00	01:19
	30/NOV	13:20	01:19
	1-5/DEC	13:20	01:19
MAG018	6/DEC	18:40	01:19
	7-12/DEC	13:20	01:19
MAG019	13/DEC	15:10	01:19
	14-17/DEC	13:20	01:19
	18-19/DEC	13:30	01:29
MAG020	20/DEC	16:40	01:29
	21-26/DEC	13:30	01:29
MAG021	27/DEC	15:10	01:29
	28-31/DEC	13:30	01:29
YEAR = 1989			
MAG021	1-2/JAN	13:30	01:29
MAG022	3/JAN	15:10	01:29
	4-9/JAN	13:30	01:29
MAG023	10/JAN	14:40	01:39
	11-16/JAN	13:40	01:39
MAG024	17/JAN	15:00	01:39
	18-23/JAN	13:40	01:39
MAG025	24/JAN	15:00	01:39
	25-26/JAN	13:40	01:39
	27/JAN	13:40	19:04
MAG026	31/JAN	15:30	01:39
	1/FEB	13:40	15:31
MAG027	1/FEB	21:00	01:39
	2-6/FEB	13:40	01:39
MAG028	7/FEB	14:30	01:39
	8-13/FEB	13:40	01:39
MAG029	14/FEB	14:40	01:39
	15-20/FEB	13:40	01:39
MAG030	22/FEB	14:40	01:39
	23-28/FEB	13:40	01:39
MAG031	1/MAR	15:30	01:39
	2-7/MAR	13:40	01:39
MAG032	8/MAR	15:30	01:39
	9-14/MAR	13:40	01:39

Malmstrom Air Force Base, Montana

TAPE #	DATE	START	STOP
MAG033	15/MAR	14:40	01:39
	16-21/MAR	13:40	01:39
MAG034	22/MAR	15:10	01:39
	23-25/MAR	13:40	01:39
	26-27/MAR	13:30	01:29
	28/MAR	13:30	15:29
MAG035	29/MAR	15:50	01:29
	30-31/MAR	13:30	01:29
	1/APR	13:30	01:19
MAG036	4/APR	20:50	01:29
	5-10/APR	13:30	01:29
MAG037	11/APR	14:30	01:29
	12-17/APR	13:30	01:29
MAG038	18/APR	14:20	01:29
	19-24/APR	13:30	01:29
MAG039	25/APR	20:30	01:29
	26-30/APR	13:30	01:29
	1/MAY	13:30	01:29
MAG040	2-8/MAY	13:30	01:29
MAG041	9/MAY	14:00	01:29
	10/MAY	13:30	01:29
	11-14/MAY	13:20	01:19
	15/MAY	13:20	13:46
MAG042	16/MAY	16:40	01:19
	17/MAY	13:20	01:19
	18-22/MAY	13:30	01:29
MAG043	23/MAY	14:00	01:29
	24-29/MAY	13:30	01:29
MAG044	30/MAY	14:30	01:29
	31/MAY	13:30	01:29
	1-5/JUN	13:30	01:29
MAG045	6/JUN	14:10	01:29
	7-12/JUN	13:30	01:29
MAG046	13/JUN	14:50	01:29
	14-19/JUN	13:30	01:29
MAG047	20/JUN	16:00	01:29
	21-26/JUN	13:30	01:29
MAG048	27-30/JUN	13:30	01:29
	1-3/JUL	13:30	01:29
MAG049	5/JUL	16:40	01:29
	6-11/JUL	13:30	01:29
MAG050	12/JUL	16:00	01:29
	13-17/JUL	13:30	01:29
	18/JUL	13:40	01:39
MAG051	19/JUL	15:00	01:39
	20-21/JUL	13:40	01:39
MAG052	16/AUG	17:10	01:29
	17-22/AUG	13:30	01:29
MAG053	23/AUG	14:40	01:29
	24-28/AUG	13:30	01:29
	29/AUG	13:30	23:41
MAG054	8/SEP	13:20	15:37
MAG055	8/SEP	16:50	01:19
	9-14/SEP	13:20	01:19
MAG056	15/SEP	13:50	01:19
	16-21/SEP	13:20	01:19
MAG057	22/SEP	14:30	01:19
	23-28/SEP	13:20	01:19
MAG058	29/SEP	16:50	01:19
	30/SEP	13:10	01:09
	1/OCT	13:10	01:09
MAG059	2/OCT	14:00	01:09
	3/OCT	13:10	01:09
MAG061	11/OCT	19:20	01:09
	12-17/OCT	13:10	01:09
MAG062	18/OCT	19:30	01:09
	19-24/OCT	13:10	01:09
MAG063	25/OCT	15:20	01:09
	26-31/OCT	13:10	01:09
MAG064	1/NOV	16:30	01:09
	2-7/NOV	13:10	01:09

Malmstrom Air Force Base, Montana

TAPE #	DATE	START	STOP
MAG067	18/NOV	18:50	01:09
	19/NOV	13:10	01:09
	20/NOV	13:10	17:52
MAG068	25/NOV	19:10	00:02
MAG069	27/NOV	22:20	01:09
	28-30/NOV	13:10	01:09
	1/DEC	13:10	01:09
	2-3/DEC	13:20	01:19
MAG070	6/DEC	23:10	01:19
	7-12/DEC	13:20	01:19
MAG071	14/DEC	15:10	01:19
	15-20/DEC	13:20	01:19

2.6 Malabar Transmitter Annex, Palm Bay, Florida

TAPE #	DATE	START	STOP
YEAR = 1988			
BAR008	8/DEC	17:00	23:19
	9-14/DEC	11:20	23:19
BAR009	15/DEC	13:40	23:19
	16-21/DEC	11:20	23:19
BAR010	22/DEC	14:10	23:19
	23/DEC	11:20	23:19
	24-28/DEC	11:30	23:29
BAR011	29/DEC	14:30	23:29
	30-31/DEC	11:30	23:29
YEAR = 1989			
BAR011	1-4/JAN	11:30	23:29
BAR012	5/JAN	13:30	23:29
	6/JAN	11:30	18:38
BAR013	6/JAN	20:30	23:29
	7-11/JAN	11:30	23:29
	12/JAN	11:30	17:21
BAR014	12/JAN	18:00	23:29
	13-15/JAN	11:30	23:29
	16-18/JAN	11:40	23:39
BAR015	19-25/JAN	11:40	23:39
BAR023	15/MAR	13:50	23:39
	16-20/MAR	11:40	23:39
	21/MAR	11:30	23:39
BAR024	23/MAR	15:50	23:29
	24-29/MAR	11:30	23:29
BAR025	30/MAR	13:30	23:29
	31/MAR	11:30	23:29
	1-5/APR	11:30	23:29
BAR026	6/APR	12:00	23:29
	7/APR	11:30	19:01
BAR027	7/APR	19:10	23:29
	8-10/APR	11:30	23:29
	11/APR	11:30	14:29
BAR028	25/APR	15:40	23:19
	26/APR	11:20	23:19
	27/APR	17:50	23:19
	28-30/APR	11:20	23:19
	1/MAY	11:20	23:19
BAR029	3/MAY	11:50	23:19
	4/MAY	11:20	23:19
BAR030	5/MAY	13:10	23:19
	6-11/MAY	11:20	23:19
BAR031	12/MAY	12:30	23:19
	13-18/MAY	11:20	23:19
BAR032	19/MAY	12:30	23:19
BAR033	22/MAY	11:50	23:19
	23-28/MAY	11:20	23:19
BAR034	30/MAY	21:20	23:19
	1-5/JUN	11:20	23:19
BAR035	6/JUN	12:20	23:19
	7-12/JUN	11:30	23:29
BAR036	13/JUN	13:30	23:29
	14-19/JUN	11:30	23:29
BAR037	20/JUN	12:40	23:29
	21-26/JUN	11:30	23:29
BAR038	27/JUN	18:50	23:29
	28-30/JUN	11:30	23:29
	1-3/JUL	11:30	23:29
BAR039	5/JUL	13:10	23:29
	6-11/JUL	11:30	23:29
BAR040	12/JUL	15:40	23:29
	13-18/JUL	11:30	23:29
BAR041	19/JUL	13:30	23:29
	20-25/JUL	11:30	23:29
BAR042	26/JUL	11:30	23:29
	27/JUL	11:30	12:11
BAR441	7/AUG	13:10	23:29
	8/AUG	11:30	11:53

Malabar Transmitter Annex, Palm Bay, Florida

TAPE #	DATE	START	STOP
BAR443	9/AUG	19:30	23:39
	10/AUG	11:30	12:30
BAR444	10/AUG	14:50	18:09
BAR045	10/AUG	18:50	23:29
	11-16/AUG	11:30	23:29
BAR046	17/AUG	11:50	23:29
	18-23/AUG	11:30	23:29
BAR047	24-26/AUG	11:30	23:29
	28-30/AUG	11:20	23:19
BAR048	1/SEP	12:00	23:19
	2-7/SEP	11:20	23:19
BAR049	8/SEP	11:50	23:19
	9-14/SEP	11:20	23:19
BAR050	15-21/SEP	11:20	23:19
BAR051	22/SEP	12:00	23:19
	23/SEP	11:20	23:19
	24-28/SEP	11:10	23:09
BAR052	29-30/SEP	11:10	23:09
	1-5/OCT	11:10	23:09
BAR053	6/OCT	11:40	23:09
	7-12/OCT	11:10	23:09
BAR054	20-26/OCT	11:10	23:09
BAR055	13/OCT	12:10	23:09
	14-19/OCT	11:10	23:09
BAR056	27-31/OCT	11:10	23:09
	1-2/NOV	11:10	23:09
BAR057	3-9/NOV	11:10	23:09
BAR058	10-16/NOV	11:10	23:09
BAR059	17-23/NOV	11:10	23:09
BAR060	24-30/NOV	11:10	23:09
BAR061	1-6/DEC	11:10	23:09
	7/DEC	11:20	23:19
BAR062	8-14/DEC	11:20	23:19
BAR063	15-21/DEC	11:20	23:19
BAR064	22/DEC	15:50	23:19
	23/DEC	11:20	23:19
	24/DEC	11:20	12:51
BAR065	27/DEC	12:30	23:19
	28/DEC	11:20	23:19
	29-31/DEC	11:30	23:29

YEAR = 1990

BAR065	1-2/JAN	11:30	23:29
BAR066	3/JAN	14:00	23:29
	4-9/JAN	11:30	23:29
BAR067	10/JAN	13:30	23:29
	11-16/JAN	11:30	23:29
BAR068	17/JAN	12:20	23:29
	18-23/JAN	11:30	23:29
BAR069	24/JAN	14:30	23:29
	25-30/JAN	11:40	23:39
BAR070	31/JAN	15:20	23:39
	1-6/FEB	11:40	23:39
BAR071	14/FEB	14:10	23:39
BAR072	7/FEB	14:00	23:39
	8-13/FEB	11:40	23:39
BAR073	15/FEB	14:50	23:39
	16-21/FEB	11:40	23:39
BAR074	22/FEB	12:40	23:39
	23-28/FEB	11:40	23:39
BAR075	1/MAR	12:10	23:39
	2-4/MAR	11:40	23:39
	5-6/MAR	11:30	23:29
	7/MAR	11:40	23:29
BAR076	8/MAR	14:20	23:29
	9-14/MAR	11:30	23:29
BAR077	15/MAR	14:00	23:29
	16-21/MAR	11:30	23:29

Malabar Transmitter Annex, Palm Bay, Florida

TAPE #	DATE	START	STOP
BAR078	22/MAR	14:50	23:29
	23-25/MAR	11:30	23:29
	26/MAR	11:30	14:00
BAR079	28/MAR	15:40	23:29
	29-31/MAR	11:30	23:29
	1-3/APR	11:30	23:29
BAR080	4/APR	12:10	23:29
	5-7/APR	11:30	23:29
	8-10/APR	11:20	23:19
BAR081	11/APR	12:10	23:19
	12-17/APR	11:20	23:19
BAR082	18/APR	11:30	23:19
	19-24/APR	11:20	23:19
BAR083	25/APR	11:40	23:19
	26-30/APR	11:20	23:19
	1/MAY	11:20	23:19
BAR084	6/JUL	15:00	23:29
	7/JUL	11:30	13:52
BAR085	7/JUL	15:20	23:29
	8-13/JUL	11:30	23:29
BAR086	15-21/JUL	11:30	23:29
BAR087	23/JUL	15:40	23:29
	24-29/JUL	11:30	23:29
BAR088	30-31/JUL	11:30	23:29
	1-5/AUG	11:30	23:29
BAR089	6/AUG	15:00	23:29
	7-12/AUG	11:30	23:29
BAR090	13/AUG	13:10	23:29
	14-19/AUG	11:30	23:29
BAR091	20/AUG	13:10	23:29
	21-26/AUG	11:20	23:19
BAR092	27-31/AUG	11:20	23:19
	1-2/SEP	11:20	23:19
BAR093	3-9/SEP	11:20	23:19
BAR094	10/SEP	12:40	23:19
	11-16/SEP	11:20	23:19

TAPE #	DATE	START	STOP
BAR095	17/SEP	13:50	23:19
	18-22/SEP	11:20	23:19
	23/SEP	11:10	23:09
BAR096	24/SEP	13:00	23:09
	25-30/SEP	11:10	23:09
BAR097	1/OCT	11:10	16:32
BAR098	1/OCT	18:10	23:09
	2-7/OCT	11:10	23:09
BAR099	8/OCT	11:20	23:09
	9/OCT	11:10	23:09
	10/OCT	11:10	20:32
BAR100	11/OCT	12:30	23:09
	12-17/OCT	11:10	23:09
BAR101	18/OCT	11:40	23:09
	19-24/OCT	11:10	23:09
BAR102	25-31/OCT	11:10	23:09
BAR103	1/NOV	11:10	16:25
BAR104	16/NOV	16:10	23:09
	17-18/NOV	11:10	23:09
	19/NOV	11:10	19:56

2.7 National Weather Facility, Columbia, Missouri

TAPE #	DATE	START	STOP
YEAR = 1989			
COL001	9/FEB	16:20	00:29
	10-14/FEB	12:30	00:29
	15/FEB	13:10	00:29
COL002	16-21/FEB	12:30	00:29
	22/FEB	13:10	00:29
COL003	23/FEB	14:00	00:29
	24-28/FEB	12:30	00:29
	1/MAR	13:10	00:29
COL004	2-3/MAR	12:30	00:29
	4-7/MAR	12:20	00:19
COL005	8-14/MAR	12:20	00:19
COL006	15-21/MAR	12:20	00:19
COL007	22-28/MAR	12:20	00:19
COL008	29-31/MAR	12:20	00:19
	1-3/APR	12:20	00:19
COL009	5/APR	12:20	00:19
	6/APR	12:40	00:19
	7/APR	12:20	00:19
	8-11/APR	12:10	00:09
COL010	12-17/APR	12:10	00:09
	18/APR	12:10	22:09
COL011	19-25/APR	12:10	00:09
COL012	26/APR	12:10	00:09
	27/APR	12:10	22:44
COL013	30/APR	19:40	00:09
	1-4/MAY	12:10	00:09
	5/MAY	12:20	00:09
	6/MAY	12:10	00:09
COL014	16/MAY	12:10	20:54
COL015	16/MAY	21:20	00:09
	17-22/MAY	12:10	00:09
COL016	23-29/MAY	12:10	00:09
COL017	22/JUN	21:20	00:09
	23-28/JUN	12:10	00:09
COL018	29-30/JUN	12:10	00:09
	1-5/JUL	12:10	00:09
COL019	6-11/JUL	12:10	00:09
	12/JUL	12:20	00:19
COL020	13-19/JUL	12:20	00:19
COL021	20-26/JUL	12:20	00:19
COL022	27/JUL	20:30	00:19
	28-30/JUL	12:20	00:19
	1-2/AUG	12:20	00:19
COL023	3-9/AUG	12:20	00:19
COL024	10-16/AUG	12:10	00:09
COL025	17-23/AUG	12:10	00:09
COL027	24-30/AUG	12:10	00:09
COL028	31/AUG	14:10	00:09
	1-6/SEP	12:10	00:09
COL029	7/SEP	15:10	00:09
	8-13/SEP	12:10	00:09
COL030	14/SEP	14:00	23:59
	15-20/SEP	12:00	23:59
COL031	21-27/SEP	12:00	23:59
COL032	28-30/SEP	12:00	23:59
	1-4/OCT	12:00	23:59
COL033	5/OCT	17:30	23:59
	6-11/OCT	12:00	23:59
COL034	12-13/OCT	12:00	23:59
	14-18/OCT	11:50	23:49
COL035	19-25/OCT	11:50	23:49
COL036	26-31/OCT	11:50	23:49
	1/NOV	11:50	23:49
COL037	2/NOV	22:40	23:49
	3/NOV	11:50	16:21
COL038	3/NOV	16:24	23:49
	4-8/NOV	11:50	23:49

National Weather Facility, Columbia, Missouri

TAPE #	DATE	START	STOP
COL039	9-15/NOV	11:50	23:49
COL040	16-17/NOV	11:50	23:49
	18-22/NOV	12:00	23:59
COL041	23-29/NOV	12:00	23:59
COL042	30/NOV	12:00	23:59
	1-6/DEC	12:00	23:59
COL043	14/DEC	12:23	23:59
COL044	15/DEC	12:00	23:59
	16-21/DEC	12:10	00:09
COL045	22/DEC	14:30	00:09
	23-27/DEC	12:10	00:09
COL046	28-31/DEC	12:10	00:09

YEAR = 1990

COL046	1-3/JAN	12:10	00:09
COL047	4/JAN	13:30	00:09
	5-6/JAN	12:10	00:09
	7-10/JAN	12:20	00:19
COL048	11-17/JAN	12:20	00:19
COL049	18-24/JAN	12:20	00:19
COL050	25-31/JAN	12:20	00:19
COL051	1-7/FEB	12:20	00:19
COL052	8-14/FEB	12:20	00:19
COL053	15/FEB	15:16	00:19
	16-21/FEB	12:20	00:19
COL054	22-28/FEB	12:20	00:19
COL055	1-7/MAR	12:20	00:19
COL056	8-10/MAR	12:20	00:19
	11/MAR	12:20	00:51
COL057	12/MAR	20:24	20:24
	13-14/MAR	12:20	00:18
COL058	15-21/MAR	12:20	00:19
COL059	22-25/MAR	12:20	00:19
	26-28/MAR	12:10	00:09
COL060	2/APR	12:50	00:09
	3-8/APR	12:10	00:09
COL061	9-11/APR	12:10	00:09
COL062	12-18/APR	12:10	00:09
COL063	19-25/APR	12:10	00:09
COL064	26-30/APR	12:10	00:09
	1-2/MAY	12:10	00:09
COL065	3-9/MAY	12:10	00:09
COL066	10-16/MAY	12:10	00:09
COL067	17-23/MAY	12:10	00:09
COL068	24-30/MAY	12:10	00:09
COL069	31/MAY	12:10	00:09
	1-4/JUN	12:10	00:09
COL070	5/JUN	13:50	00:09
	6/JUN	12:10	00:09
COL071	7-13/JUN	12:10	00:09
COL075	1/AUG	17:50	00:19
	2-7/AUG	12:20	00:19
COL076	8/AUG	12:20	00:19
	9-14/AUG	12:10	00:09
COL077	15-21/AUG	12:10	00:09
COL078	22-28/AUG	12:10	00:09
COL079	29-31/AUG	12:10	00:09
	1-4/SEP	12:10	00:09
COL080	5-11/SEP	12:10	00:09
COL081	19-25/SEP	12:00	23:59
COL082	26-30/SEP	12:00	23:59
	1-2/OCT	12:00	23:59

National Weather Facility, Columbia, Missouri

TAPE #	DATE	START	STOP
COL083	3-9/OCT	12:00	23:59
COL084	10-12/OCT	12:00	23:59
	13-16/OCT	11:50	23:49
COL085	17-23/OCT	11:50	23:49
COL086	24-30/OCT	11:50	23:49
COL087	31/OCT	11:50	23:49
	1-6/NOV	11:50	23:49
COL088	7-13/NOV	11:50	23:49
COL089	14-16/NOV	11:50	23:49
	17-20/NOV	12:00	23:59
COL090	21-27/NOV	12:00	23:59
COL091	28/NOV	19:40	23:59
	29-30/NOV	12:00	23:59
	1-4/DEC	12:00	23:59
COL092	10/DEC	17:10	23:59
	11-14/DEC	12:00	23:59
	15-16/DEC	12:10	00:09
COL093	17-23/DEC	12:10	00:09
COL094	24-30/DEC	12:10	00:09
COL095	31/DEC	12:10	00:09

OPTICAL SYSTEMS GROUP
TECHNICAL NOTE NO. 232

APPENDIX B
Sep. 1991

RATIO AND CLOUD DECISION SOFTWARE SUMMARY

T. L. Koehler

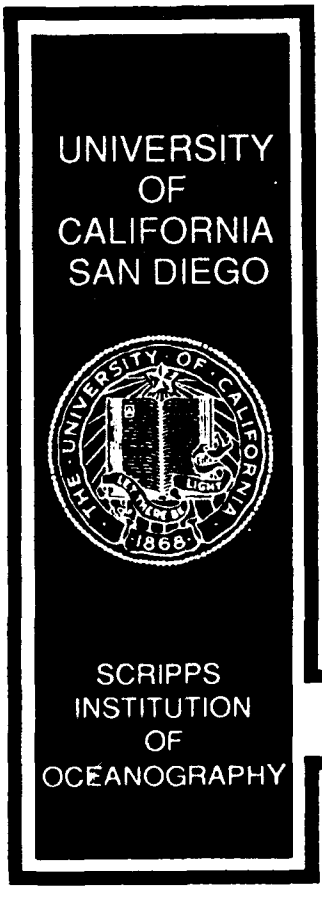

Contract Monitor, Mr. B. Kunkel
Atmospheric Sciences Division

Prepared for
The Geophysics Directorate of the Phillips Laboratory
Air Force Systems Command, United States Air Force
Hanscom AFB, Massachusetts 01731
under contract No. F19628-88-K-0005

MARINE PHYSICAL LAB San Diego, CA 92152-6400

B1.0 INTRODUCTION

This appendix provides a brief overview of the software used to produce cloud decision imagery from the raw radiance imagery collected in the field. An overview of the procedure used to produce the 1-minute and 10-minute cloud decisions for the contract is shown in Fig. B1-1. The following three sections describe the three main processing programs, TAPRATPL, CLDDECM and CMPDECTP. Section B5 describes some of the other programs used in intermediate steps. Section B6 lists brief descriptions of utility routines written at MPL that are accessed by the three major processing routines.

B2.0 TAPRATPL - The Composite Ratio Processing Program

TAPRATPL is the program that takes a set of four radiance images from a field tape, and produces a composite ratio image. The ratio image, along with its corresponding dark red image, is then copied onto an output tape that is usually referred to as a ratio tape. TAPRATPL is run either for 1 or 10 minute images. Thus, a given field tape must be processed twice if both 1 and 10 minute ratio images are needed.

To run TAPRATPL, the AT type computer must be equipped with an ITI FG-100, a PL-1250 accelerator board, and 2 ExaByte tape drives (one for input, the other for output). The PL board allowed us to cut the computation time by a factor greater than 3, enabling a TAPRATPL run to usually take less than 12 hours. It also increased the complexity of the programming effort. The following description provides a general overview of the TAPRATPL main program.

The input files needed by TAPRATPL are described in Tech Notes 230 and 231. The program also requires user input regarding the field tape number, the type of images being processed, thin and opaque values for a color ratio display option, the site number for the field tape, and the expected start date on the input tape.

The program makes several consistency checks between input parameters either from the user or the input files, and the input tape, and notifies the user of any discrepancy. Other parts of the code will check for consistency within the four image sets, and the main program also notifies the user of any unexpected time shifts. All peculiarities are written to an output diagnostic file. A log file containing date, time, quality and ratio histogram information is also produced by TAPRATPL.

Figure B2-1 shows a conceptual flowchart for the TAPRATPL program. Basically, after some initializations and input definition steps, the program consists of an outer day loop and an inner image loop. Due to the occasional date shifts in our field systems, date changes are detected by backward time skips of greater than four hours.

B2.1 TAPRATPL Subroutine Descriptions

TAPRATPL is a complex program, linking together more than 90 subprograms. The names of the routines developed here at MPL for TAPRATPL are listed in Figure B2-2. The remaining MPL utility programs are described in a later section. Additional subprograms perform specific functions on the FG-100 and PL-1250 boards, and are in documentation provided by the vendors (ITI and Eighteen Eight respectively.)

The subroutines written specifically for TAPRATPL are described below in their order of appearance. The * symbol indicates those routines that require PL-1250 access.

SETPL* - initializes the PL-1250 processor, allocates PL memory locations for subsequent programs, and transfers some of the constants used in later calculations to the PL board.

CLRCLD - creates the color lookup tables for the color ratio display hotkey option from input thin and opaque thresholds.

CALSEL - requests the site number, opens the diagnostic file, requests the start date of the field tape. Confirms the date and field tape sequence number with data from DATE_.LST. Retrieves the hardware version numbers and data quality information from VERSION.LOG for each date on the input tape.

FRSTHD - reads initial header from field tape, and determines the software version that created the tape and whether the first image is a full resolution, 10 minute image, or a subset 1 minute image. Confirms the initial date from CALSEL input and the site. Reads the iris, occultor and neutral density settings for the image.

RDCAL* - reads the calibration file (CAL_V___.RAT) specified by CALSEL for a given date. Performs some preliminary computations related to the image offset and magnifications, and the ratio multiplier factors. Transfers this information to the PL-1250.

EQTIME - using code similar to that used in the FIELD program, compute the start time (6 hours before LAN) for the specified Julian day and longitude. The start time is used to determine the expected occultor position.

TIMCOR - reads the time correction from the TIME_.COR file for the date specified.

ARMSET - reads the occultor arm number and angle offset from the OCC_.DAT file for the date specified.

GETIMG - transfers the remainder of the field image set from ExaByte to the FG-100 board.

CHCKHD - performs consistency checks on the neutral density and spectral filter designations, and the quadrant number specified in all four headers in an image set.

KEYCK - checks for new hotkey entries during processing. Activates flags that are acted upon in the main program.

LINDIG - applies the linearity correction to the radiance byte values via an input LUT on the FG-100.

RATCOM* - transfers the radiance information from the FG-100 to the PL-1250 using a double buffering technique described in Eighteen Eight (1988). Calls RATPL which performs the ratio operations on the set of 4 lines transferred. Returns the resulting composite ratio line to the FG-100 board.

RATPL* - performs the ratio operations on the 4 image lines provided. Includes setting offscale dark points on the bright red-blue pair to 0, offscale bright points on the dark red-blue pair to 240, and the remaining ratio byte values between 1 and 239.

OCCMSK - determines the arm and edge locations in 3-dimensions. Calls POSIMA to locate points on the edge in image coordinates, and DRAWLN to identify the pixel locations connecting consecutive edge points. Overlays the resulting occultor mask onto the ratio image with byte value 0. Currently, the arm mask is drawn twice its actual diameter, and the frame is expanded by 15% to compensate for mechanical play in the occultor assembly.

POSIMA - converts the 3-dimension location of a point on the occultor assembly to ratio image coordinates.

DRAWLN - determines the image pixels along a line segment defined by any two points in the image coordinates.

OBDRAW - overlays the obstacle masks onto the ratio image with byte value 0 using edges defined in RDCAL.

SMOHST* - performs two passes of a smoothing filter over the raw ratio values. Passes a double buffered set of lines from the FG-100 to the PL-1250. Calls SMTHPL to perform the smoothing operations, then returns the smoothed results to the FG-100. Computes the resulting ratio histogram distribution.

SMTHPL* - passes a 2-dimensional kernel over a full resolution 10-minute image, or a 1-dimension kernel over the subset lines of a 1-minute image. If more than half the weight of the filter is at a pixel value of 0 or 240 (offscale bright), no smoothing is performed at that point.

WRITHD - imbeds the ratio header information onto the ratio image on the FG-100 board.

PUTIMG - writes a DOS header block for this image onto the output ExaByte drive, then copies the ratio-dark red image pair from the FG-100 to ExaByte.

LOOP - loops from the colored ratio image to the red image when a certain hotkey is activated.

NEXTHD - transfer the next header on the input ExaByte to the FG-100, determines the image type, and extracts the iris, occultor and neutral density settings.

B3.0 CLDDECM - The Fixed Threshold Cloud Decision Program

In early 1990, we were tasked to provide preliminary cloud-no cloud decision data for 4 sites for up to a year to The Analytic Sciences Corporation (TASC). The cloud decisions for the 1-minute subset imagery processed for this requirement were run using the fixed threshold algorithm named CLDDECM. This program is much simpler than TAPRATPL and subsequently much faster. The cloud decision is made by passing the ratio image through an input look-up table and no PL-1250 computations are required. The thin and opaque decision thresholds are constant for the entire tape, and are specified as user inputs. In addition to the output tape, one output file is generated, and it contains sky cover results only from those minutes evenly divisible by 10.

The conceptual flow chart for CLDDECM is shown in Fig. B3-1. While not shown in the diagram, end-of-file marks are written to the output ExaByte drive at the end of each day. No dummy DOS headers are placed before the images, as done in TAPRATPL.

B3.1 CLDDECM Subroutines

CLDDECM links together more than 30 subprograms. The 7 subroutines written specifically for CLDDECM are described below. Twelve MPL utility programs are also used, along with 20 Image Tool Library routines. (Fig. 3-2)

CLRDEC - requests the thin and opaque threshold inputs and computes the cloud decision LUT. If the ratio input value is 0, its corresponding cloud decision value will also be zero. Ratio values between 1 and the thin threshold inclusive will be assigned the clear decision value of 100. The remaining values up to and including the opaque threshold will be assigned the thin cloud decision value of 150. Those points with ratios greater than the opaque threshold up to the value 239 will be given the opaque cloud value of 200. Finally, the off-scale bright points, with a ratio value of 240, will be assigned a cloud decision value of 202. The color LUT for hotkey cloud decision displays are also determined.

CHKTAP - tests of the source and target ExaByte drives are ready, and can write an EOF to the target ExaByte.

FRATHD - finds the DOS header and imbedded ratio headers in the ratio tape images.

ONERAT - reads the remaining 65 lines of the 1-minute ratio images.

CLDKEY - checks for hotkey entries during processing, and sets appropriate flags.

WRCDHD - writes the cloud decision header information to the FG-100.

ONESAV - copies the cloud decision image from the FG-100 to the target ExaByte.

B4.0 CMPDECTP - The Composite Cloud Decision Program

Our experience with the cloud decisions produced by fixed threshold algorithms such as CLDDECM, was that while opaque cloud were reasonably well identified, thin cloud in the downsun region of the sky were undetermined, while regions near the horizon, particularly at near-horizon sun angles were incorrectly identified as cloudy. To overcome these problems, a new algorithm was developed. A fixed threshold is still used to identify opaque clouds, but the thin cloud determination is now made against an estimate of the clear sky ratio that varies in both space and time. A more detailed description of the algorithm is provided in Section 5 in the main body of the report.

CMPDECPL also requires the PL-1250 board to get the run time for a 7 day tape down to about 3 1/2 hours. (Without the PL, the run time would exceed 15 hours). For a particular field tape, three input files must be present. CMPDECINP specifies the opaque thresholds for each of the 4 spatial density settings, the azimuth offset, and the thin cloud acceptance level for a particular hardware version. Another file, _ _ _ SKY.DAT contains the normalized Red/Blue clear sky radiance estimates at 5° increments of solar zenith angle that were extracted from clear day samples for the site. The first 3 letters in this file name are the 3 letter site identifier. (For example, COLSKY.DAT would contain the Columbia, MO tables.) The final file needed is _ _ _ ###.REF, containing the reference factors that vary as a function of boundary layer haze loading. File KAA050.REF would contain the reference values for tape number 50 from Kirtland AFB, NM. These files are generated in the SETREF program described in the next section.

A conceptual flowchart for CMPDECTP is shown in Fig. B4-1. CMPDECTP only processes the full resolution imagery taken at 10-minute intervals in the field, in contrast to the 1-minute imagery processed by CLDDECM. A 1-minute version of the new algorithm has yet to be developed. As in TAPRATPL, dummy DOS headers are written to the output ExaByte before each cloud decision image.

B4.1 - CMPDECTP Subroutine Description

The subroutines needed to run CMPDECTP are described in Fig. B4-2. Descriptions for those programs written specifically for the CMPDECTP routine are provided below. Those subroutines interacting with the PL-1250 board are again marked with an *.

INITCD - initializes the FG-100 board

SETPLC* - sets up the PL and passes some of the constant and fixed value arrays to the PL-1250

CLRCMP - program the color LUT for cloud decision image displays

CTRTHD - reads the next ratio header from the input ExaByte

PARCMP - on the first time called, sets the ratio image size parameters, computes latitude and longitude from the ratio header information and reads the CMPDECINP file and *.REF file for this tape. For each new date encountered, the solar declination angle, needed to compute solar zenith and azimuth, is determined.

RDTRAT - reads the remaining 479 lines of the 10-min ratio image.

CMPCMT - computes the solar zenith and azimuth angles for the image, and interpolates the normalized clear sky reference tables to the image zenith. Interpolates the haze-related reference factor in time to image time. Passes upper and lower ratio image row pairs to the PL for processing, then places the resulting cloud decision rows into the FG-100. At completion, computes sky cover parameters.

CMPPLT - interpolates the sky ratio table to the image row pixel locations, and multiplies by the reference value producing a clear sky pixel estimate. A cloud decision value is then assigned at each pixel in the following manner.

No data: RATIO = 0

DECIS = 0

Off-Scale bright: RATIO = 240

DECIS = 201

Indeterminate: CLEAR ≥ OPAQUE

DECIS = 202

Opaque Cloud: RATIO ≥ OPAQUE

DECIS = 100 (RATIO/OPAQUE) + 40

Thin Cloud: RATIO/CLEAR ≥ ACCEPT

DECIS = 40 [RATIO/(ACCEPT · CLEAR)]+60

Clear: RATIO/CLEAR < ACCEPT

DECIS = 100 (RATIO/OPAQUE)

where RATIO - ratio byte value

CLEAR - clear sky ratio estimate

OPAQUE - opaque ratio threshold

ACCEPT - thin cloud acceptance level

DECIS - cloud decision byte value

Thus, clear pixels fall between 1 and 99, thin cloud pixels between 100 and 139, and opaque cloud pixels between 140 to 200 in the composite decision imagery. Some of the original variability in the ratio image remains in the decision image, in contrast to the CLDDECM output that had single byte values for each category. The indeterminate category also was not available in CLDDECM. Following the cloud decision in subroutine CMPPLT, the decision histogram is then updated.

SKYINT - first time through loads the normalized clear sky red/blue ratio estimates for each 5° solar zenith angle. Then interpolates the tables to the observed solar zenith angle (all calls).

SUNPOS - determines the sun position in WSI zenith and azimuth space for the specified time and azimuth offset.

REFCOM - interpolates the reference values for the date specified to the time specified.

CLDKEY - checks for hot key entries during processing and sets appropriate flags.

WRCTHD - writes the cloud decision header information to the FG-100 board.

CMPSVT - writes a DOS header block and decision image on the output ExaByte drive.

B5.0 OTHER RELATED ROUTINES

Several computer routines have been written by our group for WSI data display and manipulations. The routines needed to perform many of the intermediate tasks in the ratio and cloud decision processing sequence are described in this section.

CHECKAZM - determines the azimuth offset of the sensor with respect to true North. Done for a particular hardware version from a raw radiance tape. Hourly sun positions for an entire clear day are extracted from full-resolution image with the aid of a mouse. These positions are then plotted on a nominal WSI image. The solar path for a user-input azimuth offset is then plotted. The offset can then be changed until the best visual fit to the extracted sun positions is found.

CHECKLAN - allows the user to determine the occultor arm and offset values, and the time offset for a LAN image on disk. Other quality-related comments regarding the image, and estimated cloud cover values are also manually recorded during these runs. This information forms the basis for several of the TAPRATPL input files.

NDRCALC - computes the red/blue ratios from raw radiance quadrants 1 and 2, and then from quadrants 3 and 4. Then forms the ratio between these values, and writes the histogram of the final ratio pixel values. The peak in this histogram, along with the

absolute calibration results, provide a good first estimate of the NDR correction factor in TAPRATPL.

OBSBETA - using measured ratio images, computes normalized clear sky ratio distribution from full resolution ratio tape input, usually from completely clear days. Using a mouse, nonrepresentative points in regions of stray light or covered by cloud elements can be flagged for removal from the sample (5° zenith and 15° relative azimuth intervals) extracted from the full image.

COMBNORM - combines the normalized clear sky ratio files from OBSBETA for a given site. Tables from the same solar zenith angle are averaged together for all the days with OBSBETA output. The resulting averaged tables are examined for consistency, and after some manual adjustments, provide the ___SKY.DAT files needed by CMPDECTP and GETREF.

GETREF - determines a representative clear sky reference value estimate for each ratio image on a 10-minute ratio tape. The observed ratio is divided by the normalized clear sky ratio for all points within the 70° zenith angle circle, and a histogram of the resulting values chosen. A seven count window is passed across the low value end of the histogram to find the window with the largest image area contribution. The center of the maximum window and the area of the window's contribution are written to the GETREF output files.

SETREF - plots the GETREF reference values for up to four days in different colors, and allows the user to select representative reference values for the day. Value selection is performed with a mouse. Results are written to *.REF files for use in CMPDECTP.

RATREF - reads a ratio image from a 10-minute ratio tape and constructs a ratio histogram. By use of a mouse, the user can then select different thresholds. The region of the image below that threshold is then colored blue on the ratio image. The resulting ratio image can then be compared to the dark red image that accompanies the ratio image on tape. The visual comparisons enable the selection of opaque levels at different neutral density settings needed by CMPDECTP.

EXCOPY - backs up the WSI image tapes, either raw, ratio or cloud decision.

EXQC - provides a summary of the images available on a 1-minute cloud decision tape.

ISOTEST - allows examination of different thin and opaque threshold combinations on the images stored on disk. Used primarily for CLDDECM threshold determination.

Several routines have been written for viewing WSI imagery from disk and evaluating them with a mouse. These include SHOIMG, VIEWIMG and SAMPIMG. Another set of routines manipulate the WSI images on tape include IMCIND, RDIMGS and WRIMGS.

B6.0 MPL Utility Routines Used in Ratio and Cloud Decision Processing

Several utility routines have been written for use with our processing programs. Brief descriptions of these routines are given below.

BEEP - causes an audible sound to be made by the computer.

CALEND - computes the month, day and year from the relative Julian date, and constructs the appropriate date string.

CLRSCR - clears all 4 quadrants of the FG-100 board.

DELAY - pauses the runstream for the specified number of seconds.

EOFC1 - writes an EOF to ExaByte unit 1. (Usually the write drive).

EXSNS0 - decodes the ExaByte unit 0 sense data.

EXSNS1 - decodes the ExaByte unit 1 sense data.

EX2FG1 - passes a 1K block from ExaByte to the FG-100 board.

FGREGS - sets the FG-100 registers before data is passed through an input LUT.

FGSEL1 - sets the FG-100 registers for normal ExaByte [illegible]

FG1EX1 - writes a 1K block from the FG100 board to the ExaByte unit 1.

FG60K1 - writes a 60K block from the FG-100 board to ExaByte unit 1.

FHDR - creates a dummy DOS header block for a file of specified size.

FHDR - creates a dummy DOS header for a ratio image for either a 1 or 10 min image.

INITFG - initializes the FG-100 board.

JULIAN - computes the relative Julian date from either a date string or integer month, day and year values. The relative Julian date for 1/JAN/88 is 1.

OUTEOF - writes an EOF to the ExaByte write drive.

READY - determines whether the ExaByte unit specified is ready for a command.

RSENSE - decodes the ExaByte sense data from the read drive.

SKBLK - skips the specified number of 1K blocks on the read Exabyte.

SUN - compute the solar declination angle, radius vector, and equation of time for a particular longitude and date. Based on the ephemeris algorithm of Wilson (1980).

WHBLK - writes the 1K DOS header to ExaByte.

WRFMK - write an EOF to ExaByte.

WSENSE - decodes the ExaByte sense data from the write Exabyte.

REFERENCES

Ciandro, M. L., 1991. WSI processing manual. Tech Note 230, Optical Systems Group, Marine Physical Laboratory, University of California, San Diego, Scripps Institution of Oceanography.

Koehler, T. L., 1991. WSI ratio and cloud decision processing summary. Tech Note 231, Optical Systems Group, Marine Physical Laboratory, University of California, San Diego, Scripps Institution of Oceanography.

Wilson, W. H., 1980. Solar ephemeris Algorithm. SIO Ref. 80-13. Visibility Laboratory, University of California, San Diego, Scripps Institution of Oceanography.

Eighteen Eight Laboratories, 1988. *Reference Manual for PL Series Processors*, San Diego, CA.

Werner Frei Associates, 1987. *IMAGETOOL - Toolkit for Image Processing Software Development*, Model 1000, Santa Monica, CA.

Figure B1-1
Overview of Ratio and Cloud Decision Processing Steps

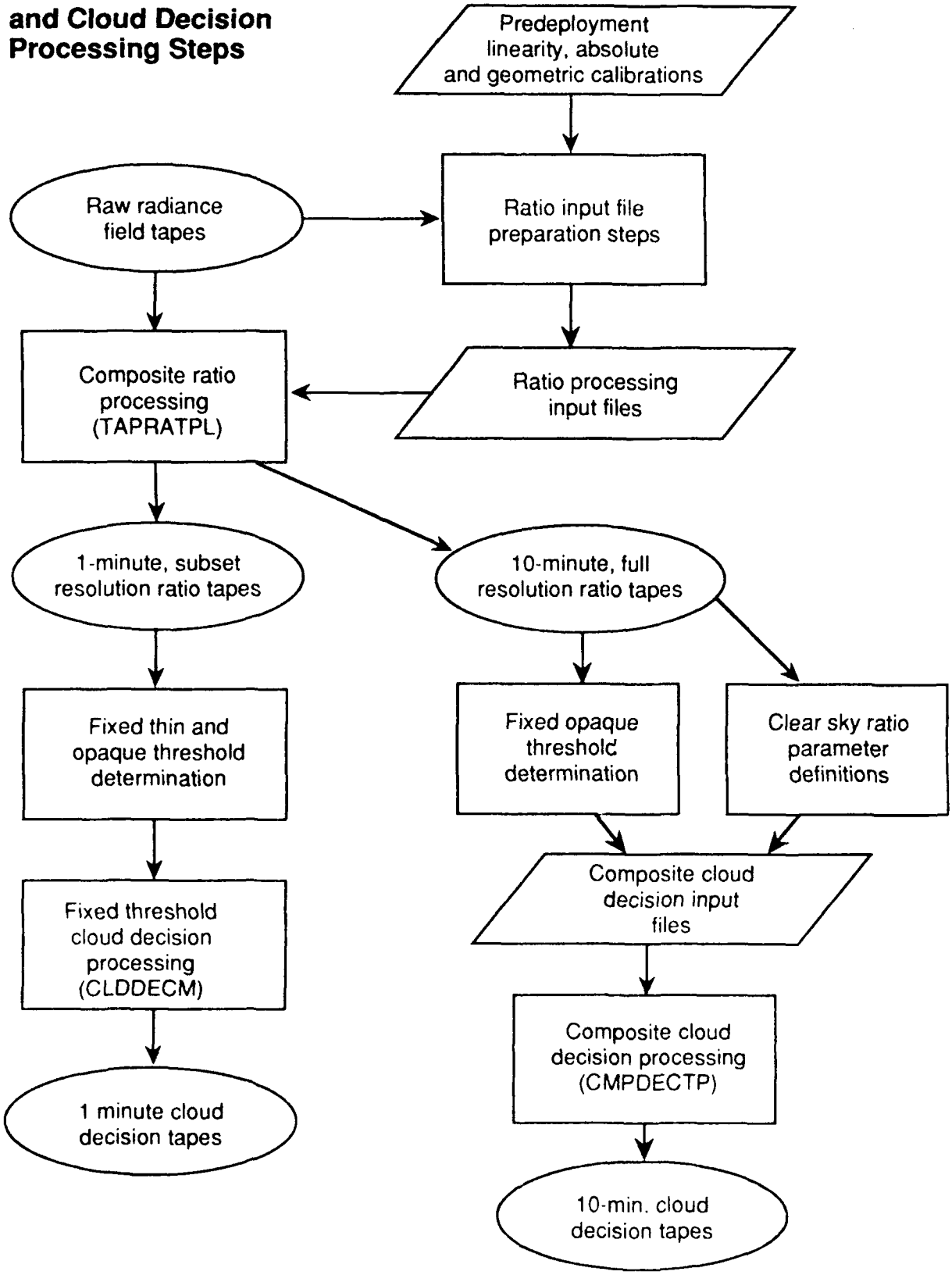

Fig. B2-1 TAPRATPL Conceptual Flowchart

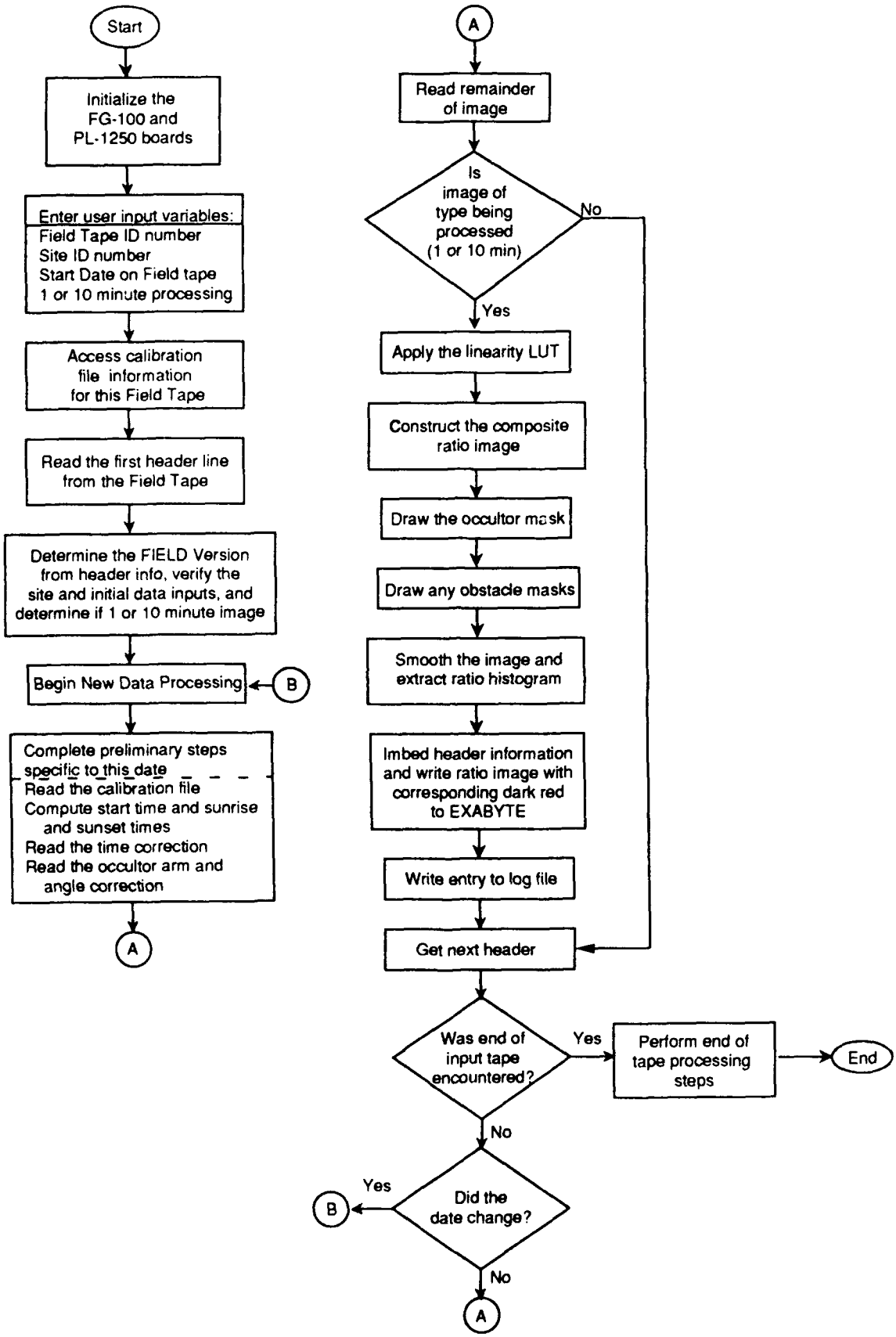

Fig. B2-2 TAPRAT PL Subroutines

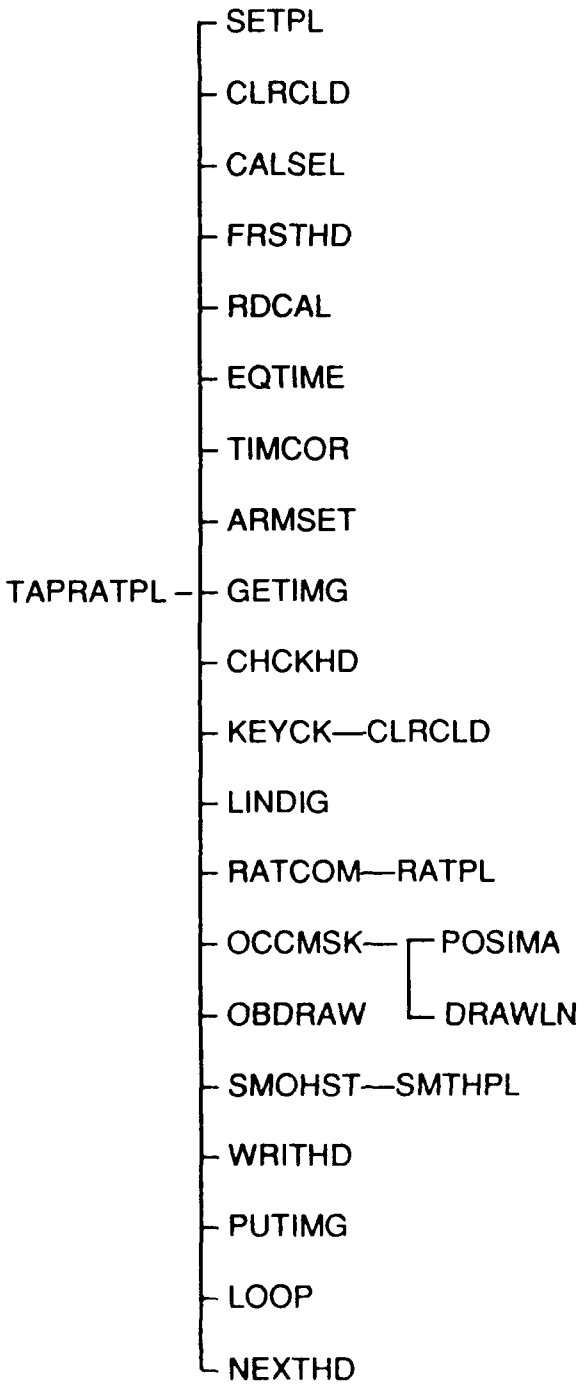

Other MPL Utility Routines Called

CALEND	FG1KU1	RSENSE
CLRSCR	FG60U1	SKBLK
DELAY	FILL	SUN
EXSNS1	INITFG	WHBLK
EX2FG1	JULIAN	WRFMK
FGREGS	OUTEOF	WSENSE
FGSET	READY	

PL - Series Subprograms Called

CNV2FP	PLSLIB	VFIEEE
ITISET	PLSPRC	VFILL8
LVGTA	PLTOIT	VFLT8
LVLTA	PLWTRN	VHIST
LVMERG	PLXFFR	VHST8
PLCKRN	PLXFTR	VIMITQ
PLFLSH	VCLI8	VSMUL
PLFMIT	VCLPHI	VTIEEE
PLINIT	VCONV	VZERO
PLITFM	VDIVR	XTIVAL
PLITPS	VFFILL	XTONEF
PLITTO		

Image Tool Library Functions Called

BRDSEL	IMMOVE	SETSCR
CHARST	INITIM	WDISK
CHARZ	LUTSEL	WRLUT
CLKSEL	PANSET	WRREC
DIGITZ	PCKMOD	WRREG
PWVEC	RDREC	WTFVB
FLREC	SCRSET	

Fig. B3-1 CLDDECM Conceptual Flowchart

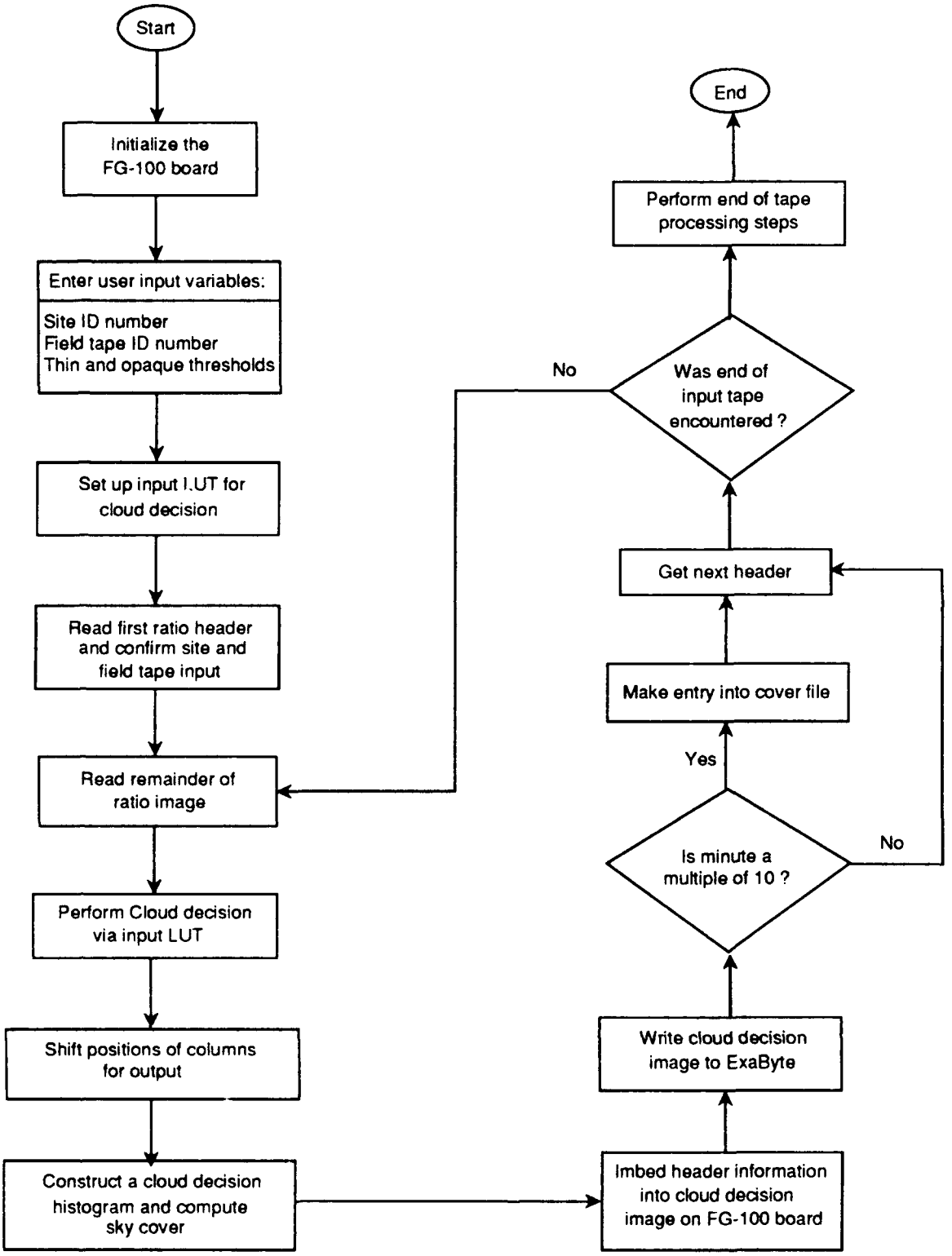

Fig. B3-2 CLDDECM Subroutines

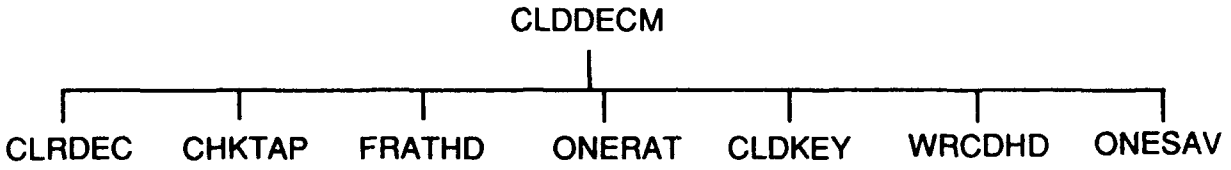

Other MPL Utility Routines Called

BEEP	CLRSCR	EQFC1	EXSNS1	FGREGS	FG1KU1	INITFG
CALEND	DELAY	EXSNS0	EX2FG1	FGSET		

Image Tool Library Functions Called

BRDSEL	CLKSEL	HISTO	LUTSEL	RDREL	WDISK	WRREG
CHARST	DWVEC	IMMOVE	PANSET	SCRSET	WRLUT	WTFVB
CHARZ	FLREC	INITIM	PCKMOD	SETSCR	WRREC	

Fig. B4-1 CMPDECTP Conceptual Flowchart

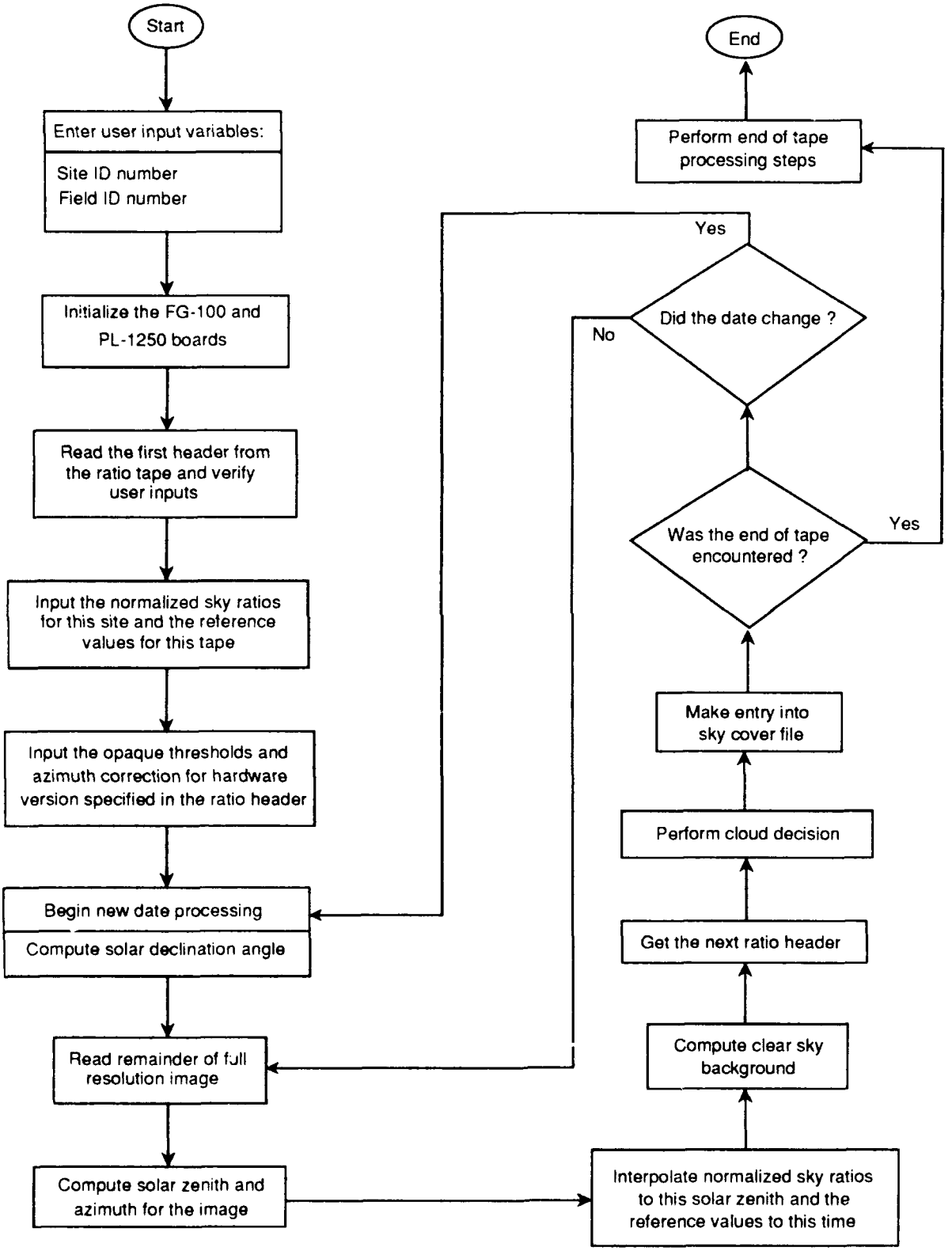

Fig. B4-2 CMPDECTP Subroutines

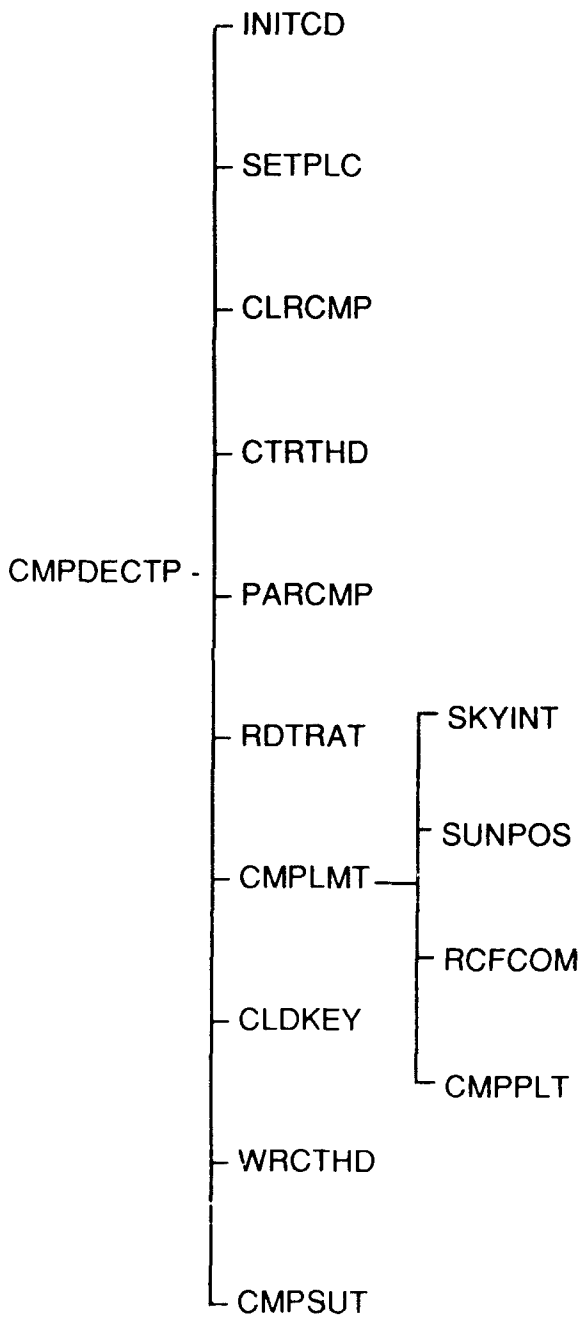

Other MPL Utility Routines Called

CALEND	OUTEOF
CLRSCR	READY
DELAY	RSENSE
EX2FG1	SKBLK
FGSET	SUN
FG60U1	WHBLK
FFILL	WRFMK
JULIAN	WSENCE

Image Tool Library Functions Called

BRDSEL	PCKMOD
CHARST	RDREC
CHARZ	SCRSET
CLKSEL	SETSCR
FLREC	WDISK
IMMOVE	WRLUT
INITIM	WRREC
LUTSEL	WRREG
PANSET	

PL - Series Subprograms Called

LVEQ	PLXFTR	VSADD
LVGT	VABS	VSDIVL
LVLE	VACOS	VSDIVR
LVMERG	VADD	VSMADD
PLCKRN	VCLI8	VSMSAD
PLFLSH	VCLPHI	VSMSSR
PLINIT	VDIVR	VSMUL
PLITFM	VFFILL	VSSUBR
PLITSE	VFIEEE	VSUBR
PLITTO	VFLT8	VSUBRM
PLSLIB	VFRAC	VTRUNC
PLSPRC	VHST8F	VZERO
PLWTRN	VIMVFT	XTONEF
PLXFFR	VRVRS	